

December 2020

## Design and Optimization of a Modular DC-DC Power Converter for Medium Voltage Shipboard Applications

Seyed Rasoul Hosseini  
*University of Wisconsin-Milwaukee*

Follow this and additional works at: <https://dc.uwm.edu/etd>



Part of the [Electrical and Electronics Commons](#)

---

### Recommended Citation

Hosseini, Seyed Rasoul, "Design and Optimization of a Modular DC-DC Power Converter for Medium Voltage Shipboard Applications" (2020). *Theses and Dissertations*. 2522.  
<https://dc.uwm.edu/etd/2522>

This Dissertation is brought to you for free and open access by UWM Digital Commons. It has been accepted for inclusion in Theses and Dissertations by an authorized administrator of UWM Digital Commons. For more information, please contact [open-access@uwm.edu](mailto:open-access@uwm.edu).

DESIGN AND OPTIMIZATION OF A MODULAR DC -DC POWER  
CONVERTER FOR MEDIUM VOLTAGE SHIPBOARD  
APPLICATIONS

by

Seyed Rasoul Hosseini

A Dissertation Submitted in  
Partial Fulfillment of the  
Requirements for the Degree of  
Doctor of Philosophy  
in Engineering

at

The University of Wisconsin-Milwaukee

December 2020

## ABSTRACT

### DESIGN AND OPTIMIZATION OF A MODULAR DC -DC POWER CONVERTER FOR MEDIUM VOLTAGE SHIPBOARD APPLICATIONS

by

Seyed Rasoul Hosseini

The University of Wisconsin-Milwaukee, 2020

Under the Supervision of Professor Robert Cuzner

Power electronic converters rated for medium voltage direct current (MVDC) are promising for electrification of future ships. In shipboard electrification, due to limitation of space, energy and technical maintenance, the high-power density, high efficiency and modularity of the power electronic converters are desired. Utilizing power modules made from wide band gap (WBG) semiconductors like silicon carbide (SiC) and high frequency power transformer (HFPT) can be beneficial for obtaining the high-power density, high efficiency and isolation that is required for the power electronic converters. To provide power for the low voltage (LV) DC loads, a conversion of the power from MVDC main bus to LVDC is needed. Therefore, a DC-DC converter is an essential component of a DC power system. DC-DC converter is a multipurpose element in Unit-based protection architecture (UBPA) which is an architecture that eliminates the need for DC circuit breaker (CB) and instead relies on isolated power electronic converters for protection of the system. Topologies based on Dual active bridge (DAB), Neutral point clamp (NPC) and Modular Multi-level Converter (MMC) are suggested for such a DC-DC converter rated for megawatt (MW) power level. Switching at MV level with high frequency in the ship environment is challenging because of the parasitic coupling that appears between the power module, MV side of the transformer and the ship haul which is made from the materials capable of conducting electricity. Moreover, the transformer used in the isolated DC-DC converter is one of the main contributors to the weight and power density of the converter. In this study, the DAB converter is suggested as a building block for an input series output parallel (ISOP) connected converter and analytical equations are provided for the design. A novel design for the HFPT is proposed and analytical formula is derived for the thermal loss and the leakage inductance of the HFPT. Optimization methodology using evolutionary algorithms method like genetic algorithm is applied to the design to extract the optimal values for a design. A case study is also provided in this study.

## TABLE OF CONTENTS

Section	Page
ABSTRACT	ii
TABLE OF CONTENT	iii
LIST OF FIGURES	v
LIST OF TABLES	vi
LIST OF ACRONYMS	vii
1 INTRODUCTION	1
1.1 MVDC architecture	4
1.2 Power Conversion Module	5
1.3 Modular PCM	6
1.4 Input series output parallel (ISOP)	6
1.5 PCM design flow	8
2 DUAL ACTIVE BRIDGE DC-DC CONVERTER	11
2.1 Operation of the DAB	12
2.2 Phase shift Modulation (PSM)	14
2.3 Soft switching	14
2.4 Power Module Loss Calculation	18
3 HIGH FREQUENCY POWER TRANSFORMER	24
3.1 HFPT design and geometrical parametrization	24
3.2 Design process of HFPT	27
3.3 Winding loss	31
3.4 Core loss	36
3.5 Isolation	37
3.6 Leakage inductance	40
3.7 Thermal Management of HFPT	50
3.8 A design case study	59
4 OPTIMIZATION OF HFPT	61
4.1 Genetic Algorithm	62
4.2 A design case study	63

4.2.1	Binary encoding	64
4.2.2	Population formation and selection	65
4.2.3	A design case study	65
4.2.4	Active cooling of the HFPT	66
5	CONCLUSION AND FUTURE WORK	70
	References	72
Appendix I	Computer code for Semiconductor module thermal calculation	77
Appendix II	Computer code for leakage inductance calculation	82
Appendix III	Computer code for design of HFPT	84
Appendix IV	Binary equivalent of one chromosome	100
Appendix V	The code for genetic algorithm optimization	101
	CURRICULUM VITAE	107

## LIST OF FIGURES

Figure		Page
Figure 1	Integrated Power Electronic system architecture of electric ship	4
Figure 2	Proposed DC-DC converter topology for PCM	8
Figure 3	Design methodology for the converter design and optimization	11
Figure 4	Operation modes of the DAB in one switching cycle	13
Figure 5	HB voltage and current of the DAB converter in time domain	15
Figure 6	HB voltage and current of the DAB converter in angular frequency domain	15
Figure 7	Thermal loss and $T_j$ of diode and transistor in MV and LV side modules	23
Figure 8	Core and heat sink structure of the HFPT	25
Figure 9	Front view of the HFPT	25
Figure 10	Side view of HFPT	26
Figure 11	Top view of the HFPT	26
Figure 12	Litz wire parameterization	27
Figure 13	Core building block for HFPT	27
Figure 14	Design flow of the HFPT	28
Figure 15	Foil winding parameterization	33
Figure 16	Thermal model of HFPT	52
Figure 17	Efficiency vs power density of transformer	60
Figure 18	Genetic algorithm for optimization	63

## LIST OF TABLES

Table		Page
Table 1	Conducting elements and the direction of power loss and loss mechanism in the time interval	14
Table 2	Parameters used for thermal calculations of SiC MOSFET	22
Table 3	List of the parameters of HFPT	28
Table 4	List of independent parameters for HFPT design	30
Table 5	Skin depth of Cu and Al versus switching frequency of converter	35
Table 6	Typical magnetic core materials used for HFPT	37
Table 7	Dielectric materials suitable for isolation layer	39
Table 8	Parameters considered for a leakage inductance case study	49
Table 9	Magnetic energy stored in elements of transformer	50
Table 10	Parameters used in thermal model of HFPT	51
Table 11	Heat transfer mechanism for different parts of the HFPT	53
Table 12	HFPT design requirements for a design case study	59
Table 13	Optimal values of the design variables for physics-based approach	60
Table 14	Design space for an HFPT case study design	64
Table 15	Calculated values for the considered $PT_{\xi\lambda}^{ij}$	65
Table 16	Optimal values of the design variables based on the genetic algorithm optimization approach	66
Table 17	Optimal values of the HFPT design variables with active cooling	69

## LIST OF ACRONYMS

MVDC	Medium voltage direct current
WBG	Wide band gap
SiC	Silicon Carbide
HFT	High frequency transformer
LV	Low voltage
LVDC	Low voltage direct current
LVDCCL	Low voltage direct current load
DAB	Dual active bridge
NPC	Neutral point clamp
MMC	Modular Multilevel converter
MO2	Multi-objective optimization
GA	Genetic algorithm
VPP	Virtual prototyping process
PEBB	Power electronic building block
LVPEBB	Low voltage power electronic building block
MVPEBB	Medium voltage power electronic building block
UBPA	Unit based protection architecture
MVPEBB	Medium voltage power electronic building block
CB	Circuit breaker
PS	Power system
HB	Half bridge



FB	Full bridge
MOSFET	Metal oxide semiconductor field effect transformer
PCM	Power conversion module
ISOP	Input series output parallel
IGBT	Insulated gate bipolar transistor
$P_{MLV}$	Power dissipation in LV side module
$P_{MMV}$	Power dissipation in MV side module
$P_{MMV_{cond}}$	Conduction loss in MV side module
$T_{JQMV}$	Junction temperature of the MOSFET in MV side module
$T_{JDMV}$	Junction temperature of the diode in MV side module
$T_{JDLV}$	Junction temperature of the diode in LV side module
$T_{JQLV}$	Junction temperature of the MOSFET in LV side module
PSM	Phase shift Modulation
ZVS	Zero voltage switching
$H_T$	Height of the transformer
$W_T$	Width of the transformer
$L_T$	Depth of the transformer
$w_c$	Width of the core
$h_c$	Height of the core
$l_c$	Depth of the core
$r_{ci}$	Inner radius of the core
$d_c$	Thickness of the core

$m_c$	Mass of the core
$V_c$	Volume of the core
$\rho_c$	Mass density of the core material
$w_p$	Width of the primary winding
$w_s$	Width of the secondary winding
$w_{iso}$	Width of the isolation layer
$r_{wip}$	Inner radius of the primary winding
$r_{wis}$	Inner radius of the secondary winding
$r_{wop}$	Outer radius of the primary winding
$r_{wos}$	Outer radius of the secondary winding
$d_{cww}$	Vertical distance between the core and winding
$w_{Litz}$	Width of the Litz wire bundle
$h_{Litz}$	Thickness of the Litz wire bundle
$d_{Litzbh}$	Horizontal distance between Litz bundles
$d_{Litzbv}$	Vertical distance between Litz bundles
$w_{Litzins}$	Thickness of the Litz wire insulation layer
$d_{st}$	Diameter of the copper strand
$T_{sf}$	Temperature of the surface
$P_{CM}$	Heat generated by the central core section
$P_{CO}$	Heat generated by the outer flat core section
$P_{CR}$	Heat generated by the side round core section
$R_{th,clf}$	Thermal resistance of the insulation layer between core and winding

$R_{th,pweq}$	thermal resistance OF the insulation layer and the middle point of windings
$R_{th,cram}$	Thermal resistance between round core part and the ambient
$R_{th,crcm}$	Thermal resistance of the vertical round side of the core and the central part
$T_{CO}$	Temperature of the outer core part
$T_{CM}$	Temperature of the central core part
$T_{CR}$	Temperature of the round core part
$T_{am}$	Ambient temperature
$T_{SWU}$	Temperature of the middle point of the secondary winding in upper half
$T_{PWU}$	Temperature of the middle point of the primary winding in upper half
$T_{SWL}$	Temperature of the middle point of the secondary winding in lower half
$T_{PWL}$	Temperature of the middle point of the primary winding in lower half
$n_g$	Number of genes
$n_{gb}$	Number of bits needed to represent a gene in binary format
$n_p$	Number of chromosomes in a population
$n_{chb}$	Number of bytes of memory needed to represent a chromosome
$N_{pb}$	Number of bytes of memory needed to store a population
$\vec{x}$	Transformer design vector
$PT_{\xi\lambda}^{ij}$	Power transformer chromosome tensor
$\hat{M}$	Mutation operator
$\hat{C}$	Cross-over operator

## ACKNOWLEDGEMENTS

I would like to thank the Office of Naval Research (ONR) for providing funding for this research project. This research was conducted under ONR grant N00014-16-1-3184 and was approved for public release.

I would like to thank Prof. Robert Cuzner who accepted me as a PhD student and provided technical support for me during the PhD program. Preparation of this document would not have been possible without the generous support of Prof. Cuzner.

I would like to thank Prof. Adel Nasiri, the director of the Center for Sustainable Electric Energy Systems (SEES) at the University of Wisconsin-Milwaukee. I learned a lot from the weekly Friday lunch and discussion sessions with topics about the state-of-the-art research in variety of subjects including power electronics converter design, microgrid control, energy management and industrial electronics.

I would like to thank my PhD committee members: Prof. Hossein Hosseini, Prof. David Yu, Prof. Chiu Law, and Prof. Ilya Avdeev who kindly accepted my invitation and provided me with constructive comments and questions.

I would like to thank the faculty members of electrical engineering department who I learned from during the PhD program.

I would like to thank the graduate students, post-doctoral researchers, visiting professors and engineers in the electrical engineering department and the SEES center for helpful discussions during the program.

I would like to thank Prof. Ethan Munson, the Associate Dean for Academic Affairs in Engineering school for providing help and support after the defense and during the graduation process.

I would like to thank all the UW-Milwaukee and University of Wisconsin system library staff for providing excellent service to me.

## 1- INTRODUCTION

The concept of electric ship propulsion was first introduced by the U.S. Navy in 1922 [1]. Steam and gas-powered plants using reciprocating engines have been the principal means for ship propulsion throughout the 19th and 20th centuries. For large ships, the steam pipe fitter played a crucial role in ship construction and operation. In the 20th century, with the advent of steam turbines and liquid natural gas internal combustion engines, combined with marine reduction gears, the construction and operation of ship propulsion systems shifted towards mechanical drive systems. Ships also require electrical power generation to support personnel and passengers and, increasingly, to support a host of hull mechanical and electrical loads throughout the ship, such as pumps, auxiliary loads that provide coolant to main mechanical systems, hoists and capstans.

The large-scale adoption of electric propulsion has been driven by global initiatives to reduce the greenhouse gasses produced by the commercial shipping industry, which, if conventional mechanical propulsion were to continue, would, by 2050, be responsible for a fifth of global CO<sub>2</sub> emissions [2]. The result would be a rise in air pollution to as high as 250% from container and cruise ships, oil tankers and cargo vessels alone [3, 4]. As of 2014, maritime shipping was reportedly responsible for 2 to 3 percent of global carbon dioxide emissions [5] and is predicted to increase to as high 17 percent by 2050 [6].

Compared to commercial ships, the electrification of naval shipboard systems overall has proceeded at a slow and measured rate. While the naval ship electrification is motivated by some of the same factors as commercial ships, i.e. the movement away from steam-based systems and the need for increased fuel economy and reduced environmental impact; the principal motivation for navy shipboard electrification is to ensure survivability of personnel and mission support systems. The design philosophy for naval power systems is expressed by the Naval Sea Systems Command (NAVSEA) Design Practices and Criteria Manual, Electrical Systems for Surface Ships, Chapter 300 as follows: "The primary aim of the electric power system design will be for survivability and continuity of the electrical power supply. To ensure continuity of service, consideration shall be given to the number, size and location of generators, switchboards, and to the type of electrical distribution systems to be installed and the suitability for segregating or isolating damaged sections of the system."

DC electrical distribution on navy ships became a serious consideration for new ship designs in the 1990s. This shift in the way ship electrical systems were designed and implemented came about because of a significant growth in the ratio of shipboard electronic loads (i.e. instrumentation, communications, mission loads, etc.) to purely fixed frequency electrical loads (i.e. heaters, pumps, fan coil units, etc.). The Navy is currently facing an unprecedented challenge to develop new ship designs under compressed schedules that incorporate emerging technologies for high power energy conversion in order to enable smaller ship designs with a high degree of electrification and survivability enabled by high power, high density power electronic conversion [6, 7].

Medium voltage direct current (MVDC) technology is considered for electric systems with direct current and the voltage level above 1500 V and less than 52 kV [8]. MVDC power distribution system is an emerging technology suitable for applications with power requirement in the range of multi megawatt [9]. This technology relies on utilization of power electronic converters. Designing power electronic converters rated for MV level has attracted attention among the researchers active in the field of power electronic [10].

DC systems are accepted technology for low voltage applications, and they are widely used because of simple structure and high reliability. High power conversion efficiency and fault management are the two main challenges for the MVDC power systems. Using DC circuit breaker has been common for interrupting the fault current in DC system. However, for applications like shipboard electrification when there is a limitation of space for power converters, utilizing DC circuit breakers can decrease the whole system power density. Unit based protection architecture (UBPA) [11] on the other hand relies on power electronic converters for fault management. Such an architecture can be beneficial in terms of increasing the power density of the whole system by reducing the space allocated for circuit breakers (CBs). If such an architecture can be implemented, eliminating the CBs can reduce the cost of MVDC power system (PS).

The unit-based architecture provides control over the flow of electric power since all the electric power flows through power electronic converters. If such a scenario is pursued, isolated power electronic converter topologies are necessary to use for increasing the reliability of the system. The electric isolation can take place by using transformers. Thus, development of efficient high frequency transformers is essential for having reliable unit based MVDC power system. The

design and development of high frequency power transformers is an enabler for isolated DC-DC converters [12-16]. Topologies that are based on dual active bridge (DAB) and enable soft switching techniques at high switching frequency are promising for implementation of the unit based MVDC power system. Topologies based on Modular Multi-level Converter (MMC) are also attractive for such application. For the case of MMC, gaining soft switching is challenging which decreases the converter efficiency. Also, the device conduction loss is high contributing to low efficiency and low reliability of the semiconductor modules. Moreover, MMC is less modular compared to DAB based topologies because of the inductor. Furthermore, gaining high switching frequency is more difficult compared to DAB based topologies. Because of these reasons, in this study only topologies based on DAB are considered.

For modular DAB based converters, there is an option of using half-bridge (HB) for full bridge (FB) to create the ac waveform. Using HB submodules increase the efficiency of the system as well as the power density of the converter. However, for the case of UBPA, the fault handling capability of the DAB will be essential to system reliability and recoverability. Thus, in this study, only FB based DAB topology is considered. There is an option of combining variations of DAB, MMC and Neutral Point Clamp (NPC) based topologies and come with creative topologies, but that is considered for future work. For shipboard electrification application, the power conversion module (PCM) is very important element of the MVDC system specially for the unit-based approach. Therefore, this study is focused on PCM design options considering the available semiconductor modules.

SiC based Metal oxide semiconductor field effect transformer (MOSFET) is considered as a semiconductor module because of the capability for obtaining high switching frequency which is essential for gaining high power density of the PCM. Considering the isolation requirements for MVDC power system and the modularity aspect of the converter, the design challenges of input series output parallel (ISOP) configuration of multiple DAB converters is investigated in this study and recommendations are provided for obtaining feasible solution for PCM converter.

### 1.1 MVDC Architecture

Future shipboard systems must fully integrate propulsion and electric weaponry with all other electrical load demands in the ship to enable future Naval ship demands [17-22]. In this way the full capabilities based on Integrated Power System (IPS) Direct Current (DC) Zonal Electrical Distribution System (DCZEDS) can be achieved to Medium Voltage (MV) and multi-Mega Watt (MW) feed levels. An Integrated Power and Energy System (IPES), shown in Fig. 1, is the way forward for these future electrified ships. The MVDC-based IPES will most effectively enable the delivery of power and energy to any part of the ship and optimization of use and placement of ESS's throughout the system. The MVDC-based IPES enables dynamic, bi-directional power and energy transfer between distributed generation and energy storage and all shipboard electrical loads.

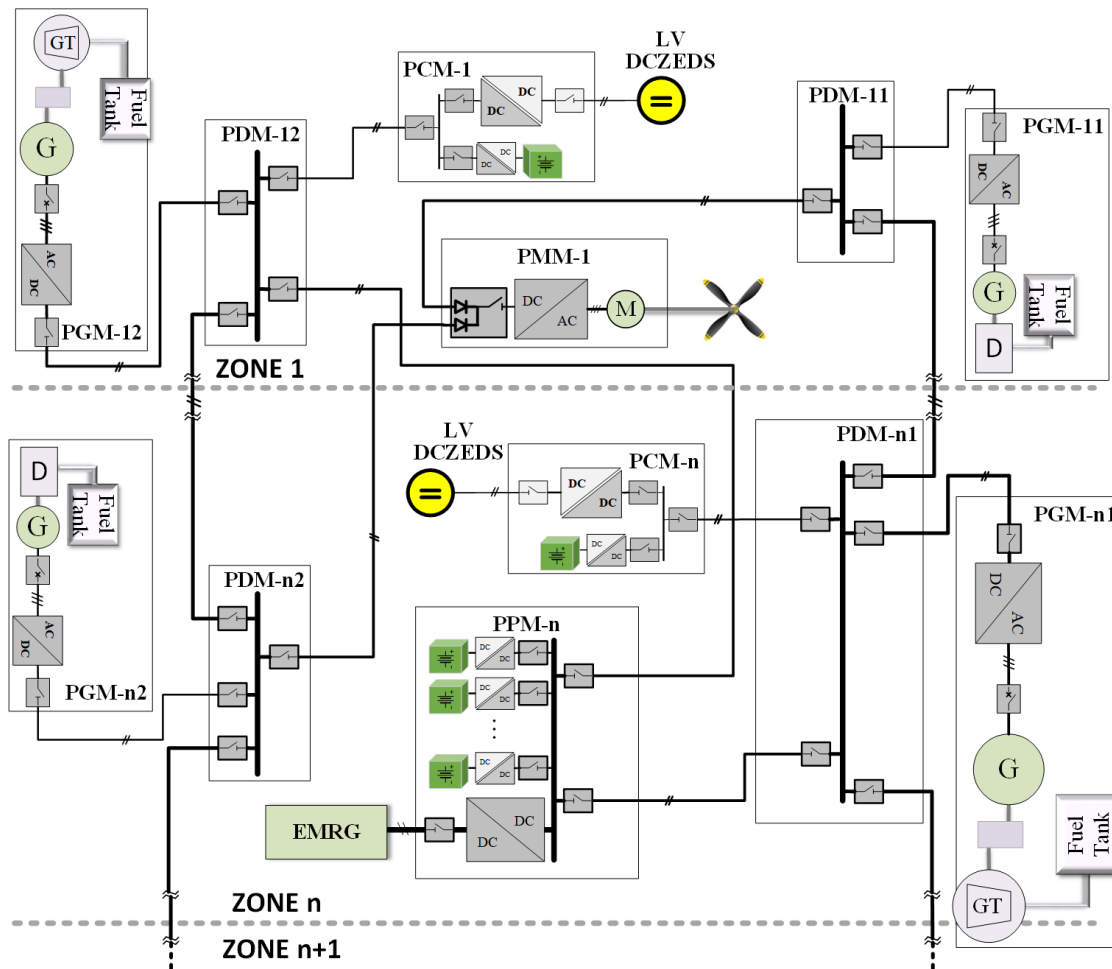


Fig. 1 Integrated Power Electronic system architecture of electric ship



Protection of the MVDC system for shipboard application is challenging and ground faults are very common in shipboard power system. Determination of the MVDC bus voltage level is also a challenge that system architects are facing. Using higher voltages will decrease the transmission loss but at the same time it makes the development of power converters more complex. Recent studies have shown that if the optimum value of the bus voltage should be a multiplication of 6kV. Various topologies may be possible for the MVDC power system. There are different types of converters necessary for the MVDC system such as Power Generation Module (PGM), Power Conversion Module (PCM) and Power distribution Module (PDM). In this study, design and optimization of PCM is considered.

## 1.2 Power conversion module

Power conversion module (PCM) is primarily a DC-DC converter that provides electrical energy for the Low Voltage Direct Current (LVDC) loads by conversion from the MVDC bus. To suggest a topology that is modular and power dense and capable of providing the isolation between the MV and LV sides, DAB topology with ISOP configuration is considered in this work. Recent advances in fabrication and packaging of wide band gap (WBG) semiconductor modules rated for MV applications will allow utilization of high switching frequency in the DC-DC converter. On the other hand, the idea of using power electronic building block (PEBB) that could be used for many kinds of converters. An ideal PEBB is power dense, efficient, reliable, robust and resilient. Additionally, the modular design using PEBB is affordable if economy of scale is considered.

Using appropriate connection of PEBBs, development of power electronic converters for high voltage and high power is possible. Therefore, in this study only the Silicon Carbide (SiC) MOSFET is considered for the design. Design of the High Frequency Power Transformer (HFPT) remains an important part of the PCM design considering the high-power rating of the system and it will be discussed separately in Chapter 3.

Multi-objective optimization approach is implemented for the design of HFPT in [16]. However, for the converter level, there are other parameters that need to be considered like the standoff distance between the converter modules and the chassis. Switching at high frequencies with high current and at MV level, arises compatibility concerns. Electromagnetic compatibility (EMC) is necessary for PCM converter. In order to provide the isolation required in ship environment, the HFPT must have an isolation layer and the design should be carried out in a way to minimize the

parasitic capacitive coupling between the primary and the secondary of the HFPT. These concerns are considered and discussed with more details in chapter 3.

### 1.3 Modular PCM

LVPEBB and MVPEBB as considered as the available building blocks for construction of the PCM. There are three topologies that are considered for PCM. Topology (1) is called PCM61 utilizes SiC based MVPEBB on the MV side of the PCM and SiC based LVPEBB on the LV side of the PCM. Topology (2) is called PCM11, and in this topology only LVPEBB is used for the DC-DC conversion. Topology (3) is called PCM61G and in this topology there is an SiC based MVPEBB on the MV side and one Insulated gate bipolar transistor (IGBT) based LVPEBB (LVPEBBG) on the LV side. This is due to capability of IGBTs in handling high currents. The operating frequency of topology (3) is lower than the topologies (1) and (2) due to using the IGBT. The HFT in topology (3) is called HFT61G. In PCM61, assuming the availability and right functionality of MVPEBB, design of the HFT is the main challenge.

HFT designed for PCM61 is called HFT61. The HFT61 is multi-winding HFT. MVPEBB is connected to the primary side of the HFT61 and four LVPEBBs are connected to secondary windings of the HFT61. Design and optimization of HFT61 is left as a future work. Design and optimization of HFT11 is discussed in chapter 3. In this study, only the PCM11 is considered and studying other possible converters are left as future work. The rating power of HFT11 is lower than the HFT61, therefore more practical currently. Using only LVPEBB has another benefit that is high degree of modularity. With this design approach, there will only be two kinds of building blocks, one LVPEBB and another HFT.

### 1.4 Input Series Output Parallel (ISOP)

Voltage conversion from MVDC to LVDC using modular design would need series connection of the DC-DC modules on the input side and parallel connection of them on the output side. Fig. 2 shows the schematics of this topology. Using this configuration, low voltage switches can be used for higher voltage applications. Therefore, a more practical choice if economy of scale is considered. To increase the stability of the converter and increasing the lifetime of the modules, equal power sharing control strategy is applied to the DC-DC converter.

The reliability of ISOP configuration during the fault on the series side of the ISOP should be subject of research. For example, if one power module is sending an over temperature fault which is a result of a malfunction of a fan in one of the DAB converters, the master controller in the cabinet will send a shut-down command to the faulted module. Therefore, the DC-DC converter shuts down.

One way to improve the reliability of the ISOP DC-DC converter can be adding two or multiple legs of series modules. This topology can be called Parallel Input Series Output Parallel (PISOP) which will have higher number of modules but higher reliability. Another approach to increase the reliability of the converter is by including the parallel leg inside the PEBB. But this method won't help for the over temperature fault because the added leg will also experience the over temperature fault.

One idea is to connect the input and output of the DAB layers in a matrix format. In this configuration, the input and output of the DAB converters are connected in series and parallel with a switch. Therefore, the same converter can be used as ISOP or parallel input series output (PISO) for conversion from LV to MV level. The same converter can also be used as input series output series (ISOS) or input parallel output parallel (IPOP) in MV and LV networks as a buffer converter. Adding such a capability will turn the modular and isolated DC-DC converter a universal converter that can be configured to either of the four configurations by a command from the controller.

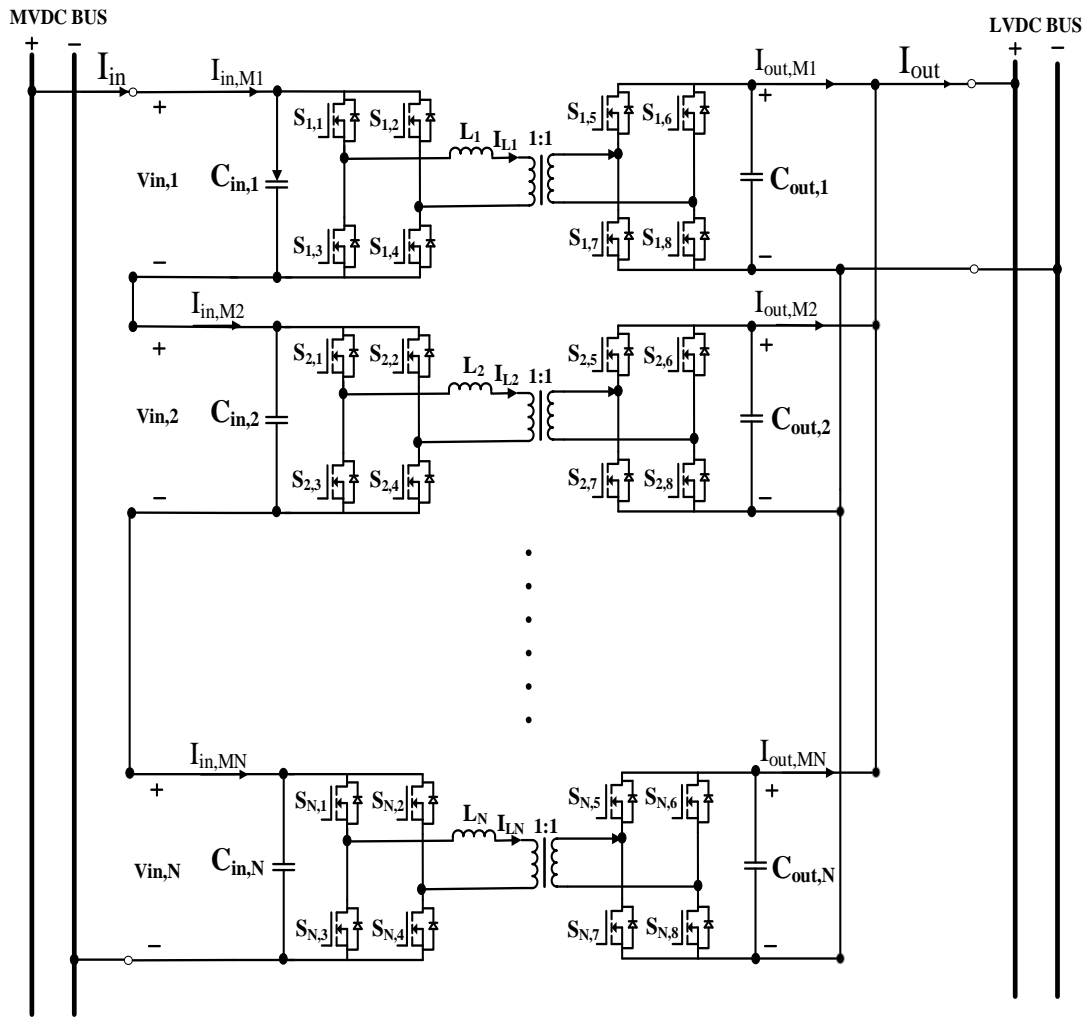


Fig. 2 Proposed DC-DC converter topology for PCM

### 1.5 PCM design flow

The design flow of the PCM converter considering the ISOP topology of multiple DAB levels are depicted in Fig. 3. The design parameters are determined by the system architects. For example the MV bus voltage ( $V_{MV}$ ), the LV bus voltage ( $V_{LV}$ ), the required isolation voltage which will be used in the design of the HFT ( $V_{iso}$ ), rated power of the PCM ( $P_{rt}$ ) and the temperature of the coolant that will be use in liquid cooled PEBBs for cooling the SiC MOSFETs ( $T_C$ ). These values could be considered as a vector and the design algorithm will consider all the possible combinations of these values and a multi-objective optimization routine to find the most power dense and yet feasible design.

The suggested approach could be used for designing other converters in the MVDC system. The next step is to determine the number of DAB layers (N) in the PCM converter. For determining the value of N, a few criteria should be considered, one is that the input series of N DAB layer is to step up the MV side converter voltage to the value of MV bus. Another aspect is the rated power or the needed output current that the LV side of the PCM should provide for the load using parallel configuration of the N DAB converters. The proposed design algorithm which is shown in Fig. 3 calculates these two values and then chooses the bigger number to use as N. Once the number of DAB layers is determined, to gain the maximum reliability and lifetime of each DAB layer, equal distribution of power between the N DAB layers is considered initially. In other words, each DAB layer should provide equal power to the LV load and that is  $P_{out}/N$ .

The rated current of the DAB layer can be calculated and if this value is larger than the rated current of the semiconductor module used in the DAB or the PEBB semiconductor module, another DAB layer will be added. This process will continue until the DAB current rating is lower than the rated current of the semiconductor module used in the DAB. Next step is determining the optimal switching frequency of the DAB layers ( $f_{sw-opt}$ ). Theoretically speaking, by increasing the switching frequency, the size of the transformer of the DAB will decrease leading to higher power density of the PCM. However, increasing the switching frequency will increase the switching loss of the converter. Although Zero voltage switching (ZVS) can be implemented for turn on event in a properly designed DAB converter, the turn off event is hard switched. Thus, increasing the switching frequency has direct impact on increasing the turn off loss of the DAB and PCM. It is possible to dissipate the loss with applying appropriate thermal management but for specific coolant temperature, there is maximum switching frequency that keeps the junction temperature of the SiC MOSFET module under the  $T_{jmax}$  which is determined by the manufacturer of the device. This maximum switching frequency is considered as the  $f_{sw-opt}$ . The next step is determining the leakage inductance of the HFT. To obtain the leakage value, we need to use the power flow equation of the DAB converter in Eq. (1).

$$P = \frac{V_1 V_2 n \phi (\pi - \phi)}{2\pi^2 f_{sw} L} \quad (1)$$

where  $V_1$  is the DC voltage of the primary side,  $V_2$  is the DC voltage of the secondary side,  $f_{sw}$  is the switching frequency,  $L$  is the leakage inductance of the transformer,  $\phi$  is the phase shift between the rectifier and inverter gate signals,  $n$  is the ratio of the secondary turns over the primary

turns of the transformer. Using Eq. (1) and considering  $P = P_{out}/N$ ,  $V_1 = V_{MV}/N$ ,  $V_2 = V_{LV}$ ,  $n=1$  and the modulation phase shift  $\varphi = \pi/2$  will determine the leakage inductance of the HFT.

$$L = \frac{V_{MV}V_{LV}n}{8f_{sw}P_{out}} \quad (2)$$

Next step is designing the HFT. The HFT design will be discussed in details in chapter 3.

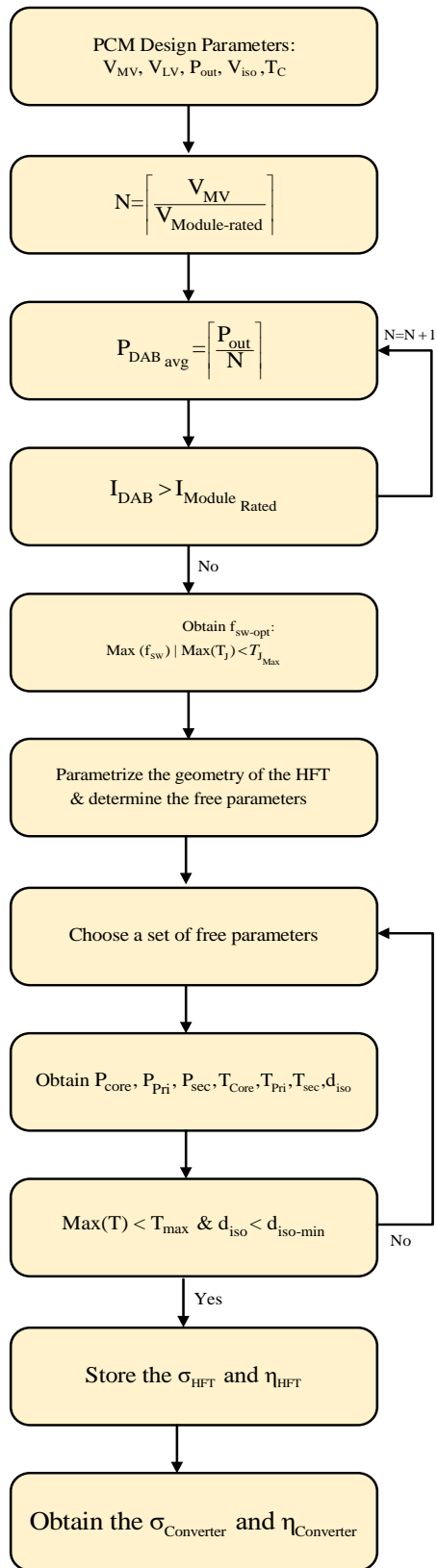


Fig. 3 Design methodology for the converter design and optimization

## 2- DUAL ACTIVE BRIDGE DC-DC CONVERTER

Dual active bridge converter topology was introduced in 1991 [23]. Since its invention, the topology has found application in renewable energy storage [24], uninterruptable power supply (UPS) systems [25], aerospace [26] and shipboard applications [27]. This topology has interesting and important features like bi-directional power flow capability, galvanic isolation between input and output of the converter and high efficiency. The bi-directional power flow capability of this topology makes it a suitable choice for applications that utilize energy storage. Additionally, the symmetrical structure of this topology makes it an ideal choice for modular applications. Therefore, this topology can be used as a building block for getting to higher voltage and higher power applications. Input series output parallel (ISOP) configuration is considered in this work for getting to medium voltage level and high operating power. In this chapter, a review of the operation of dual active bridge topology is provided. The high frequency transformer for this topology can be either single phase or three phase. In this work, only single phase HFT is considered. Utilizing SiC MOSFET switches and applying high switching frequency requires small leakage inductance of the high frequency transformer which makes the design of the transformer more challenging. On the other hand, small inductance eliminates the need for additional inductor which leads to using lower number of components and higher power density of the system.

### 2.1 Operation of the DAB

Fig. 4 shows the operation modes of the dual active bridge DC-DC converter. There are six different modes of operation in one switching frequency. Table 1 explains the conducting elements in each operating mode in the converter. The power flowing from input to the output of the converter depends on the input voltage ( $V_1$ ), output voltage ( $V_2$ ), switching frequency ( $f_{sw}$ ), leakage inductance of the transformer ( $L$ ), turns ratio of the transformer ( $n$ ) and finally the modulation scheme. Eq. 1 indicates the power flow of the DAB converter:



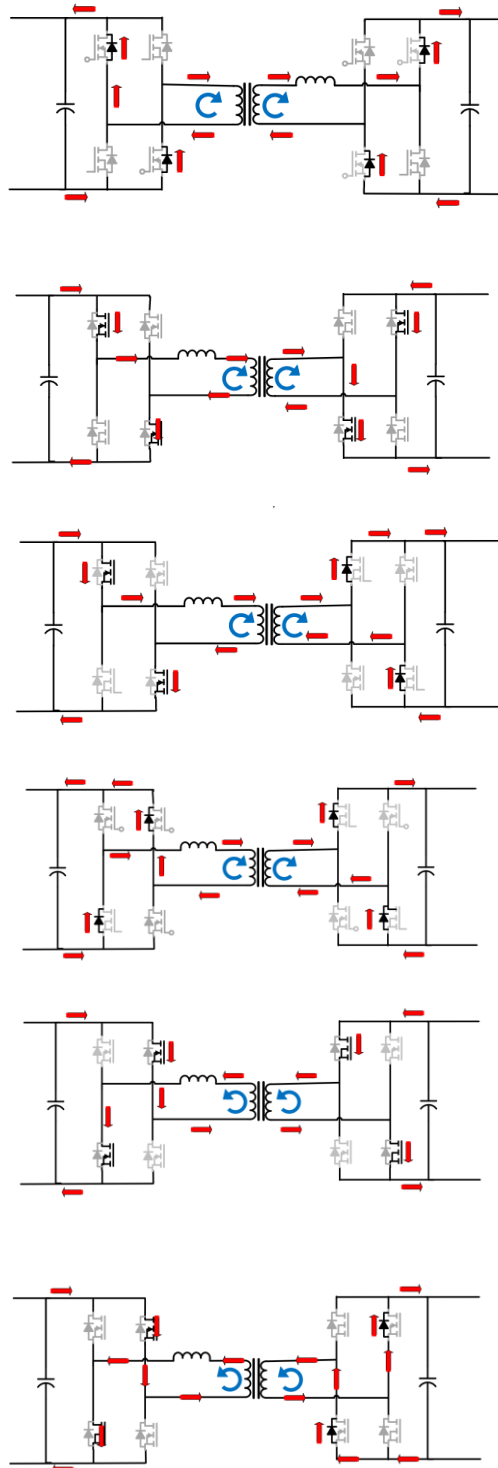


Fig. 4 Operation modes of the DAB in one switching cycle

Table 1 Conducting elements and the direction of power loss and loss mechanism in the time interval

	Conducting in primary	Conducting in secondary	Power flow	Loss
$[0, t_1]$	Diode	Diode	Outward	ZVS
$[t_1, t_\phi]$	MOSFET	MOSFET	Inward	conduction
$[t_\phi, \frac{T_s}{2}]$	MOSFET	Diode	Primary to secondary	Turn off loss
$[\frac{T_s}{2}, \frac{T_s}{2} + t_1]$	Diode	Diode	Outward	ZVS
$[\frac{T_s}{2} + t_1, \frac{T_s}{2} + t_\phi]$	MOSFET	MOSFET	Inward	Condition
$[\frac{T_s}{2} + t_\phi, T_s]$	MOSFET	Diode	Primary to secondary	Turn off loss

## 2.2 Phase shift Modulation (PSM)

Phase shift modulation (PSM) is used to transmit power between the two H-bridges through the high frequency transformer. The term phase shift refers to a time delay between switching functions applied to the input side H-bridges compared to the output side. The value of the time delay or phase shift determines the transmission of electric power in this topology. There are multiple forms phase shifting modulation reported in the literature.

Single phase shift (SPS), extended phase shift (EPS), dual phase shift (DPS), and triple phase shift (TPS) are suggested by the researchers. In this work, the SPS modulation technique is considered. In SPS modulation, the duty cycle of all switches is fixed and equal to 50%. The primary and secondary side voltages of the transformer are square wave. The phase shift between the input side H-bridge and the output side H-bridge ( $\phi$ ) controls the amount of power flow from primary to secondary or vice versa. The phase shift  $\phi$ , can take values between zero to  $\frac{\pi}{2}$  for power flow from primary to secondary and zero to  $-\frac{\pi}{2}$  for power flow from secondary to primary.

Fig. 5 shows the typical voltage and current waveforms of a dual active bridge circuit. The symmetrical behavior of the inductor current is visible in this figure. During  $[0, t_1]$  the diode is conducting on the both sides and the ZVS takes place in this period. At  $t_1$  the natural commutation takes place between diode and MOSFET.  $t_\phi$  is the time when the natural commutation happens

on the secondary side. And during  $[t_\phi, \frac{T_s}{2}]$ , the power flow is from primary to secondary and the MOSFET is conducting on the primary side as an inverter and diodes are conducting on the secondary side as a rectifier. At time  $\frac{T_s}{2}$ , the hard turn off takes place and the cycle repeats on another leg of the H-bridge.

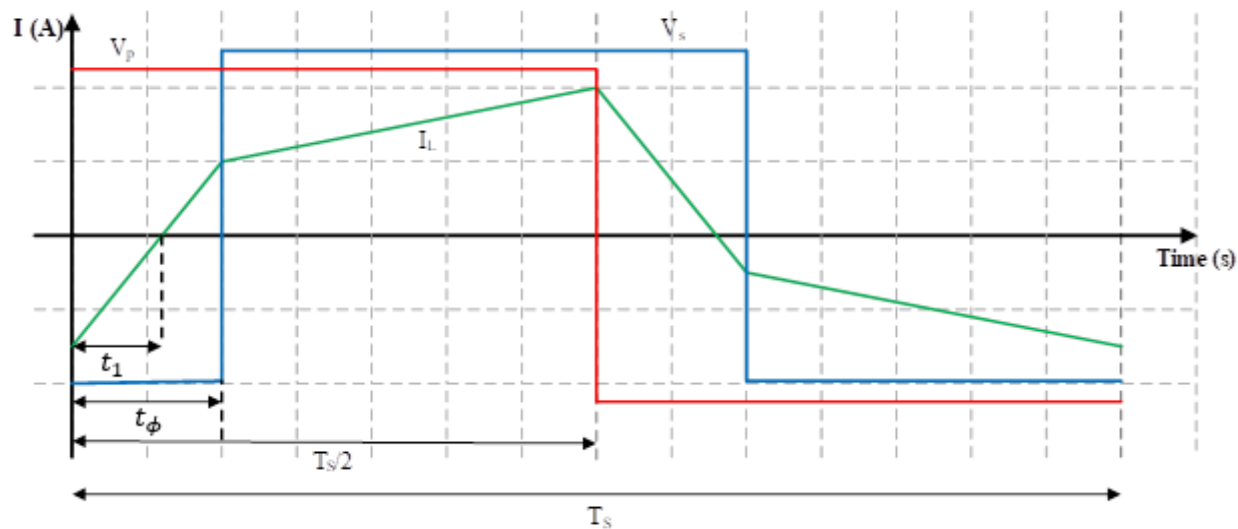


Fig. 5 HB voltage and current waveforms of the DAB converter in time domain

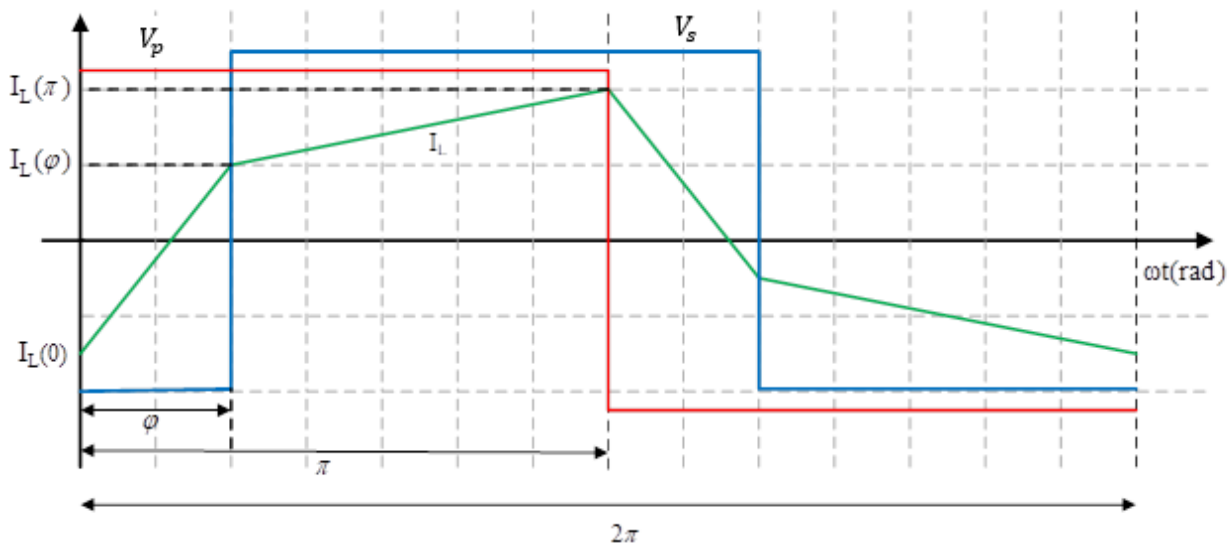


Fig. 6 HB voltage and current of the DAB converter in angular frequency domain

### 2.3 Soft switching

In the following we will derive the requirements for obtaining soft switching using phase shift modulation technique [13]. For all equations the equal turns ratio for transformer is assumed.

Mode 1:  $0 < \theta < \phi$ ,  $V_p(\theta) = V_i$ ,  $V_s(\theta) = -V_o$  where  $V_p(\theta)$  and  $V_s(\theta)$  are the primary and secondary voltages of the transformer respectively. In this mode the anti-parallel diode is conducting on the primary bridge and provides the ZVS condition for the switch to turn on. The current in this mode can be written as:

$$i_L(\theta) = \frac{V_i + V_o}{\omega L}(\theta) + i_L(0) \quad (3)$$

After this mode the current will flow through the switch and therefore the following equation will hold: Mode 2:  $\phi < \theta < \pi$ ,  $V_p(\theta) = V_i$ ,  $V_s(\theta) = +V_o$

$$i_L(\theta) = \frac{V_i - V_o}{\omega L}(\theta - \phi) + i_L(\phi) \quad (4)$$

Symmetry condition requires that  $i_L(\pi) = -i_L(0)$ , and  $d = \frac{V_o}{V_i}$  thus using  $i_L(\theta) = \frac{V_i(1+d)}{\omega L}(\theta) + i_L(0)$ , we can write:

$$i_L(\phi) = \frac{V_i(1+d)}{\omega L}(\phi) + i_L(0) \quad (5)$$

Similarly using the equation of the second mode of operation we can write:

$$i_L(\pi) = \frac{V_i - V_o}{\omega L}(\pi - \phi) + i_L(\phi) \quad (6)$$

Using Eq. (3-6) we can obtain:

$$i_L(\pi) = \frac{V_i(1-d)}{\omega L}(\pi - \phi) + \frac{V_i(1+d)}{\omega L}(\phi) + i_L(0) \quad (7)$$

Simplifying Eq. (7) we can write:

$$i_L(\pi) - i_L(0) = \frac{V_i(1-d)}{\omega L}(\pi - \phi) + \frac{V_i(1+d)}{\omega L}(\phi) \quad (8)$$

Now using the symmetry in the waveform, we can replace  $i_L(0)$  by  $i_L(\pi)$  and after some simple mathematics we will have:

$$i_L(\pi) = \frac{V_i}{\omega L} \left( \frac{(1-d)\pi}{2} + d\phi \right) \quad (9)$$

And for the  $i_L(0)$  we will get the Eq. (10)

$$i_L(0) = \frac{-V_i}{\omega L} \left( \frac{(1-d)\pi}{2} + d\phi \right) \quad (10)$$

Using Eq. (3) and replacing the Eq. (8) we can write

$$i_L(\phi) = \frac{V_i(1+d)}{\omega L}(\phi) + \frac{-V_i}{\omega L} \left( \frac{(1-d)\pi}{2} + d\phi \right) \quad (11)$$

Further simplifying the equation (11) will result into the following equation for  $i_L(\phi)$

$$i_L(\phi) = \frac{V_i}{\omega L} \left( \phi + \frac{\pi}{2}(-1+d) \right) \quad (12)$$

Soft-switching constraints will require that at  $t = 0$  the anti-parallel diode is conducting on the MV side bridge and at  $t = \phi$  diode is conducting on the LV side bridge, considering the direction of the current, soft switching conditions require  $i_L(0) \leq 0$  &  $i_L(\phi) \geq 0$  &  $d \geq 0$  using equation (8) and after doing some math we can find a condition for soft switching based on the voltages of the two sides of the DAB converter:

$$d < \frac{1}{(1-\frac{2\phi}{\pi})} \quad (0 \leq \phi < \frac{\pi}{2}) \quad (13)$$

For the second mode of operation where  $\phi < \theta < \pi$ , or  $t_\varphi < t < \frac{T_s}{2}$ , the current flowing through the converter can be written as Eq. (14)

$$i_L(\theta) = \frac{V_i - V_o}{\omega L}(\theta - \varphi) - \frac{V_i}{\omega L} \left( -\phi + \frac{\pi}{2}(1-d) \right) \quad (14)$$

Equations (3-14) shows that the inductor current is a function of input voltage, output voltage, the phase shift, leakage inductance of the transformer and switching frequency.

$$\begin{cases} i_L(\theta) = \frac{V_i + V_o}{\omega L}(\theta) - \frac{V_i}{\omega L} \left( \frac{(1-d)\pi}{2} + d\pi \right) & \theta \in [0, \varphi] \\ i_L(\theta) = \frac{V_i - V_o}{\omega L}(\theta - \varphi) - \frac{V_i}{\omega L} \left( -\varphi + \frac{\pi}{2}(1-d) \right) & \theta \in [\varphi, \pi] \end{cases} \quad (15)$$

## 2.4 Power module loss calculation

The exact amount of switching loss can be measured using double pulse test method. Such a test is usually done by the manufacturer and the results are provided as curves in the datasheet. To analytically calculate the switching loss using the datasheet values, interpolation might be necessary to extract the right amount of switching loss at the operating point of the converter and at the rated switch temperature. Switching loss can take place both at turn on and turn off. In dual active bridge topology, zero voltage switching (ZVS) can take place in turn on by allowing the current to flow through the parallel diode in the semiconductor module at the time of the turn on. In dual active bridge topology, the turn off event is hard switching and the loss needs to be calculated analytically.

Analytical calculation of the power loss in semiconductor switches is necessary for choosing the optimal switching frequency ( $f_{sw-opt}$ ). At the operating switching frequency ( $f_{sw}$ ), the junction temperature of the semiconductor elements must remain below the  $T_{j-max}$  which is also provided in the data sheet. Therefore, analytical loss calculation is a necessary step that needs to take place in designing any power electronic converter. To calculate the losses the current waveform needs to be known. In the case of dual active bridge topology with phase shift modulation, the operation of the converter can be divided into six different states within one switching cycle.

Summation of the power loss in these six states would result to the total power loss in one switching cycle. The equations for such calculation is provided in appendix I. A computer code is developed to calculate the power loss of the semiconductor module and to monitor the junction temperature of the semiconductors both on the rectifier side and the inverter side of the DAB converter. Fig. 7 shows the calculated power loss and the junction temperature of the MOSFETs and diodes in the DAB based on the datasheet values for CAS300M17BM2 module.

Effective thermal management of the module requires accurate estimation of the generated heat in the module because of conduction loss and switching loss. The temperature of the semiconductor junction in diode and MOSFET cannot go beyond a set limit by the manufacturer. Each module contains two MOSFET and two Diodes in half bridge configuration. TJQ1U is the junction temperature of the upper switch in module 1 and TJDMV shows the junction temperature of the diode in the inverter side. The resistance of diode and switch during conduction is provided by manufacturer data sheet. To calculate the power loss, it is needed to know the time interval that

the diode or the switch in conducting in the converter topology. In this study, the dual active bridge topology is considered. To calculate the junction temperatures, the operation of the converter is divided into 6 different states and it is determined which component is conducting during the specified state. Then the generated heat can be calculated with average value of  $Q_{loss}/T_s$  where  $T_s$  is the switching period. Eq. 16 shows the average total loss of the SiC module on the MV side during one switching cycle.

$$P_{MMV} = \frac{1}{T_s} \left[ \int_0^{t_1} (v_{FD1} + R_{FD1} i_{D1}(t)) i_{D1}(t) dt + \int_{t_1}^{t_\phi} r_{Q1} i_{Q1}(t)^2 dt + \int_{t_\phi}^{T_s/2} r_{Q1} i_{Q1}(t)^2 dt + \int_{T_s/2}^{T_s/2+t_1} (v_{FD1} + R_{FD1} i_{D1}(t)) i_{D1}(t) dt + \int_{T_s/2+t_1}^{T_s/2+t_\phi} r_{Q1} i_{Q1}(t)^2 dt + \int_{T_s/2+t_\phi}^{T_s} r_{Q1} i_{Q1}(t)^2 dt + 2(E_{turn\ on\ (ZVS)} + E_{turn\ off}) \right] \quad (16)$$

where  $P_{MMV}$  is the average total power loss on the SiC module on the MV during one switching cycle,  $t_1$  and  $t_\phi$  are the duration of time that components of the circuit conduct based on Table 1, Fig. 5 and Fig. 6,  $v_{FD1}$  forward voltage drop of the diode on the MV side,  $R_{FD1}$  is the forward resistance of the diode on the MV side,  $i_{D1}(t)$  is the electric current passing through the diode on MV side at time t,  $E_{turn\ on}$  is the turn on energy of MOSFET,  $r_{Q1}$  is the forward resistance of the MOSFET on the MV side,  $i_{Q1}(t)$  is the electric current passing through the MOSFET on the MV side at time t,  $E_{turn\ on}$  is the turn on loss of the MOSFET which can be minimized using Zero Voltage Switching technique and  $E_{turn\ off}$  is the turn off loss of the MOSFET. Eq. 17 indicates the total loss of the SiC module on the LV side during one switching cycle.

$$P_{MLV} = \frac{1}{T_s} \left[ \int_0^{t_1} (v_{FD2} + R_{FD2} i_{D2}(t)) i_{D2}(t) dt + \int_{t_1}^{t_\phi} r_{Q2} i_{Q2}(t)^2 dt + \int_{t_\phi}^{T_s/2} r_{D2} i_{D2}(t)^2 dt + \int_{T_s/2}^{T_s/2+t_1} (v_{FD2} + R_{FD2} i_{D2}(t)) i_{D2}(t) dt + \int_{T_s/2+t_1}^{T_s/2+t_\phi} r_{Q2} i_{Q2}(t)^2 dt + \int_{T_s/2+t_\phi}^{T_s} r_{D2} i_{D2}(t)^2 dt + 2(E_{turn\ on\ (ZVS)} + E_{turn\ off}) \right] \quad (17)$$

where  $P_{MLV}$  is the total power loss of the SiC module on the MV during one switching cycle,  $t_1$  and  $t_\phi$  are the duration of time that components of the circuit conduct based on Table 1, Fig. 5 and Fig. 6,  $v_{FD2}$  is the forward voltage drop of the diode on the LV side,  $R_{FD2}$  is the forward resistance of the diode on the LV side,  $i_{D2}(t)$  is the electric current passing through the diode on MV side at time t,  $E_{turn\ on}$  is the turn on energy of MOSFET,  $r_{Q2}$  is the forward resistance of the MOSFET on the LV side,  $i_{Q2}(t)$  is the electric current passing through the MOSFET on the MV side at time t and  $E_{turn\ off}$ , is the turn off loss of the MOSFET.

The conduction loss of the MV side module can be calculated using Eq. (18) by direct plug in of the inductor current formula to the module loss formula extracted based on the current circulation of the DAB. After integration, we can write:

$$\begin{aligned}
P_{MMVcond} = & \frac{1}{2\pi} \left\{ v_{FD1} \frac{V_i+V_o}{\omega^2 L} \frac{\theta_1^2}{2\omega^2} - v_{FD1} \frac{V_i}{\omega L} \left( \frac{(1-d)\pi}{2} + d\phi \right) \frac{\theta_1}{\omega} + R_{FD1} \frac{V_i^2 + V_o^2 + 2V_i V_o}{\omega^4 L^2} \frac{\theta_1^3}{3\omega^3} + \right. \\
& R_{FD1} \left\{ \left( \frac{V_i}{\omega L} \right)^2 \left[ \left( \frac{(1-d)\pi}{2} \right)^2 + (d\phi)^2 + (1-d)\pi d\phi \right] \right\} \frac{\theta_1^2}{2\omega^2} - R_{FD1} \frac{V_i(V_i+V_o)}{\omega^3 L^2} [(1-d)\pi + 2d\phi] \frac{\theta_1}{\omega} \\
& + r_{Q1} \left\{ \frac{V_i^2 + V_o^2 + 2V_i V_o}{\omega^4 L^2} \left( \frac{\phi^3 - \theta_1^3}{3\omega^3} \right) + \left( \frac{V_i}{\omega L} \right)^2 \left[ \left( \frac{(1-d)\pi}{2} \right)^2 + (d\phi)^2 + (1-d)\pi d\phi \right] \frac{\phi - \theta_1}{\omega} + \right. \\
& \left. \frac{V_i(V_i+V_o)}{\omega^3 L^2} [(1-d)\pi + 2d\phi] \right\} \left( \frac{\phi^2 - \theta_1^2}{2\omega^2} \right) + r_{Q1} \left\{ \frac{V_i^2 + V_o^2 - 2V_i V_o}{\omega^4 L^2} \left( \frac{\pi^3 - \phi^3}{3\omega^3} \right) + 2V_i \left( \frac{V_i - V_o}{\omega^3 L^2} \right) (d\phi - \frac{\pi}{2} (1-d)) \frac{\pi^2 - \phi^2}{2\omega^2} \right. \\
& \left. \left. + \frac{V_i^2}{\omega^2 L^2} (d\phi - \frac{\pi}{2} (1-d))^2 \frac{\pi - \phi}{\omega} \right\} \right. \quad (18)
\end{aligned}$$

where according to Fig. 6, one switching cycle is converted to  $2\pi$  and  $\theta_1$  and  $\phi$  are the equivalent values of  $t_1$  and  $t_\phi$  in polar coordinate system where  $\theta_1 = \frac{2\pi t_1}{T_s}$  and  $\phi = \frac{2\pi t_\phi}{T_s}$ .  $V_i$  and  $V_o$  are the input and output voltages of one DAB converter,  $L$  is the leakage inductance of the transformer,  $\omega = 2\pi f_{sw}$  where  $f_{sw}$  is the switching frequency,  $d = \frac{V_o}{V_i}$  is the voltage conversion ratio. The conduction loss of the module in the LV side can be calculated using Eq. (17) by plugging in the inductor current equation and obtain the Eq. 19.

$$\begin{aligned}
P_{MLVcond} = & \frac{1}{2\pi} \left\{ v_{FD1} \frac{V_i+V_o}{\omega^2 L} \frac{\theta_1^2}{2\omega^2} - v_{FD1} \frac{V_i}{\omega L} \left( \frac{(1-d)\pi}{2} + d\phi \right) \frac{\theta_1}{\omega} + R_{FD1} \frac{V_i^2 + V_o^2 + 2V_i V_o}{\omega^4 L^2} \frac{\theta_1^3}{3\omega^3} + \right. \\
& R_{FD1} \left\{ \left( \frac{V_i}{\omega L} \right)^2 \left[ \left( \frac{(1-d)\pi}{2} \right)^2 + (d\phi)^2 + (1-d)\pi d\phi \right] \right\} \frac{\theta_1^2}{2\omega^2} - R_{FD1} \frac{V_i(V_i+V_o)}{\omega^3 L^2} [(1-d)\pi + 2d\phi] \frac{\theta_1}{\omega} \\
& + r_{Q1} \left\{ \frac{V_i^2 + V_o^2 + 2V_i V_o}{\omega^4 L^2} \left( \frac{\phi^3 - \theta_1^3}{3\omega^3} \right) + \left( \frac{V_i}{\omega L} \right)^2 \left[ \left( \frac{(1-d)\pi}{2} \right)^2 + (d\phi)^2 + (1-d)\pi d\phi \right] \frac{\phi - \theta_1}{\omega} + \right. \\
& \left. \frac{V_i(V_i+V_o)}{\omega^3 L^2} [(1-d)\pi + 2d\phi] \right\} \left( \frac{\phi^2 - \theta_1^2}{2\omega^2} \right) + r_{Q1} \left\{ \frac{V_i^2 + V_o^2 - 2V_i V_o}{\omega^4 L^2} \left( \frac{\pi^3 - \phi^3}{3\omega^3} \right) + v_{FD1} \frac{V_i+V_o}{\omega^2 L} \frac{\pi^2 - \phi^2}{2\omega^2} - \right. \\
& v_{FD1} \frac{V_i}{\omega L} \left( \frac{(1-d)\pi}{2} + d\phi \right) \frac{\pi - \phi}{\omega} + R_{FD1} \left\{ \frac{V_i^2 + V_o^2 - 2V_i V_o}{\omega^4 L^2} \left( \frac{\pi^3 - \phi^3}{3\omega^3} \right) + 2V_i \left( \frac{V_i - V_o}{\omega^3 L^2} \right) (d\phi - \frac{\pi}{2} (1-d)) \frac{\pi^2 - \phi^2}{2\omega^2} \right. \\
& \left. \left. + \frac{V_i^2}{\omega^2 L^2} (d\phi - \frac{\pi}{2} (1-d))^2 \frac{\pi - \phi}{\omega} \right\} \right. \quad (19)
\end{aligned}$$



To calculate the junction temperatures of the diode and the MOSFET on the MV side and the LV side, we should break down the loss of the module into individual losses of the diode and the MOSFET. The loss of the diode in the MV side module can be calculated using Eq. (20)

$$P_{DMV} = \frac{1}{2\pi} \left\{ v_{FD1} \frac{V_i + V_o}{\omega^2 L} \frac{\theta_1^2}{2\omega^2} - v_{FD1} \frac{V_i}{\omega L} \left( \frac{(1-d)\pi}{2} + d\phi \right) \frac{\theta_1}{\omega} + R_{FD1} \frac{V_i^2 + V_o^2 + 2V_i V_o}{\omega^4 L^2} \frac{\theta_1^3}{3\omega^3} + \right. \\ \left. R_{FD1} \left\{ \left( \frac{V_i}{\omega L} \right)^2 \left[ \left( \frac{(1-d)\pi}{2} \right)^2 + (d\phi)^2 + (1-d)\pi d\phi \right] \frac{\theta_1^2}{2\omega^2} - R_{FD1} \frac{V_i(V_i + V_o)}{\omega^3 L^2} [(1-d)\pi + 2d\phi] \frac{\theta_1}{\omega} \right\} \right. \quad (20)$$

The loss of the diode in the LV side module can be calculated using Eq. (21)

$$P_{DLV} = \frac{1}{2\pi} \left\{ v_{FD1} \frac{V_i + V_o}{\omega^2 L} \frac{\theta_1^2}{2\omega^2} - v_{FD1} \frac{V_i}{\omega L} \left( \frac{(1-d)\pi}{2} + d\phi \right) \frac{\theta_1}{\omega} + R_{FD1} \frac{V_i^2 + V_o^2 + 2V_i V_o}{\omega^4 L^2} \frac{\theta_1^3}{3\omega^3} + \right. \\ \left. R_{FD1} \left\{ \left( \frac{V_i}{\omega L} \right)^2 \left[ \left( \frac{(1-d)\pi}{2} \right)^2 + (d\phi)^2 + (1-d)\pi d\phi \right] \frac{\theta_1^2}{2\omega^2} - R_{FD1} \frac{V_i(V_i + V_o)}{\omega^3 L^2} [(1-d)\pi + 2d\phi] \frac{\theta_1}{\omega} \right\} \right. \\ + v_{FD1} \frac{V_i + V_o}{\omega^2 L} \frac{\pi^2 - \phi^2}{2\omega^2} - v_{FD1} \frac{V_i}{\omega L} \left( \frac{(1-d)\pi}{2} + d\phi \right) \frac{\pi - \phi}{\omega} + R_{FD1} \frac{V_i^2 + V_o^2 + 2V_i V_o}{\omega^4 L^2} \frac{\pi^3 - \phi^3}{3\omega^3} + \\ \left. R_{FD1} \left\{ \left( \frac{V_i}{\omega L} \right)^2 \left[ \left( \frac{(1-d)\pi}{2} \right)^2 + (d\phi)^2 + (1-d)\pi d\phi \right] \frac{\pi^2 - \phi^2}{2\omega^2} - R_{FD1} \frac{V_i(V_i + V_o)}{\omega^3 L^2} [(1-d)\pi + \right. \right. \\ \left. \left. 2d\phi] \frac{\pi - \phi}{\omega} \right\} \right. \quad (21)$$

The conduction loss of the switch in the MV side module can be calculated using Eq. (22)

$$P_{QMV} = \frac{1}{2\pi} \left\{ r_{Q1} \left\{ \frac{V_i^2 + V_o^2 + 2V_i V_o}{\omega^4 L^2} \left( \frac{\phi^3 - \theta_1^3}{3\omega^3} \right) + \left( \frac{V_i}{\omega L} \right)^2 \left[ \left( \frac{(1-d)\pi}{2} \right)^2 + (d\phi)^2 + (1-d)\pi d\phi \right] \frac{\phi - \theta_1}{\omega} + \right. \right. \\ \left. \frac{V_i(V_i + V_o)}{\omega^3 L^2} [(1-d)\pi + 2d\phi] \left( \frac{\phi^2 - \theta_1^2}{2\omega^2} \right) + r_{Q1} \left\{ \frac{V_i^2 + V_o^2 - 2V_i V_o}{\omega^4 L^2} \left( \frac{\pi^3 - \phi^3}{3\omega^3} \right) + 2V_i \left( \frac{V_i - V_o}{\omega^3 L^2} \right) (d\phi - \frac{\pi}{2} (1-d)) \right. \right. \\ \left. \left. \frac{\pi^2 - \phi^2}{2\omega^2} \right) + \frac{V_i^2}{\omega^2 L^2} (d\phi - \frac{\pi}{2} (1-d))^2 \frac{\pi - \phi}{\omega} \right\} \right\} \quad (22)$$

And finally, the conduction loss of the switch on the LV side can be calculated using Eq. (21)

$$P_{QLV} = \frac{1}{2\pi} \left\{ r_{Q1} \left\{ \frac{V_i^2 + V_o^2 + 2V_i V_o}{\omega^4 L^2} \left( \frac{\phi^3 - \theta_1^3}{3} \right) + \left( \frac{V_i}{\omega L} \right)^2 \left[ \left( \frac{(1-d)\pi}{2} \right)^2 + (d\phi)^2 + (1-d)\pi d\phi \right] \left( \frac{\phi^2 - \theta_1^2}{2} \right) + \right. \right. \\ \left. \frac{V_i(V_i + V_o)}{\omega^3 L^2} [(1-d)\pi + 2d\phi] \frac{\phi - \theta_1}{\omega} \right\} \right\} \quad (23)$$

Another approach to calculate the module losses and the junction temperatures would be to use discretized model of the current and calculate the losses and the  $T_J$  based on statistical averaging. For example, the conduction loss of the diode on the MV side can be calculated using  $\frac{1}{N} \sum_n (i_n^2 r_d + V_{on} i_n)$  and the thermal model for heat sink and ambient temperature is used to calculate the junction temperature of the switch and the diode on the inverter side or the rectifier side of the converter. A computer code is developed for this purpose and it is included in the Appendix I.

The third approach would be using the average and root mean squared (rms) values of the current passing through every diode and MOSFET. The loss of the semiconductor would become

$$P_{D_j} = V_{drop} I_{avg_{ij}} + r_{on} I_{rms_{ij}}^2 \quad (24)$$

$$P_{MOS_j} = r_{on} I_{rms_{ij}}^2 \quad (25)$$

where  $P_{D_j}$  is the power loss of the diode  $j$  in the  $i^{\text{th}}$  DAB layer, or the amount of electric energy that turns into thermal energy during one switching cycle.  $V_{drop}$  is the voltage drop of the semiconductor,  $I_{avg}$  is the average current passing through the semiconductor during one switching cycle,  $r_{on}$  is the resistance of the semiconductor device during forward conduction.  $I_{rms}$  is the rms value of the current passing through the device. The values of  $V_{drop}$  and  $r_{on}$  are provided by the manufacturer and the values of the  $I_{avg}$  and  $I_{rms}$  should be calculated.

The loss is evaluated using analytical and numerical methods for a converter with modes of operations as provided in Table I. The results of the calculations are provided in Fig. 7 for the system with CAS300M17BM2 module. The code that was developed for the calculation and generation of the curves in Fig. 7 is provided in Appendix I. The parameters of the DC-DC converter were used are indicated in Table 2. According to Fig. 7, to keep the junction temperature of the diode and MOSFET in MV and LV side below 120°C, the coolant temperature of 25°C and lower is needed. This figure also shows correctly that the losses of the module on the inverter side and rectifier side are not equal.

Table 2 Parameters used for thermal calculations of SiC MOSFET

Parameter	Description	Value
$V_i$	Primary side DC voltage (V)	6k
$V_o$	Secondary side DC voltage (V)	1k
$P_r$	Rated power of the converter	1.5 MW
$T_c$	Coolant temperature	[5- 35]°C

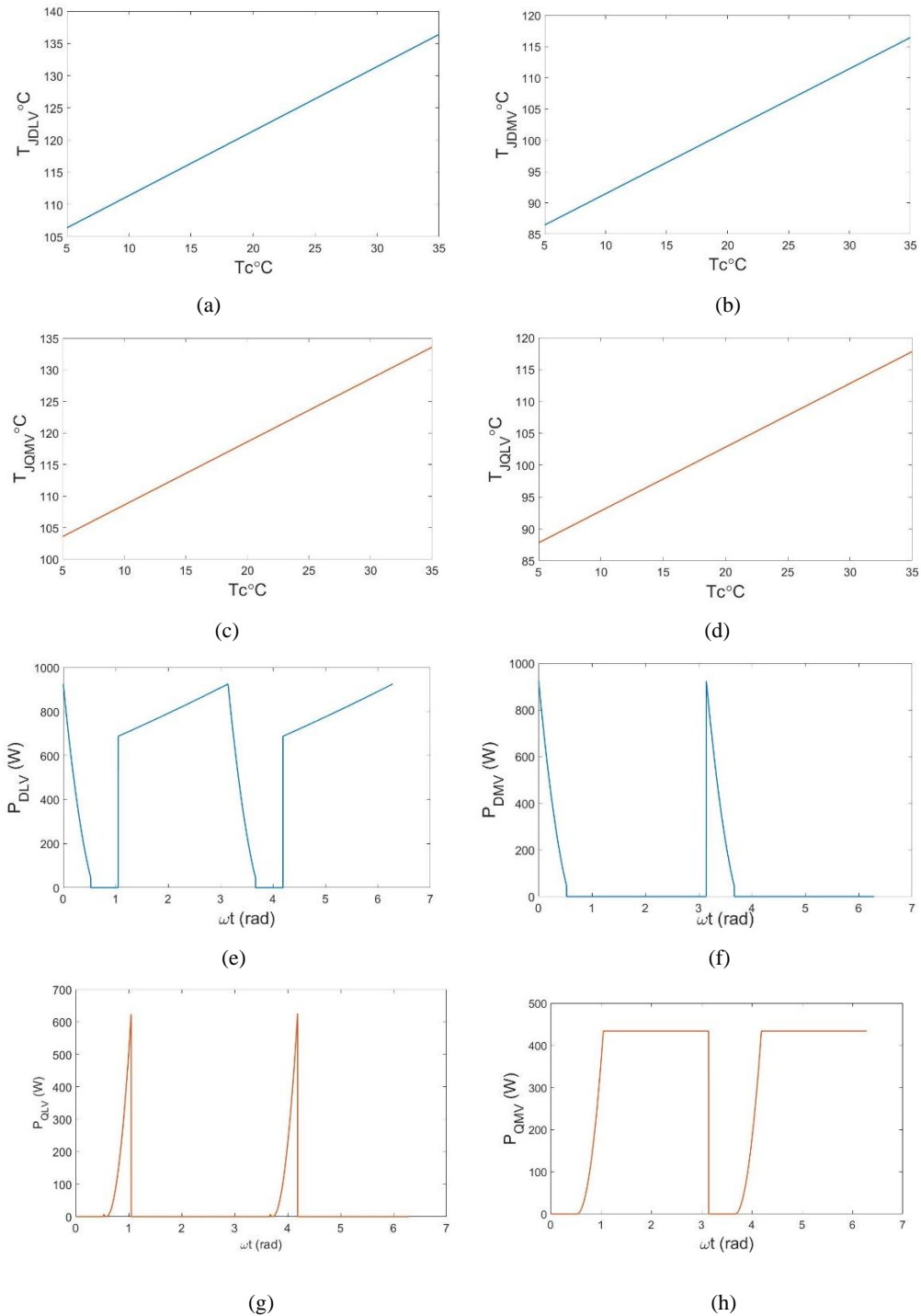


Fig. 7, Junction temperature and thermal loss of diode and transistor in MV and LV side modules: (a) junction temperature of diode on LV side vs coolant temperature, (b) junction temperature of diode on MV side vs coolant temperature, (c) junction temperature of transistor on MV side vs coolant temperature, (d) junction temperature of transistor on LV side vs coolant temperature, (e) instantaneous power loss of diode on LV side, (f) instantaneous power loss of diode on MV side, (g) instantaneous power loss of diode on LV side and (h) instantaneous power loss of transistor on MV side

### 3- HIGH FREQUENCY POWER TRANSFORMER

High frequency transformer (HFT) is an important component in DAB converter. It provides the isolation between the MV side and LV side. Design of the high frequency transformer is an important part of the PCM design because HFT is a contributor to power density and the power transfer happens through HFT. Obtaining low loss and low leakage inductance is important for DAB made of SiC modules with high switching frequency. Both winding loss and core loss are a function of the switching frequency. HFT can be designed in various geometrical topologies. Core type, shell type, matrix type and coaxial are the most popular ones. The winding of such a transformer can be a foil, round wire, or Litz wire. For high frequency applications, Litz wire is recommended to obtain more efficiency.

#### 3.1 HFPT design and geometrical parametrization

In this study, a novel topology is proposed for the high frequency power transformer that is used in DAB converter to obtain a low value of leakage inductance. The capacitive coupling between the primary winding and secondary winding should be minimum for high frequency applications. Additionally, the capacitive coupling between the windings and the core should also be minimized. Therefore, the split winding configuration is considered in this study. The core and heatsink structure of the transformer is shown in Fig. (8), front view is shown in Fig (9), side view is shown in Fig. (10), top view in Fig. (11), the Litz wire winding configuration is shown in Fig. (12) and the magnetic core building block is shown in Fig. (13).

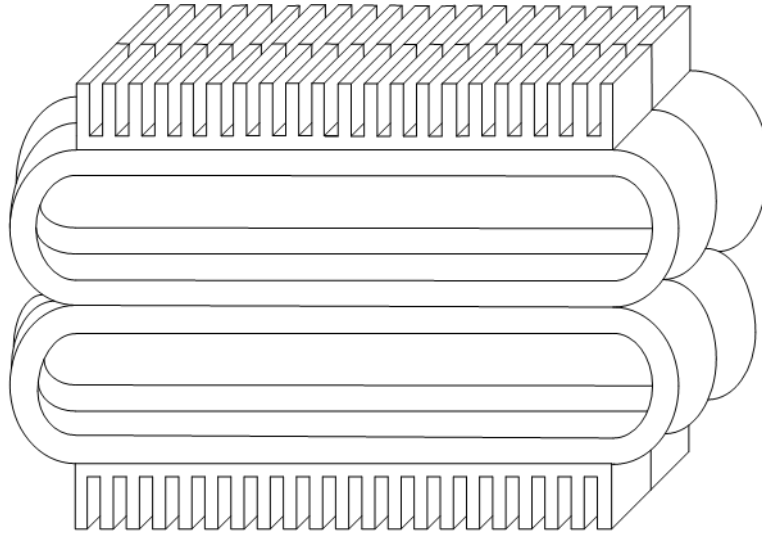


Fig. 8 Core and heat sink structure of the HFPT

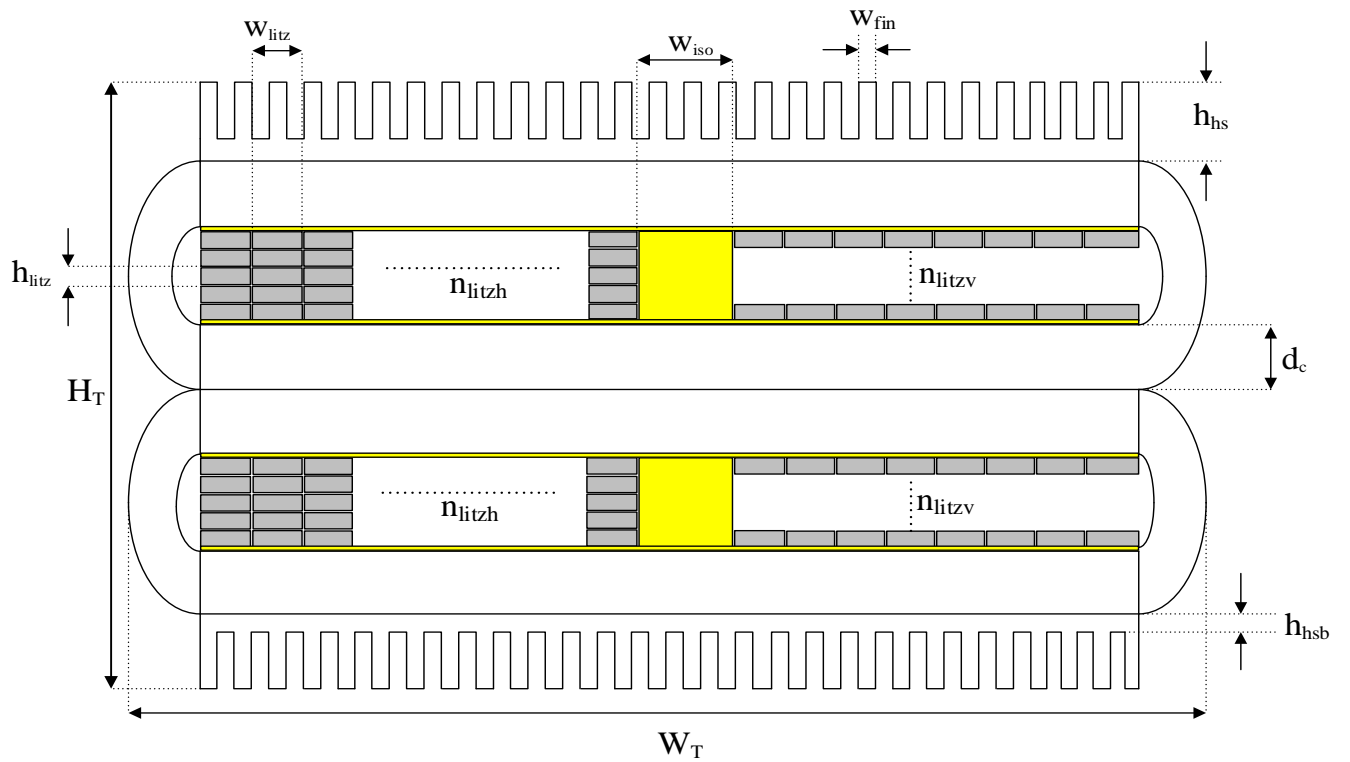


Fig. 9 Front view of the HFPT

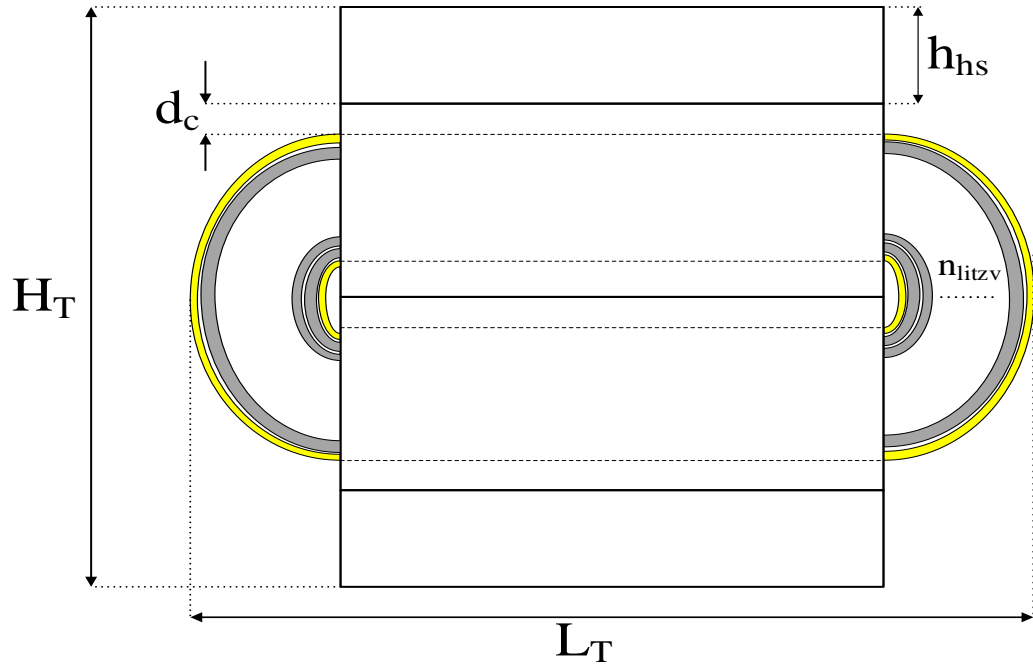


Fig. 10 Side view of HFPT

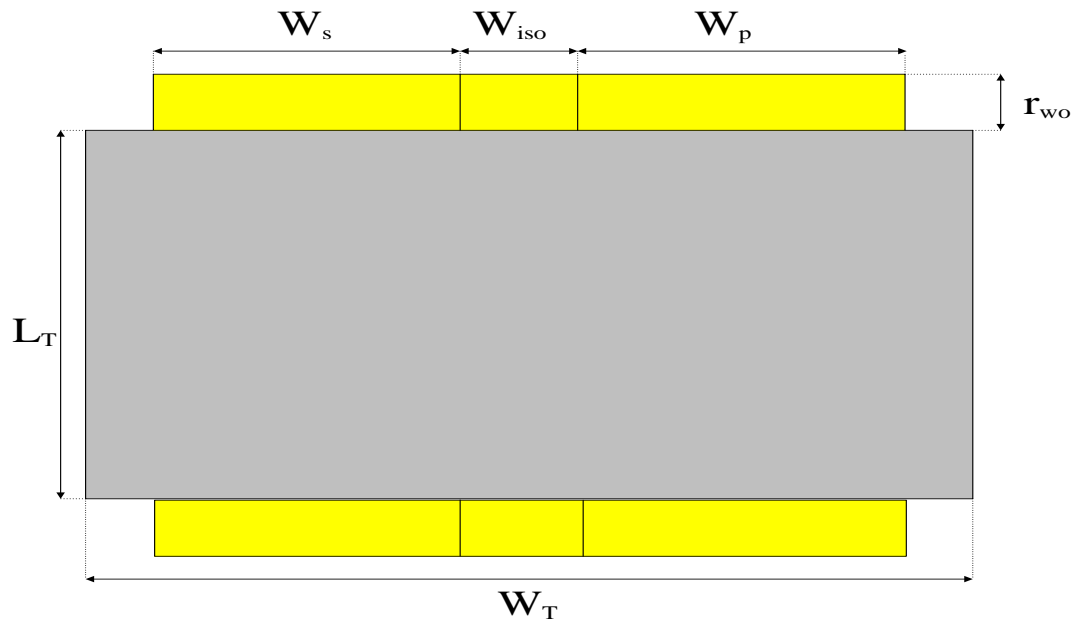


Fig. 11 Top view of the HFPT

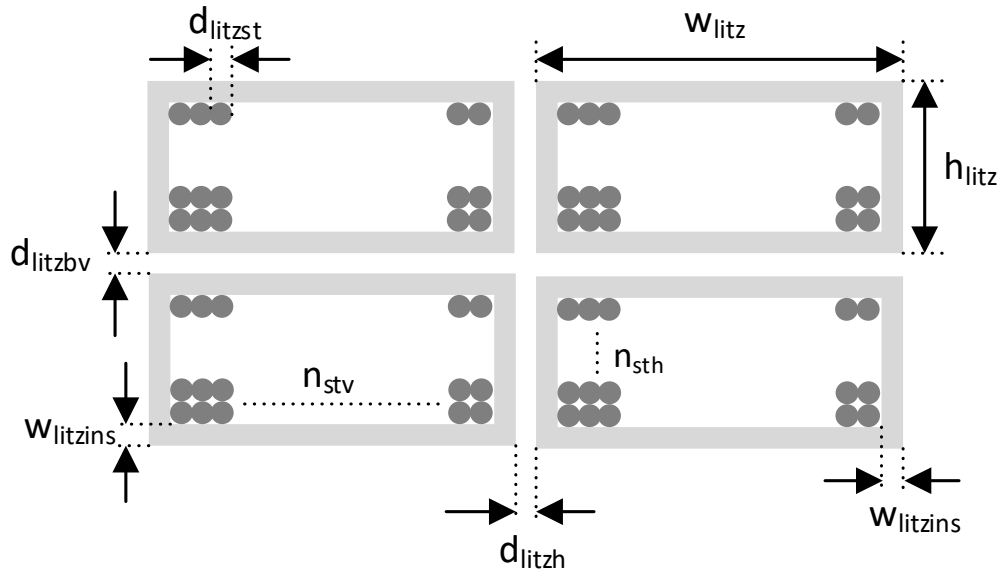


Fig. 12 Litz wire parameterization

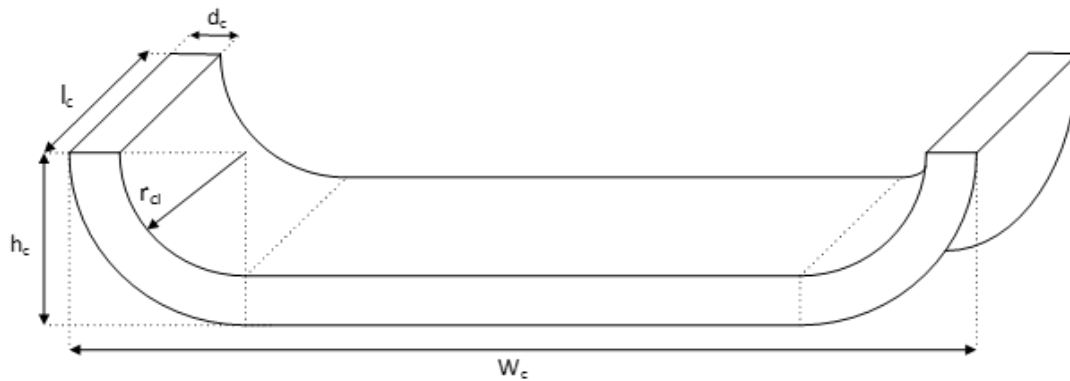


Fig. 13 Core building block for HFPT

### 3.2 Design process of HFPT

Design process of HFPT is an iterative process. There are several reports exist in the literature for HFT design [28-42] In this study, the multi-objective optimization of the HFPT is considered and maximum power density of the HFPT is considered as the primary goal. Given that there is a height limitation in the dedicated space for power electronics converters in the ship environment, the design must take a laminar form. This will also increase the surface of the heatsink which helps with thermal management of the HFPT. The parameters of the HFPT are listed in table 3. However,

not all these parameters are independent. The first design step is determining the independent design parameters and extracting the relationship between dependent parameters and the independent ones.

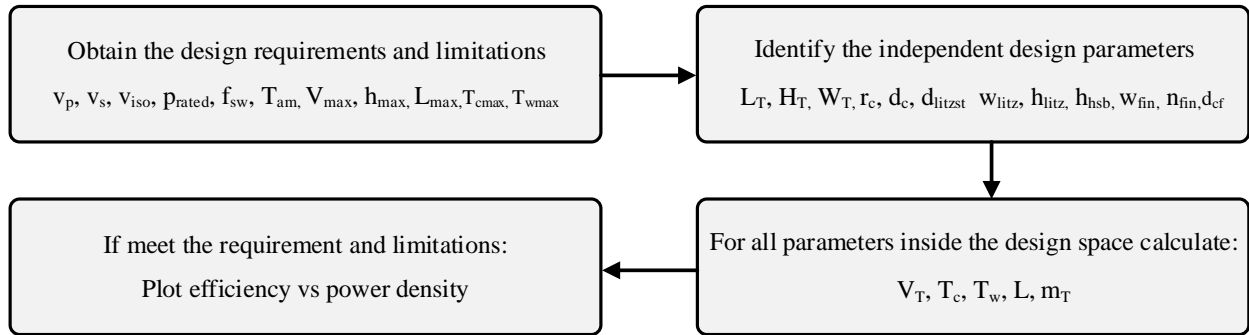


Fig. 14 Design flow of the HFPT

Table 3 List of the parameters of HFPT

Parameter	Description
$H_T$	Height of the transformer
$W_T$	Width of the transformer
$L_T$	Depth of the transformer
$M_T$	Mass of the transformer
$V_T$	Volume of the transformer
$w_c$	Width of the core
$h_c$	Height of the core
$l_c$	Depth of the core
$r_{ci}$	Inner radius of the core
$d_c$	Thickness of the core
$m_c$	Mass of the core
$V_c$	Volume of the core
$\rho_c$	Mass density of the core material
$w_p$	Width of the primary winding
$w_s$	Width of the secondary winding



$r_{wip}$	Inner radius of the primary winding
$r_{wis}$	Inner radius of the secondary winding
$r_{wop}$	Outer radius of the primary winding
$r_{wos}$	Outer radius of the secondary winding
$w_{Litz}$	Width of the Litz wire bundle
$h_{Litz}$	Thickness of the Litz wire bundle
$d_{Litzbh}$	Horizontal distance between Litz bundles
$d_{Litzbv}$	Vertical distance between Litz bundles
$w_{Litzins}$	Thickness of the Litz wire insulation layer
$d_{st}$	Diameter of the copper strand
$n_{stv}$	Number of strands placed vertically in a Litz bundle
$n_{sth}$	Number of strands placed horizontally in a Litz bundle
$l_{pw}$	Length of the primary winding
$l_{sw}$	Length of the secondary winding
$n_{Litzv}$	Number of Litz bundles placed vertically in the core window
$n_{Litzh}$	Number of Litz bundles placed horizontally in the core window
$d_{cwv}$	Vertical distance between winding and core
$w_{iso}$	Width of the isolation layer
$d_{cww}$	Vertical distance between the core and winding
$n_{iso}$	Number of turns of the isolation layer
$d_{iso}$	Thickness of the isolation layer between the windings
$h_{hs}$	Height of the heatsink
$w_{hs}$	Width of the heatsink
$d_{hs}$	Depth of the heatsink
$h_{hsb}$	Height of the heatsink base layer
$w_{hsf}$	Width of the heatsink fin
$w_{hsa}$	Width of the heatsink air channel
$n_{hsf}$	Number of fins in the heatsink

The DAB converter considered in this study has a symmetry and therefore the HFPT also has a symmetry between the winding variables. This means that not all the parameters in the Table 3 are independent parameter, many of them are dependent parameters and their value can be determined based on the values of the independent parameters. The independent parameters that can be used in the design of the HFPT are listed in Table 4.

The values of the independent parameters sweep between a minimum and maximum values determined by the designer or the optimization machine. For every combination of the independent parameter values, the leakage inductance, temperature of the core and windings will be calculated and only for those designs that the leakage and temperature are within the acceptable range will be kept and the rest will be removed. For all the feasible designs, the power density, efficiency, reliability and cost will be calculated, and the Pareto front will be identified based on the selection criteria.

There can be different ways to identify the independent parameters depending the design approach being considered. For example, a top down approach starts with considering the limitations of the HFPT, like power density and efficiency and then the optimal values of the Litz wire, the core dimensions, heatsink size and isolation layer thickness will be identified. A bottom up approach can start with the dimensions of the Litz wire, magnetic core and the heatsink and find the most optimal design and then calculation of the features of the HPFT. Identification of the independent parameters depends on the design approach. In this study the bottom up approach is used. Table 4 shows the independent design parameters for the bottom up approach.

Table 4 List of independent geometrical parameters for HFPT design for bottom up design approach

Parameter	Description	Variable
$d_{st}$	Diameter of the copper strand inside the Litz bundle	$x_1$
$n_{stv}$	Number of copper strands placed in a Litz bundle vertically	$x_2$
$n_{sth}$	Number of copper strands placed in a Litz bundle horizontally	$x_3$
$w_{litzins}$	Width of the insulation layer of Litz wire	$x_4$
$d_{litzbv}$	Vertical distance between Litz bundles	$x_5$
$d_{litzbh}$	Horizontal distance between Litz bundles	$x_6$

$n_{litzh}$	Number of Litz bundles placed horizontally in a core window	$x_7$
$n_{litzv}$	Number of Litz bundles placed vertically in a core window	$x_8$
$r_{wi}$	Inner radius of the windings	$x_9$
$d_c$	Thickness of the core	$x_{10}$
$r_{ci}$	Inner radius of the core	$x_{11}$
$l_c$	Length of the magnetic core	$x_{12}$
$w_{iso}$	Width of the insulation layer	$x_{13}$
$d_{cww}$	Thickness of the insulation layer between the core and the winding	$x_{14}$
$h_{hs}$	Height of the heatsink	$x_{15}$
$h_{hsb}$	Height of the base part of the heatsink	$x_{16}$
$w_{fin}$	Width of the fin	$x_{17}$

Dependent variables of the HPFT can be extracted from the independent variables based on the following equations:

$$l_w = 2n_{litzv}n_{litzh}(l_c + \pi r_{wi} + (n_{litzv} - 1)(d_{litzbv} + h_{litz})) \quad (26)$$

$$l_{iso} = 2n_{iso}l_c + \pi(2n_{iso}r_{iso} + d_{iso}n_{iso}(n_{iso} - 1)) \quad (27)$$

$$n_{iso} = \frac{n_{litzv}h_{litzv} + (n_{litzv} - 1)d_{litzbv}}{d_{iso}} \quad (28)$$

### 3.3 Winding loss:

Calculating the winding loss is necessary for the design of transformer. Analytical approach to calculation of winding loss considering the eddy current was first done by Dowell [43] where an effective resistance of the winding was extracted for alternating current operation. This methodology has been used by other researchers [14, 15]. One approach is to calculate the loss for foil winding and then extend the results to Litz wire winding. If we assume one layer of Litz winding that consists of  $n_{litzh}$  Litz bundles placed horizontally to form a geometry like a foil with

width of  $W_w$  and thickness of  $d_{cu}$ , then we can apply the methodology that was introduced in [14] to obtain an estimate of the winding loss for this topology. The cross-sectional current distribution function is needed. Given that there is magnetic field inside the core window where the foil winding is placed, Maxwell's equations are used to extract the current density.

$$\nabla \cdot \vec{E} = \frac{\rho_v}{\epsilon} \quad (29)$$

$$\nabla \cdot \vec{H} = 0 \quad (30)$$

$$\nabla \times \vec{E} = -\mu \frac{\partial \vec{H}}{\partial t} \quad (31)$$

$$\nabla \times \vec{H} = \vec{J} + \epsilon \frac{\partial \vec{E}}{\partial t} \quad (32)$$

For ac current with angular frequency of  $\omega$ , the Eqs. (31) and (32) will take the following form:

$$\nabla \times \vec{E} = -j\omega\mu\vec{H} \quad (33)$$

$$\nabla \times \vec{H} = \vec{J} + j\omega\epsilon\vec{E} \quad (34)$$

Within the conductive material, the current density and electric field have the following relationship:

$$\vec{J} = \sigma\vec{E} \quad (35)$$

Therefore, the eq (34) can be rewritten as:

$$\nabla \times \vec{H} = \sigma\vec{E} + j\omega\epsilon\vec{E} \quad (36)$$

The second term in eq (36) is known as the displacement current, if we ignore the displacement current, then the electric field and magnetic field will have the following relation:

$$\nabla \times \vec{H} = \sigma\vec{E} \quad (37)$$

And plugging eq (33), the following can be extracted:

$$\nabla \times (\nabla \times \vec{H}) = \sigma(\nabla \times \vec{E}) \quad (38)$$

$$\nabla^2 \vec{H} = \sigma j\omega\mu \vec{H} \tag{39}$$

Fig. (15) shows one foil layer within the HFPT and the corresponding coordinate system. Based on this coordinate system, if the current is flowing through the foil in the x direction, the cross sectional current density of the foil is  $J = J_x(y, z)$ , and then the magnetic field is  $\vec{H} = \vec{a}_y H_y(z)$ .

In order to calculate the field distribution within the foil, the Eq. (39) will be in the form of Eq. (40)

$$\frac{\partial^2 H_y(z)}{\partial z^2} - j\sigma\omega\mu H_y(z) = 0 \tag{40}$$

This equation has a solution in the form of Eq. (41)

$$H_y(z) = Ae^{\alpha z} + Be^{-\alpha z} \tag{41}$$

where  $\alpha^2 = j\sigma\omega\mu$ , now applying the boundary conditions, the magnetic field takes the following form

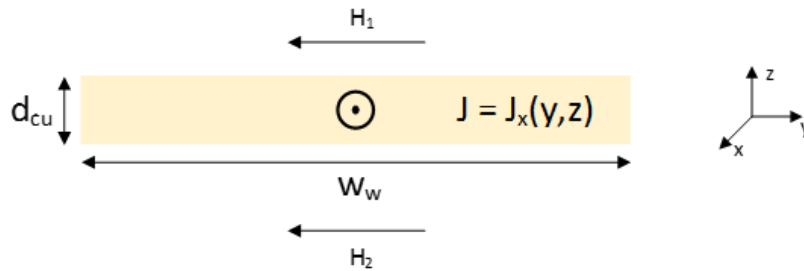


Fig. 15 foil winding parameterization

$$H_y(z) = H_1 \frac{\sinh(\alpha z)}{\sinh(\alpha d_{cu})} - H_2 \frac{\sinh(\alpha(z - d_{cu}))}{\sinh(\alpha d_{cu})} \tag{42}$$

And the current density can be calculated using Eq. (43)

$$\nabla \times \vec{H} = \vec{J} \tag{43}$$

If we assume the cross section current density distribution is homogenous in y direction, then the following equations can be derived:

$$\frac{\partial H_y(z)}{\partial z} = J_x(z) \quad (44)$$

$$J_x(z) = \alpha H_1 \frac{\cosh(\alpha z)}{\sinh(\alpha d_{cu})} - \alpha H_2 \frac{\cosh(\alpha(z-d_{cu}))}{\sinh(\alpha d_{cu})} \quad (45)$$

Having the current density, the power loss of the foil can be calculated using Eq (46):

$$P_\sigma = \frac{1}{\sigma} \int \vec{j} \cdot \vec{j}^* dv \quad (46)$$

$$P_\sigma = \frac{1}{\sigma} \int_{z=0}^{z=d_{cu}} |J_x(z)|^2 w_w d_f dz \quad (47)$$

where  $d_f$  is the length of the foil in x direction. Using Eq. (42), we can write

$$|J_x(z)|^2 = \left| \alpha H_1 \frac{\cosh(\alpha z)}{\sinh(\alpha d_{cu})} - \alpha H_2 \frac{\cosh(\alpha(z-d_{cu}))}{\sinh(\alpha d_{cu})} \right|^2 \quad (48)$$

Using this equation and mathematical simplification the loss of the foil with the existing boundary conditions will take the following form [16]:

$$P_{foil} = \frac{l_f d_{cu}}{2\delta\sigma} \left[ (H_1 - H_2)^2 \frac{\sinh(2\Delta) + \sin(2\Delta)}{\cosh(2\Delta) - \cos(2\Delta)} + 2H_1 H_2 \frac{\sinh(\Delta) - \sin(\Delta)}{\cosh(\Delta) + \cos(\Delta)} \right] \quad (49)$$

where  $\Delta = \frac{d_{cu}}{\delta}$ , the penetration ratio and  $\delta = \sqrt{\frac{2}{\omega\mu\sigma}}$  is the skin depth of the foil conductor. The

two expressions in Eq. (49), represent the skin and proximity effect. For a design that has multiple layers of foil winding, the  $H_1$  and  $H_2$  are generated by the other layers of winding, therefore, for the  $i^{\text{th}}$  winding layer from the center to the top in the HFPT structure, the values of

boundary fields will be as  $H_1 = i \frac{I}{w_w}$  and  $H_2 = (i-1) \frac{I}{w_w}$  where  $I$  is the peak current for the

waveforms that were shown in Fig. 5 and Fig. 6.

Another approach is to calculate the loss for one strand and then sum the loss of strands. Considering the magnetic field inside the core window the transverse current density of strands will be different based on the layer they are placed in and the horizontal position that they are placed in. However, to find an approximation for this case, we will ignore the proximity and the impact of external magnetic field on the current density.

The strands of copper assumed in this work have cylindrical geometry, therefore, the transverse cross section of the strands is circular. The intensity of current density on a cylinder of radius  $r$  from the middle of one copper strand where ( $r < d_{st}$ ) takes the following form if the proximity effect and the external magnetic field effects are neglected:

$$J(r) = J_s e^{-\frac{(d_{st}-r)}{\delta}} \quad (50)$$

where  $J_s$  is the current density at the surface of the wire,  $r$  is the radius of the cylindrical layer considered, and  $\delta = \sqrt{\frac{2}{\omega\mu\sigma}}$  is the skin depth of the conductor.  $\sigma$  is the electric conductivity of the material used for winding. Copper and Aluminum are the two common conductors used for windings. The electric conductivity of copper is  $\sigma_{cu} = 5.87 \times 10^7 \left(\frac{S}{m}\right)$  and the electric conductivity of Aluminum is  $\sigma_{Al} = 3.47 \times 10^7 \left(\frac{S}{m}\right)$ .  $\omega$  is angular frequency where  $\omega=2\pi f_{sw}$  and  $f_{sw}$  (Hz) is the switching frequency of the converter.  $\mu$  is the magnetic permeability of the conducting material and  $\mu=\mu_r\mu_0$   $\left(\frac{H}{m}\right)$  where the relative permeability for Copper is  $\mu_{r,cu} = 0.999994$ , and for Aluminum is  $\mu_{r,Al} = 1.000022$  and  $\mu_0 = 1.25663753 \times 10^{-6} \left(\frac{H}{m}\right)$ . The skin depth versus the switching frequency for Copper and Aluminum is provided in Table 5 for switching frequency that ranges from 1kHz to 100kHz.

Table 5 Skin depth of Cu and Al vs switching frequency of converter

$f_{sw}$ (kHz)	1kHz	10kHz	20kHz	40kHz	60kHz	80kHz	100kHz
$\delta_{cu}$ (mm)	2.1	0.65	0.47	0.32	0.27	0.23	0.2
$\delta_{Al}$ (mm)	2.7	0.85	0.6	0.42	0.35	0.3	0.27

It can be seen from Table 5 that the skin depth of both of conductors of the choice decrease with high rate when switching frequency is between 1kHz to 20kHz, but then the rate of decline is decreasing when switching frequency is above 20kHz. This means, when switching frequency increases, more electrons are pushed to the surface of the conducting wire. For converters with Silicon Carbide modules, the switching frequency is usually between 20kHz and 100kHz, and according to Table 5 the skin depth of Copper and Aluminum are less than 1mm.

Considering the radial distribution of electric current in copper strands, the thermal loss of one strand of wire winding can be calculated using the following formula:

$$P_{st} = \frac{1}{\sigma} \int J \cdot J^* dv \quad (51)$$

Incorporating Eq. (50) to Eq. (51), we can obtain a thermal loss for one strand of copper:

$$\begin{aligned} P_{st} &= \frac{1}{\sigma} l_w J_s^2 \int_0^{\frac{d_{st}}{2}} e^{-\frac{2(d_{st}-r)}{\delta}} dr = \frac{1}{\sigma} l_w J_s^2 e^{-\frac{2d_{st}}{\delta}} \int_0^{\frac{d_{st}}{2}} e^{\frac{2r}{\delta}} dr = \frac{1}{\sigma} l_w J_s^2 e^{-\frac{2d_{st}}{\delta}} \frac{\delta}{2} \left( e^{\frac{d_{st}}{\delta}} - 1 \right) = \\ &= \frac{1}{\sigma} l_w \left( \frac{\mu_0 I_{st}}{2\pi \frac{d_{st}}{2}} \right)^2 e^{-\frac{2d_{st}}{\delta}} \frac{\delta}{2} \left( e^{\frac{d_{st}}{\delta}} - 1 \right) = \frac{1}{\sigma} l_w \left( \frac{\mu_0 I}{\pi d_{st} n_{stv} n_{sth}} \right)^2 e^{-\frac{2d_{st}}{\delta}} \frac{\delta}{2} \left( e^{\frac{d_{st}}{\delta}} - 1 \right) \end{aligned} \quad (52)$$

And therefore, the winding loss of the proposed transformer can be approximated by Eq. (53):

$$\begin{aligned} P_w &= 2(n_{stv} n_{sth} n_{litzv} n_{litzh}) P_{st} = 2(n_{stv} n_{sth} n_{litzv} n_{litzh}) \frac{1}{\sigma} l_w \left( \frac{\mu_0 I}{\pi d_{st} n_{stv} n_{sth}} \right)^2 e^{-\frac{2d_{st}}{\delta}} \frac{\delta}{2} \\ &= \frac{2n_{litzv} n_{litzh}}{\sigma n_{stv} n_{sth}} l_w \left( \frac{\mu_0 I}{\pi d_{st}} \right)^2 e^{-\frac{2d_{st}}{\delta}} \frac{\delta}{2} \end{aligned} \quad (53)$$

Another approach is to think of a rectangular Litz wire bundle as a foil and obtain the effective AC resistance for the bundle using equations that exist in the literature for foil winding [43].

$$RF = \frac{R_{AC}}{R_{DC}} = M(\Delta) + \frac{m^2-1}{3} D(\Delta) \quad (54)$$

$$M(\Delta) = \Delta \frac{\sinh 2\Delta + \sin 2\Delta}{\cosh 2\Delta - \cos 2\Delta} \quad (55)$$

$$D(\Delta) = 2\Delta \frac{\sinh \Delta - \sin \Delta}{\cosh \Delta + \cos \Delta} \quad (56)$$

where  $R_F$  is the ratio of AC resistance to DC resistance of the winding,  $R_{DC}$  is the resistance of the conducting material with DC excitation,  $R_{AC}$  is the resistance of the conducting material with AC excitation,  $m$  is the layer number. Delta, the penetration ratio, takes the form of  $\Delta = \frac{n_{stv} d_{st}}{\delta}$  in this case where  $\delta = \sqrt{\frac{2}{\omega \mu \sigma}}$  is the skin depth of the conductor. For example, if  $n_{stv} = 10$ ,  $d_{st} = 0.5mm$

and  $\delta = 0.32mm$ , then  $\Delta = 15.223$  and considering,  $RF \cong 15$  can be achieved.

### 3.4 Core loss



Steinmtz's equation, a practical formula that was obtained using interpolation of laboratory test results is commonly used to estimate the low frequency core loss of the transformer and it is shown in Eq. (57)

$$P_c = Kf^\alpha B_m^\beta \quad (57)$$

where  $P_c$  (kW/m<sup>3</sup>) represents the core loss density of the transformer,  $f$  is the frequency of the current passing through the windings in kHz,  $B_m$  is the peak magnetic field in Tesla and  $K$ ,  $\alpha$  and  $\beta$  are constants related to a magnetic core material. Modifications on Steinmtz's equation were reported in the literature to estimate the core loss for high frequency applications [28].

Waveform coefficient Steinmtz's equation (WCSE) is used in this study to obtain an estimate of the core loss for high switching frequency and for non-sinusoidal waveform [39]. The flux waveform coefficient (FWC) is defined as the ratio of the area of the flux waveform of the non-sinusoidal waveform to the area of the flux waveform of the sinusoidal waveform [28]. Therefore, the improved Steinmtz's equation for loss calculation will take the following form:

$$P_c = FWCKf^\alpha B_m^\beta \quad (58)$$

For the case of DAB application with squared waveform, the FWC coefficient for a square waveform is  $\pi/4$ . For HFT application, various options exist to choose a core material with the most popular ones being from the families of ferrites, amorphous materials, nanocrystalline, Si iron, Ni Fe and powdered iron. Ref. [44] provides comprehensive explanations about the physics of magnetic materials and their manufacturing process. Laboratory measurements of the core loss for nanocrystalline cores are reported in [39].

To calculate the  $B_m$ , the knowledge about the voltage waveform created by FB circuit on the inverter side of the HFPT and DAB current waveform is helpful. For a typical magnetic circuit consist of magnetic core and a winding there is a relationship between the voltage across the winding and corresponding magnetic field, Eq. (59) shows this relationship:

$$v(t) = NA_c \frac{dB}{dt} \quad (59)$$

where the  $v(t)$  is the voltage across the winding,  $N$  is the number of turns,  $A_c$  is the cross-sectional area and  $B$  is the magnetic field propagating through the core. In the case of DAB circuit,  $v(t)$  the

voltage across the transformer windings takes rectangular form and the magnetic field inside the core,  $B(t)$  takes ramp form and the  $B_m$ , the maximum value of the  $B$  takes place at  $t_\phi$  and  $T_s/2 + t_\phi$  where  $\phi$  is the phase shift between the MV and LV side HBs.

Table 6 shows the values of these coefficients for a few popular core materials used for HFT design [44]. It should be noted that the physical characteristics of the core materials are temperature and frequency dependent. Also, special attention should be paid to the units that are used in Eq. (57).

Table 6 Typical magnetic core materials used for HFPT [44]

Material	Ferrite, N87	Amorphous, Metglas 2605	Si iron Unisil 23M3	Nanocrystalline Vitroperm500F	Permalloy 80
$\mu_r$	2200	$10^4$ - $10^5$	5000-10000	15000	20000-50000
$B_{max}$ (T)	0.49	1.2	2	1.2	0.60-1.3
$T_C$ (°C)	210	600	745	600	665
$\alpha$	1.25	1.32	1.7	1.32	1.02
$\beta$	2.35	2.1	1.9	2.35	1.89
K	16.9	2.3	3.38	2.3	1.798

### 3.5 Isolation

Isolation is an essential topic for high voltage electrical engineering because with increasing the voltage level, confinement of the electric field in designated area becomes more important. Therefore, utilization of insulating materials to provide isolation voltage between the conducting materials is a fundamental task in designing components and systems that work with high voltage levels. The DC-DC converter that is considered in this study for shipboard electrification will connect the two networks with different voltage levels, one network with LV voltage level and the other with MV voltage level. If the core of the transformer is grounded, there will be a MV voltage difference between the MV and core of the transformer which can cause capacitive coupling and electric leakage of current. Therefore, it is necessary to provide enough thickness of the isolation layer placed between the windings and the magnetic core material. The common mode coupling that takes place between points with MV voltage level and the ground through the parasitic path should be minimized in the MVDC power system. In the case of fault, this path could prevent

isolating scenarios and will cause ground faults to flow in the system even when preventive methodologies are applied. The transformer could provide the isolation between the MVDC and the LVDC and ground by properly utilizing an isolation layer between the primary and the secondary windings of the transformer. There are two main design categories for transformer as far as winding configuration is concerned, one is concentric when one winding is wound on the other, and there is split winding when the windings are wound on different part of the core and there is no overlap between the windings. Since in the split winding configuration, the windings are not placed on top of each other there will be lower probability for the parasitic coupling. For integrated power electronic system for shipboard electrification application, the isolation capability of the system is very important since ground faults could be common in ship environment. Therefore, in this study only the split winding arrangement is considered. Calculating the required thickness of the isolation material is a design criterion for a transformer. Selecting a thick isolation material could provide better electric isolation while increasing the size of the transformer or decreasing the power density of the transformer. Also, isolation material has power dissipation which is usually not significant compared to core loss or winding loss, but it should be considered during the design phase. Lifetime and insulation profile of the material should also be considered for the design because the isolation capability of the material degrades with time. List of potential dielectric materials that can be used as an isolation layer is provided in Table 7.

Dielectric strength is the maximum electric field that can exist in the insulating material before the electric breakdown takes place and the unit is provided as  $\left(\frac{kV}{mm}\right)$ . Dielectric constant or relative permittivity is the electric permittivity compared to air which is shown by  $\epsilon_r$ . Dielectric constant or relative permittivity of the material is a factor that the electric force between the electric charges in the material decreases compared to the air.

Table 7 Dielectric materials suitable for isolation layer

Material	Dielectric strength kV/mm	Dielectric constant ( $\epsilon_r$ )	Thermal conductivity W/mk	Tan ( $\delta$ )
Paper	22-49	2.3-5	0.05	6e-5
NOMEX	27	2.5-4	-	5e-3
Mica	11-43	2.5-7	0.71	-
Epoxy resin	15	3.6	0.25	0.021

Air	3	1	0.03	0
-----	---	---	------	---

The isolating materials of the transformer contribute to leakage inductance and thermal behavior of the transformer as well. Therefore, obtaining the optimum value of the thickness can be included in the multi-objective optimization routine. To ensure that the selected thickness that meets the isolation voltage, the minimum value for the design space should be chosen in a way that meets the required voltage isolation, and therefore all the points in the design space will provide the required voltage isolation level. Then, the optimization problem will determine the optimum value that ensures the leakage inductance and the thermal behavior.

Table 7 contains information about insulating materials that can be used in this type of transformer. There are more materials that could be considered as well, like different types of polymers. For all these materials, the dielectric strength (kV/mm) is a determining factor for choosing the thickness of the material. Higher dielectric strength is desirable because it will lead to thinner thickness of the material and higher power density. This value is provided by the manufacturer of the material. The minimum thickness of the isolation layer can be calculated using Eq. (60):

$$d_{cvw-min} = \frac{V_{iso-wc}}{E_{ins}} \quad (60)$$

where  $d_{cvw-min}$  is the minimum distance between the core and winding and  $V_{iso-wc}$  is the required isolation voltage between the core and winding, and  $E_{ins}$  is the dielectric strength of the insulating material that is used between winding and core. Similarly, the minimum thickness of the isolation layer between the primary and secondary winding can be extracted using Eq. (61):

$$w_{iso-min} = \frac{V_{iso-ww}}{E_{ins}} \quad (61)$$

where  $w_{iso-min}$  is the minimum distance between the primary winding and secondary winding and  $V_{iso-ww}$  is the required isolation voltage between the primary winding and secondary winding, and  $E_{ins}$  is the dielectric strength of the insulating material that is used between primary and secondary windings.

It should be noted that the dielectric strength of the insulating material degrades with time and this profile should be considered for extraction of estimated lifetime of the transformer. One way to address this issue is to add a coefficient when calculating the thickness of the insulating material.

For example,  $d_{cvw} > 2d_{cvw-min}$  or  $w_{iso} > 2w_{iso-min}$ . The coefficient can change based on the problem and the lifetime profile of the material. These limitations can be imposed to the optimization problem or they can be considered when determining the design space minimum values.

The second column of the Table 7 is showing the dielectric constant of the material which is also important for calculating the parasitic or capacitive coupling that might happen between windings and core or chassis of the converter. The third column of the Table 7 is showing the thermal conductivity of the insulating material. Higher thermal conductivity is desirable for the insulating material.

### 3.6 Leakage inductance

The leakage inductance is the inductance associated with the portion of magnetic flux that does not couple between the primary and secondary windings. The leaking flux and therefore the leakage inductance of the transformer will cause storage of magnetic energy within the window of the transformer. Therefore, the value of leakage inductance is dependent to the geometry of the transformer and the arrangement of the components of the transformer.

The leakage inductance of the transformer is an important design parameter for DAB applications because it has direct impact on the throughput power between input and output and it also has impact on the rate of increase and decrease of the switched current. To calculate the leakage inductance of the transformer, the idea that has been suggested in the literature is to calculate the energy stored inside the window of the transformer and relating this stored energy with the leakage inductance using Eq. (62). The total energy stored in primary and secondary windings in addition to the isolation layer is calculated in the following:

$$E_{CW} = E_{pcu} + E_{pbair} + E_{pins} + E_{pintwh} + E_{pintwv} + E_{pisowc} + E_{pairch} + E_{scu} + E_{sbair} + E_{sins} + E_{sintwh} + E_{sintwv} + E_{sisowc} + E_{sairch} + E_{iso} \quad (62)$$

$$E_{CW} = \frac{1}{2}LI^2 \quad (63)$$

where  $E_{cw}$  is the total energy stored in the core window,  $E_{pcu}$  is the energy stored in the copper of Litz bundles of the primary winding,  $E_{pins}$  is the energy stored in the insulation layer of the Litz bundles in the primary winding,  $E_{scu}$  is the energy stored in the secondary Litz bundles winding

$E_{sins}$  is the stored energy in the insulation layer of the secondary winding and  $E_{iso}$  is the stored energy in the isolation layer and  $E_{pintwh}$  is the energy stored in the air between the horizontal distance in Litz bundles of primary windings and of the primary winding and  $E_{sintwh}$  is the energy stored in the air and between the horizontal distance of Litz bundles of the secondary windings. Similarly,  $E_{pintwv}$  is the energy stored in the vertical air between the Litz bundles in the primary winding and  $E_{sintwv}$  is the same energy in the secondary windings.  $E_{pisowc}$  is the energy stored in the isolation layer between the winding and core of the primary winding and  $E_{sisowc}$  is the energy stored in the isolation layer between the secondary winding and the core.  $E_{pairch}$  is the magnetic energy stored in the air channel of the primary side winding and  $E_{sairch}$  is the energy stored in the air channel on the secondary winding side.  $E_{pbair}$  and  $E_{sbair}$  are the magnetic energy stored in the air between the strands in Litz bundle. It should be mentioned that  $E_{pcu}$  and  $E_{scu}$  are frequency dependent while  $E_{pins}$ ,  $E_{sins}$  and  $E_{iso}$  are not frequency dependent.  $L$  is the leakage inductance of the transformer referred to the primary side and  $I$  is the rms value of the primary current. In the following each of these components will be calculated. For this topology, the intensity of magnetic field ( $\vec{H}$ ) inside the Litz bundles in different layers are not equal and it is lower for the layers that are closer to the middle section of the core and it is higher for the layers that are closer to the outer layer of the transformer. The intensity of magnetic field in the insulation material of each layer is constant and it is equal to the peak value of the intensity in that layer. The stored energy inside the air between the copper strands is assumed to be negligible.

The components of energy stored in the window will be calculated in the following. Because of the symmetry of the design,  $E_{pins} = E_{sins} = E_{ins}$ ,  $E_{pintwh} = E_{sintwh} = E_{intwh}$ ,  $E_{pintwv} = E_{sintwv} = E_{intwv}$ ,  $E_{pisowc} = E_{sisowc} = E_{isowc}$ ,  $E_{pairch} = E_{sairch} = E_{airch}$ ,  $E_{pbair} = E_{sbair} = E_{bair}$  and  $E_{pcu} = E_{scu} = E_{cu}$ . Therefore, only three components of the total energy should be calculated, and the total energy takes the following form:

$$E_{CW} = 2(E_{cu} + E_{bair} + E_{ins} + E_{intwh} + E_{intwv} + E_{isowc} + E_{airch}) + E_{iso} \quad (64)$$

First, we calculate the  $E_{cu}$  which is the energy stored in the copper winding of either primary or secondary windings. Since the Litz wire winding is considered, the current density must be obtained inside the copper strand and the impact of skin effect must be incorporated. The intensity

of current density at radius  $r$  from the middle of one copper strand takes the following form if the proximity effect is neglected:

$$J(r) = J_s e^{-\frac{(d_{st}-r)}{\delta}} \quad (65)$$

where  $J_s$  is the current density at the surface of the wire,  $r$  is the radius of the cylindrical layer considered, and  $\delta = \sqrt{\frac{2}{\omega\mu\sigma}}$  is the skin depth of the conductor while  $\sigma$  is the conductivity of the conductor,  $\omega=2\pi f_{sw}$  where  $f_{sw}$  is the switching frequency and  $\mu=\mu_r\mu_0$  is the permeability of the conductor material.

To calculate the stored magnetic energy in the components of the transformer, we can integrate the magnetic energy density over the volume of the component. The magnetic energy density can be calculated using Eq. (66):

$$U_{st} = \frac{|\vec{B}|^2}{2\mu_0} \quad (66)$$

where  $U_{st}$  is the magnetic energy density of one copper strand in Litz bundle,  $\vec{B}$  is the magnetic flux density ( $\frac{Wb}{m^2}$ ) inside the copper strand, and  $\mu_0$  is the permeability of free space. Amper's law ( $\oint \vec{B} \cdot \vec{dl} = \mu_0 I_{enc}$ ) can be used to obtain the magnetic flux density ( $\vec{B}$ ) on the circumference of the considered area and  $I_{enc}$  is the total electric current passing through the considered area. For this application,  $I_{enc}$  is the peak current as it was shown in Fig. 5 and Fig. 6. The direction of the  $\vec{B}$  can be determined using right hand rule where if the thumb is placed on the direction of the electric current, the fingers will show the direction of magnetic flux density.

If the length of the winding layers assumed to be equal, total energy stored in one copper strand can be calculated as:

$$\begin{aligned} E_{st} &= l_w \int_0^{\frac{d_{st}}{2}} U_{st} dr = l_w \int_0^{\frac{d_{st}}{2}} \frac{(J_s e^{-\frac{(d_{st}-r)}{\delta}})^2}{2\mu_0} dr = \frac{1}{2\mu_0} l_w J_s^2 \int_0^{\frac{d_{st}}{2}} e^{-\frac{2(d_{st}-r)}{\delta}} dr = \\ & l_w \frac{1}{2\mu_0} J_s^2 \int_0^{\frac{d_{st}}{2}} e^{-\frac{2d_{st}}{\delta}} e^{\frac{2r}{\delta}} dr = l_w \frac{1}{2\mu_0} J_s^2 e^{-\frac{2d_{st}}{\delta}} \int_0^{\frac{d_{st}}{2}} e^{\frac{2r}{\delta}} dr = l_w \frac{1}{2\mu_0} J_s^2 e^{-\frac{2d_{st}}{\delta}} \frac{\delta}{2} (e^{\frac{d_{st}}{\delta}} - 1) = \\ & l_w \frac{1}{2\mu_0} \left(\frac{\mu_0 I_{st}}{2\pi \frac{d_{st}}{2}}\right)^2 e^{-\frac{2d_{st}}{\delta}} \frac{\delta}{2} (e^{\frac{d_{st}}{\delta}} - 1) = l_w \frac{\mu_0 I_{st}^2 \delta}{4\pi^2 d_{st}^2} e^{-\frac{2d_{st}}{\delta}} (e^{\frac{d_{st}}{\delta}} - 1) \end{aligned} \quad (67)$$

If it is assumed that magnetic field of each strand is only caused by the same strand, then total magnetic energy stored in one Litz bundle can be calculated using Eq. (68):

$$E_{litzcu} = n_{stv}n_{sth}l_w \frac{\mu_0 I_{st}^2 \delta}{4\pi^2 d_{st}^2} e^{-\frac{2d_{st}}{\delta}} \left( e^{\frac{d_{st}}{\delta}} - 1 \right) \quad (68)$$

and if we assume that the magnetic field in each Litz bundle on the same layer is only created by the same bundle, the total magnetic energy stored in the copper of first layer of winding can be calculated using Eq. (69):

$$E_{culayer} = n_{litzh}n_{stv}n_{sth}l_w \frac{\mu_0 I_{st}^2 \delta}{4\pi^2 d_{st}^2} e^{-\frac{2d_{st}}{\delta}} \left( e^{\frac{d_{st}}{\delta}} - 1 \right) \quad (69)$$

The total amount of energy stored in copper winding layers can be estimated by Eq. (70) using the assumptions made to derive Eq. (69):

$$E_{cu} = \sum_{i=1}^{n_{litzv}} n_{litzh}n_{stv}n_{sth}l_w \frac{\mu_0 (iI_{st}^2) \delta}{4\pi^2 d_{st}^2} e^{-\frac{2d_{st}}{\delta}} \left( e^{\frac{d_{st}}{\delta}} - 1 \right) = \\ n_{litzh}n_{stv}n_{sth}l_w \frac{\mu_0 (I_{st}^2) \delta}{4\pi^2 d_{st}^2} e^{-\frac{2d_{st}}{\delta}} \left( e^{\frac{d_{st}}{\delta}} - 1 \right) \left( \frac{1}{6} \right) (n_{litzv})(n_{litzv} + 1)(2n_{litzv} + 1) \quad (70)$$

It is seen from Eq. (70) that having multiple layers of winding significantly increases the total energy stored in copper layers of the windings. Therefore, for high switching frequency applications when low value of leakage inductance is preferred, it might be practical to only use one layer of Litz wire winding.

The second term of the stored energy is the energy stored in the air inside the Litz bundle. The magnetic field intensity of the air inside the Litz bundle is assumed to be constant in one layer of strand inside each bundle and equal to the magnetic field intensity of the outer layer of strand in the specific layer of strands considered. Therefore, the magnetic energy stored in the air between the copper strands of the first layer of winding strands closest to the core inside the Litz bundle will take the following form:

$$E_{bair_{st1}} = \int U_{bair_{st1}} dv \quad (71)$$

$$E_{bair_{st1}} = \int \frac{1}{\mu_0} \left( \frac{\mu_0 I_{st}}{2\pi \left( \frac{d_{st}}{2} \right)} \right)^2 l_w ds \quad (72)$$

$$E_{bair_{st1}} = l_w n_{sth} * d_{st}^2 \left( 1 - \frac{\pi}{4} \right) \frac{\mu_0 I_{st}^2}{\pi^2 d_{st}^2} \quad (73)$$



The total energy of the air between the copper strands in one Litz bundle will take the following form:

$$E_{bair_{litz}} = \sum_{i=1}^{i=n_{stv}} l_w n_{sth} * d_{st}^2 \left(1 - \frac{\pi}{4}\right) i \frac{\mu_0 I_{st}^2}{\pi^2 d_{st}^2} = l_w \frac{n_{stv}(n_{stv}+1)}{2} n_{sth} d_{st}^2 \left(1 - \frac{\pi}{4}\right) \frac{\mu_0 I_{st}^2}{\pi^2 d_{st}^2} \quad (74)$$

If a winding layer consisting of  $n_{litzh}$  and  $n_{litzv}$  bundles considered, then the total energy inside the air of the strands for the winding layer will take the form shown in Eq. (75):

$$E_{bair} = n_{litzh} \sum_{i=1}^{n_{litzv}} l_w \frac{n_{stv}(n_{stv}+1)}{2} n_{sth} d_{st}^2 \left(1 - \frac{\pi}{4}\right) \frac{\mu_0 I_{st}^2}{\pi^2 d_{st}^2} \quad (75)$$

$$E_{bair} = l_w n_{litzh} \frac{n_{litzv}(n_{litzv}+1)}{2} \frac{n_{stv}(n_{stv}+1)}{2} n_{sth} d_{st}^2 \left(1 - \frac{\pi}{4}\right) \frac{\mu_0 I_{st}^2}{\pi^2 d_{st}^2} \quad (76)$$

The third term in  $E_{CW}$  is the magnetic energy produced by insulation layers of the Litz bundles. If the coordinate system of Fig. 15 is considered, the magnetic field inside the insulating material of the Litz bundle will have four terms as the rectangular Litz bundle has four sides. The total energy stored in insulating material of the Litz bundle can be calculated as follow:

$$\vec{B}_{litzinlower} = \frac{\mu_0 I_{st}}{\pi d_{st}} \quad (77)$$

$$\vec{B}_{litzinupper} = \frac{\mu_0 n_{litzv} I_{st}}{\pi d_{st}} \quad (78)$$

$$\vec{B}_{litzinside} = \frac{\mu_0 I_{st} n_{litzv}}{\pi d_{st} 2} \quad (79)$$

$$E_{litzinsbundle} = \int U_{litzins} dv \quad (80)$$

$$E_{Litzinsbundle} = \int_0^{W_{litzins}} U_{litzinslower} dv + \int_0^{W_{litzins}} U_{litzinsupper} dv + 2 \int_0^{h_{litz} - 2W_{litzins}} U_{litzinside} dv \quad (81)$$

$$E_{Litzinsbundle} = \int_0^{W_{litzins}} l_w w_{litz} \frac{\mu_0 I_{st}^2}{\pi^2 d_{st}^2} dz + \int_0^{W_{litzins}} l_w w_{litz} \frac{\mu_0 (n_{stv} I_{st})^2}{\pi^2 d_{st}^2} dz + 2 \int_0^{h_{litz} - 2W_{litzins}} l_w w_{litzins} \frac{\mu_0 I_{st}^2}{\pi^2 d_{st}^2} \left(\frac{n_{litzv}}{2}\right)^2 dz \quad (82)$$

$$E_{Litzinsbundle} = l_w \frac{\mu_0 I_{st}^2}{\pi^2 d_{st}^2} (w_{litzins} w_{litz} (1 + n_{stv}^2) + 2w_{litzins} \frac{n_{litzv}^2}{4} (h_{litz} - 2w_{litzins})) \quad (83)$$

$$E_{Litzinslayer} = n_{litzh} E_{litzinsbundle} \quad (84)$$

$$E_{Litzinslayer} = n_{litzh} l_w \frac{\mu_0 I_{st}^2}{\pi^2 d_{st}^2} (w_{litzins} w_{litz} (1 + n_{stv}^2) + 2w_{litzins} \frac{n_{litzv}^2}{4} (h_{litz} - 2w_{litzins})) \quad (85)$$

$$E_{ins} = \sum_{i=1}^{n_{litzv}} n_{litzh} l_w \frac{\mu_0 (i I_{st})^2}{\pi^2 d_{st}^2} (w_{litzins} w_{litz} (1 + n_{stv}^2) + 2w_{litzins} \frac{n_{litzv}^2}{4} (h_{litz} - 2w_{litzins})) \quad (86)$$

$$E_{ins} = n_{litzh} l_w \frac{\mu_0 I_{st}^2}{\pi^2 d_{st}^2} (w_{litzins} w_{litz} (1 + n_{stv}^2) + 2w_{litzins} \frac{n_{litzv}^2}{4} (h_{litz} - 2w_{litzins})) \left(\frac{1}{6}\right) (n_{litzv})(n_{litzv} + 1)(2n_{litzv} + 1) \quad (87)$$

Next contributor to leakage energy is  $E_{intwh}$  which is the energy stored in the air between the horizontal distance between the Litz wires in one layer. This distance can provide control over the leakage inductance and the temperature of the winding. The magnetic flux density in this area is primarily formed by the two adjacent Litz bundles surrounding the area. The impact of the rest of the Litz bundles are ignored for this calculation. The first step in calculating the magnetic stored energy is calculation of magnetic flux density. If the coordinate system of Fig. 15 is considered, the following can be written:

$$y \in \left[-\frac{d_{litzh}}{2}, \frac{d_{litzh}}{2}\right], z \in [0, h_{litz}], x \in [0, l_w], \vec{B} = B_z(y) \vec{a}_z \quad (88)$$

In this area, considering the geometry, it is considered that the magnetic flux density has only component in z direction. Before deriving the formula for the magnetic flux density, the boundary conditions are investigated.

$$B_z(y = 0) = 0, B_z\left(y = -\frac{d_{litzh}}{2}\right) = -\frac{\mu_0 I}{n_{sth} h_{litz}}, B_z\left(y = \frac{d_{litzh}}{2}\right) = \frac{\mu_0 I}{n_{sth} h_{litz}} \quad (89)$$

$$B_z(y) = \frac{2\mu_0 I}{n_{sth} h_{litz} d_{litzh}} y \quad (90)$$

Therefore, the magnetic energy density takes the following form:

$$U_{intwh} = \frac{\left(\frac{2\mu_0 I}{n_{sth} h_{litz} d_{litzh}} y\right)^2}{\mu_0} = \frac{4\mu_0 I^2 y^2}{n_{sth}^2 h_{litz}^2 d_{litzh}^2} \quad (91)$$

The magnetic energy stored in this area can be calculated using integration of magnetic flux density over the volume:

$$E_{intwhb} = 2l_w \int_0^{\frac{d_{litzh}}{2}} \frac{4\mu_0 I^2 y^2}{n_{sth}^2 h_{litz}^2 d_{litzh}^2} dy = l_w \frac{\mu_0 I^2 d_{litzh}}{3n_{sth}^2 h_{litz}} \quad (92)$$

Total magnetic energy stored in the area between the Litz bundles can be calculated using summation of such energy over the volume:

$$E_{intwh} = n_{litzh} \sum_{i=1}^{n_{litzv}} l_w \frac{\mu_0 (iI)^2 d_{litzh}}{3n_{sth}^2 h_{litz}} = l_w n_{litzh} \frac{\mu_0 I^2 d_{litzh}}{3n_{sth}^2 h_{litz}} \left(\frac{1}{6}\right) (n_{litzv})(n_{litzv} + 1)(2n_{litzv} + 1) \quad (93)$$

The next component of leakage energy is the energy stored in the air between the horizontal area between the winding bundles in different layers, as it is shown by  $E_{intwv}$ . Similar approach that was taken to calculate the  $E_{intwh}$  can be taken. We start by assigning the coordinate system based on the Fig. 15 geometry and considering the boundary condition in the area:

$$z \in \left[-\frac{d_{litzv}}{2}, \frac{d_{litzv}}{2}\right], y \in [0, w_{litz}], x \in [0, l_w], \vec{B} = B_y(z) \vec{a}_y \quad (94)$$

$$B_y(z = 0) = 0, B_y\left(y = -\frac{d_{litzv}}{2}\right) = -\frac{\mu_0 I}{n_{stv} w_{litz}}, B_y\left(y = \frac{d_{litzv}}{2}\right) = \frac{\mu_0 I}{n_{stv} w_{litz}} \quad (95)$$

$$B_y(z) = \frac{2\mu_0 I}{n_{stv} w_{litz} d_{litzv}} z \quad (96)$$

The magnetic energy density will take the following form:

$$U_{intwv} = \frac{\left(\frac{2\mu_0 I}{n_{stv} w_{litz} d_{litzv}} z\right)^2}{\mu_0} = \frac{4\mu_0 I^2 z^2}{n_{stv}^2 w_{litz}^2 d_{litzv}^2} \quad (97)$$

The magnetic energy stored for one horizontal area between the two bundles will be:

$$E_{intwvb} = 2l_w \int_0^{\frac{d_{litzv}}{2}} \frac{4\mu_0 I^2 z^2}{n_{stv}^2 w_{litz}^2 d_{litzv}^2} dy = l_w \frac{\mu_0 I^2 d_{litzv}}{3n_{stv}^2 w_{litz}^2} \quad (98)$$

Total magnetic energy stored in the horizontal air area between the bundles can be calculated using Eq. (99):

$$E_{intwv} = n_{litzv} \sum_{i=1}^{n_{litzh}} l_w \frac{\mu_0 (iI)^2 d_{litzv}}{3n_{stv}^2 w_{litz}^2} l_w n_{litzv} \frac{\mu_0 I^2 d_{litzv}}{3n_{stv}^2 w_{litz}^2} \left(\frac{1}{6}\right) (n_{litzh})(n_{litzh} + 1)(2n_{litzh} + 1) \quad (99)$$

The next component that stores magnetic energy in the core window of the transformer is the isolation layers used between winding and core. There are two layers of isolation materials between winding and core in this topology. One that is used in the middle part of the core and one that is used between the outer layer of the winding and the inner side of the outer part of the core. The magnetic flux density in these two areas are different therefore, they store different amount of energy. We start by considering the isolation layer between the winding and middle side of the core component.

$$y \in [0, n_{litzh} w_{litz}], z \in [0, d_{cww}], x \in [0, l_w], \vec{B} = B_y(z) \vec{a}_y \quad (100)$$

$$B_y(z=0) = 0, B_y(z=d_{cww}) = -\mu_0 n_{litzh} I \quad (101)$$

$$B_y(z) = \frac{n_{litzh} \mu_0 I}{d_{cww}} z \quad (102)$$

$$U = \frac{n_{litzh}^2 \mu_0 I^2}{2d_{cww}^2} z^2 \quad (103)$$

$$E_{isowc} = \int_0^{d_{cww}} l_w n_{litzh} w_{litz} \frac{n_{litzh}^2 \mu_0 I^2}{2d_{cww}^2} z^2 dz = l_w w_{litz} \frac{n_{litzh}^3 \mu_0 I^2 d_{cww}}{6} \quad (104)$$

Similar approach can be taken to calculate the energy stored in the isolation layer between the outer layer of the winding with the inner layer of the outer layer of the core. The level of magnetic flux density is higher in that region that therefore, higher level of magnetic energy is stored in the insulation material. The approach to do the calculation is similar to the procedure that was done for the inner layer of the isolating material with modified magnetic flux density.

We start by considering the isolation layer between the winding and middle side of the core component.

$$y \in [0, n_{litzh}w_{litz}], z \in [0, d_{cww}], x \in [0, l_w], \vec{B} = B_y(z)\vec{a}_y \quad (105)$$

$$B_y(z=0) = 0, B_y(z=d_{cww}) = -\mu_0 n_{litzh} n_{litzv} I \quad (106)$$

$$B_y(z) = \frac{n_{litzh} n_{litzv} \mu_0 I}{d_{cww}} z \quad (107)$$

$$U = \frac{n_{litzh}^2 n_{litzv}^2 \mu_0 I^2}{2 d_{cww}^2} z^2 \quad (108)$$

$$E_{isowc} = \int_0^{d_{cww}} l_w n_{litzh} w_{litz} \frac{n_{litzh}^2 n_{litzv}^2 \mu_0 I^2}{2 d_{cww}^2} z^2 dz = l_w w_{litz} \frac{n_{litzh}^3 n_{litzv}^2 \mu_0 I^2 d_{cww}}{6} \quad (109)$$

The next component contributing to the stored energy is the isolation layer between the windings. The approach to calculate the stored energy in this insulating material is similar to the rest of the components. First, the functionality of the magnetic flux density should be determined and then integration over the volume of the material should take place. The coordinate system and the boundary conditions will take the following format:

$$y \in [-\frac{w_{iso}}{2}, \frac{w_{iso}}{2}], z \in [0, n_{litzv} h_{litz}], x \in [0, l_w], \vec{B} = B_z(y)\vec{a}_z \quad (110)$$

Since in this design the ratio of the turns and the voltage of the primary and secondary windings are the same and there is a symmetry in the system, the current that is flowing in the primary and secondary windings are equal in amplitude but in opposite direction. Therefore, we can write:

$$B_z(y=0) = 0, B_z(y=-\frac{w_{iso}}{2}) = -\frac{\mu_0 I}{2 h_{litz}}, B_z(y=\frac{w_{iso}}{2}) = \frac{\mu_0 I}{2 h_{litz}} \quad (111)$$

$$B_z(y) = \frac{\mu_0 I}{w_{iso} h_{litz}} z \quad (112)$$

$$U = \frac{\mu_0^2 I^2}{w_{iso}^2 h_{litz}^2} z^2 \quad (113)$$

$$E_{iso} = 2 \int_0^{w_{iso}} l_w \frac{\mu_0^2 I^2}{w_{iso}^2 h_{litz}^2} z^2 dz = l_w \frac{2 \mu_0^2 I^2 w_{iso}}{3 h_{litz}^2} \quad (114)$$

Finally, the magnetic energy stored in air channels on the right side and left side of the windings should be calculated. If this area is considered as a round area can write:

$$r \in [0, \frac{n_{lithv} h_{litz}}{2}], \varphi \in [0, \pi], x \in [0, l_w], \vec{B} = B_\varphi(r)\vec{a}_\varphi \quad (115)$$

$$B_\varphi\left(\frac{n_{lithv} h_{litz}}{2}\right) = \frac{\mu_0 I}{h_{litz} n_{litzv}} \quad (116)$$

$$U = \frac{\mu_0^2 I^2}{h_{litz}^2 n_{litzv}^2} \quad (117)$$

$$E_{airch} = 2 \int_0^\pi l_w \frac{\mu_0^2 I^2}{h_{litz}^2 n_{litzv}^2} d\varphi = l_w \frac{2 \mu_0^2 I^2 \pi}{h_{litz}^2 n_{litzv}^2} \quad (118)$$

Total energy stored in the transformer window can be calculated as follow:

$$\begin{aligned}
 E_{CW} = & 2(n_{litzh}n_{stvh}n_{sth}l_w \frac{\mu_0 I^2 \delta}{n_{st}^2 4\pi^2 d_{st}^2} e^{-\frac{2d_{st}}{\delta}} (e^{\frac{d_{st}}{\delta}} - 1) (\frac{1}{6})(n_{litzv})(n_{litzv} + 1)(2n_{litzv} + 1) + \\
 & l_w n_{litzh} \frac{n_{litzv}(n_{litzv}+1)}{2} \frac{n_{stvh}(n_{stvh}+1)}{2} n_{sth} (1 - \frac{\pi}{4}) \frac{\mu_0 I_{st}^2}{\pi^2} + n_{litzh} l_w \frac{\mu_0 I^2}{n_{st}^2 \pi^2 d_{st}^2} (w_{litzins} w_{litz} (1 + n_{stvh}^2) + \\
 & l_w n_{litzh} \frac{\mu_0 I^2 d_{litzh}}{3n_{sth}^2 h_{litz}^2} (\frac{1}{6})(n_{litzv})(n_{litzv} + 1)(2n_{litzv} + 1) + 2w_{litzins} \frac{n_{litzv}^2}{4} (h_{litz} - \\
 & 2w_{litzins})) (\frac{1}{6})(n_{litzv})(n_{litzv} + 1)(2n_{litzv} + 1) + l_w n_{litzv} \frac{\mu_0 I^2 d_{litzv}}{3n_{stvh}^2 w_{litz}^2} (\frac{1}{6})(n_{litzh})(n_{litzh} + 1)(2n_{litzh} + \\
 & 1) w_{litz} \frac{n_{litzh}^3 \mu_0 I^2 d_{cww}}{6} + l_w w_{litz} \frac{n_{litzh}^3 n_{litzv}^2 \mu_0 I^2 d_{cww}}{6} + l_w \frac{2\mu_0^2 I^2 \pi}{h_{litz}^2 n_{litzv}^2} + l_w \frac{2\mu_0^2 I^2 w_{iso}}{3h_{litz}^2}
 \end{aligned} \tag{119}$$

Therefore, the leakage inductance will be:

$$\begin{aligned}
 L = & 4(n_{litzh}n_{stvh}n_{sth}l_w \frac{\mu_0 \delta}{n_{st}^2 4\pi^2 d_{st}^2} e^{-\frac{2d_{st}}{\delta}} (e^{\frac{d_{st}}{\delta}} - 1) (\frac{1}{6})(n_{litzv})(n_{litzv} + 1)(2n_{litzv} + 1) + \\
 & l_w n_{litzh} \frac{n_{litzv}(n_{litzv}+1)}{2} \frac{n_{stvh}(n_{stvh}+1)}{2} n_{sth} (1 - \frac{\pi}{4}) \frac{\mu_0}{n_{st}^2 \pi^2} + n_{litzh} l_w \frac{\mu_0}{n_{st}^2 \pi^2 d_{st}^2} (w_{litzins} w_{litz} (1 + n_{stvh}^2) + \\
 & 2w_{litzins} \frac{\mu_0 n_{litzv}^2}{4} (h_{litz} - 2w_{litzins})) (\frac{1}{6})(n_{litzv})(n_{litzv} + 1)(2n_{litzv} + 1) + \\
 & l_w n_{litzv} \frac{\mu_0 d_{litzv}}{3w_{litz}^2} (\frac{1}{6})(n_{litzh})(n_{litzh} + 1)(2n_{litzh} + 1) + l_w w_{litz} \frac{n_{litzh}^3 \mu_0 d_{cww}}{6} + l_w w_{litz} \frac{n_{litzh}^3 n_{litzv}^2 \mu_0 d_{cww}}{6} + \\
 & l_w \frac{2\mu_0^2 \pi}{h_{litz}^2 n_{litzv}^2} + 2l_w \frac{2\mu_0^2 w_{iso}}{3h_{litz}^2}
 \end{aligned} \tag{120}$$

To investigate the accuracy of Eq. (120), a case study with the parameters as shown in Table 8 is performed. The computer code that was used to obtain these values are provided in Appendix II.

Table 8 Parameters considered for a leakage inductance case study

Parameter	Description	Value
$d_{st}$	Diameter of the copper strand inside the Litz bundle	0.5 (mm)
$n_{stvh}$	Number of copper strands placed in a Litz bundle vertically	10
$n_{sth}$	Number of copper strands placed in a Litz bundle horizontally	30
$w_{litzins}$	Width of the insulation layer of Litz wire	1 (mm)
$d_{litzbv}$	Vertical distance between Litz bundles	1 (mm)
$d_{litzbh}$	Horizontal distance between Litz bundles	1 (mm)
$n_{litzh}$	Number of Litz bundles placed horizontally in a core window	10

$n_{litzv}$	Number of Litz bundles placed vertically in a core window	1
$r_{wi}$	Inner radius of the windings	15 (mm)
$r_{ci}$	Inner radius of the core	10 (mm)
$l_c$	Length of the magnetic core	30 (mm)
$w_{iso}$	Width of the insulation layer	10 (mm)
$d_{cww}$	Thickness of the insulation layer between the core and the winding	10 (mm)
$n_c$	Number of core stacks	10

Table 9 shows the value of magnetic energy stored in each section of the core during one switching period when  $f_{sw} = 40$  kHz. The computer code that was used to extract these values is provided in Appendix III.

Table 9 Magnetic energy stored in elements of transformer inside the core window due to leakage flux

Parameter	Description	Value
$E_{cu}$	Energy stored in the copper strands in the windings	0.1994 (J)
$E_{bair}$	Energy stored in the air inside the Litz bundle	0.0008 (J)
$E_{ins}$	Energy stored in the insulation layer of Litz bundle	0.0382 (J)
$E_{intwh}$	Energy stored in the air in horizontal distance between Litz bundles	0.0369 (J)
$E_{intwv}$	Energy stored in the air in vertical distance between Litz bundles	0.0264 (J)
$E_{isowc}$	Energy stored in the isolation layer between winding and core	0.0010 (J)
$E_{iso}$	Energy stored in the isolation layer between the windings	0.0560 (J)
$E_{airch}$	Energy stored in the air channel on the sides of the windings	0.0046 (J)
$E_{cw}$	Total energy stored in the core window	0.3646 (J)
$L$	Leakage Inductance	18.2 ( $\mu H$ )

### 3.7 Thermal management of the HFPT

The heat dissipation process between the suggested HFPT topology and the ambient environment is through convection and radiation processes. The thermal conduction takes place inside the HFPT and between the internal components, for example, between the core and the insulation material or between the winding layers. Therefore, it is necessary to study the convection and radiation heat transfer mechanisms as well as developing a thermal network model that incorporates the thermal conduction process.

The newton formula for the heat transfer for convection is shown in Eq. (121):

$$P_{conv} = h_{conv}A_{conv}(T_{sf} - T_a) \quad (121)$$

where  $P_{conv}$  is the dissipated heat through the convection process,  $h_{conv}$  is the convection heat transfer coefficient,  $A_{conv}$  is the surface area that the convection process takes place,  $T_{sf}$  is the surface temperature and  $T_a$  is the ambient temperature. Calculation of the convection heat transfer coefficient can be done using Nusselt number and the following expression is reported in [16]:

$$h_{conv} = \left( 0.68 + \frac{0.67(g(\frac{2}{T_{sf}+T_a})(T_{sf}-T_a)L^3Pr/v^3)^{0.25}}{((1+0.492/Pr)^{9/16})^{4/9}} \right) \frac{k}{L} \quad (122)$$

where  $g$  ( $m/s^2$ ) is the gravity,  $L$  is the distance propagated by the coolant,  $Pr$  is Prandtl number,  $v$  is the kinematic viscosity and  $k$  is the thermal conductivity of the coolant which in this case is the air and Prandtl number can be calculated from the following equation [16]:

$$Pr = c_p \frac{\mu}{k} \quad (123)$$

where  $\mu$  is the dynamic viscosity and  $c_p$  is the specific heat capacity. Similar formula is used for the radiation process:

$$P_{rad} = h_{rad}A_{rad}(T_{sf} - T_a) \quad (124)$$

where  $P_{rad}$  is the dissipated heat through the radiation process,  $h_{rad}$  is the radiation heat transfer coefficient. The radiation heat transfer coefficient can be calculated using eq (63):

$$h_{rad} = \frac{\varepsilon_{rad}\sigma_{sb}(T_{sf}^4 - T_a^4)}{T_{sf} - T_a} \quad (125)$$





different thermal conductivity. Therefore, for accurate practical calculations, the thermal conductivity should be checked with the manufacture. In this study, the pure aluminum is considered in analytical and optimization calculations. Thermal conductivity of the materials used for extracting the thermal resistance can be found in Table 10.

Table 10 Parameters used in thermal model of HFPT

Parameter	Description
$P_{CM}$	Heat generated by the central core section
$P_{CO}$	Heat generated by the outer flat core section
$P_{CR}$	Heat generated by the side round core section
$R_{th,clf}$	Thermal resistance of the insulation layer between core and winding
$R_{th,pweq}$	thermal resistance between the insulation layer and the middle point of windings
$R_{th,cram}$	Thermal resistance between round core part and the ambient
$R_{th,rcrm}$	Thermal resistance of the vertical round side of the core and the central part
$T_{CO}$	Temperature of the outer core part
$T_{CM}$	Temperature of the central core part
$T_{CR}$	Temperature of the round core part
$T_{am}$	Ambient temperature
$T_{SWU}$	Temperature of the middle point of the secondary winding in upper half
$T_{PWU}$	Temperature of the middle point of the primary winding in upper half
$T_{SWL}$	Temperature of the middle point of the secondary winding in lower half
$T_{PWL}$	Temperature of the middle point of the primary winding in lower half

Table 11 shows the heat transfer mechanism for different areas of the HFPT.

Table 11 Heat transfer mechanism for different parts of the HFPT

Heat transfer	Mechanism
Core to coil former insulator	Conduction
winding insulation to coil former	Conduction

Core to heatsink	Conduction
Heatsink to ambient	Convection and radiation
Core to ambient	Convection and radiation
Coil former insulation to air	Convection and radiation

The thermal resistance of the metal can be calculated using Eq. (126)

$$R_{th} = \frac{l_{cond}}{\sigma_{cond} A_{cond}} \tag{126}$$

where  $l_{cond}$  is the length of the material that the conduction is taking place through it,  $\sigma_{cond}$  is the conductivity of the material and  $A_{cond}$  is the cross sectional area where the conduction process takes place. In the HFPT problem, there is a thermal conduction inside the Litz bundle and between the strands. Depending on the cross-sectional current density inside the bundle this temperature of the strands can be different. However, in this study we assume that there is a uniform current density distribution inside the Litz bundle.

If the bundles are arranged with no distance between the bundles, there will be a thermal conduction between the Litz bundles as well. However, in this study it is assumed that the Litz bundle has an insulator and the conduction between the two bundle is assumed to be negligible. Therefore, we assume that the temperature of the conducting conductors are the same. The variable  $T_w$  is associated to this temperature. Regarding the temperature of the core, we assign three different core temperatures,  $T_{CO}$  which refers to the temperature of the I core on the outside where it is in contact with heatsink,  $T_{CM}$  which refers to the temperature of the I core in the middle parts of the HFPT and  $T_{CR}$  which refers to the temperature of the C core which is in contact with air without heatsink. The heat transfer differential equation can be written as follow [16, 23]:

$$C_{SWU} \frac{dT_{PWU}}{dt} = \frac{1}{R_{th,sweq} + R_{th,clf}} (T_{COU} - T_{SWU}) + \frac{1}{R_{th,pweq} + R_{th,clf}} (T_{CM} - T_{SWU}) + \frac{1}{R_{th,crswu}} (T_{CRU} - T_{SWU}) + P_{SWU} \tag{127}$$

$$C_{PWU} \frac{dT_{PWU}}{dt} = \frac{1}{R_{th,pweq} + R_{th,clf}} (T_{COU} - T_{PWU}) + \frac{1}{R_{th,pweq} + R_{th,clf}} (T_{CM} - T_{PWU}) + \frac{1}{R_{th,crpwu}} (T_{CRU} - T_{PWU}) + P_{PWU} \tag{128}$$

$$C_{SWL} \frac{dT_{SWL}}{dt} = \frac{1}{R_{th,sweq} + R_{th,clf}} (T_{COL} - T_{SWL}) + \frac{1}{R_{th,sweq} + R_{th,clf}} (T_{CM} - T_{SWL}) + \frac{1}{R_{th,crswL}} (T_{CRL} - T_{SWL}) + P_{SWL} \quad (129)$$

$$C_{PWL} \frac{dT_{PWL}}{dt} = \frac{1}{R_{th,pweq} + R_{th,clf}} (T_{COL} - T_{PWL}) + \frac{1}{R_{th,pweq} + R_{th,clf}} (T_{CM} - T_{PWL}) + \frac{1}{R_{th,crpwL}} (T_{CRL} - T_{PWL}) + P_{PWL} \quad (130)$$

$$C_{CM} \frac{dT_{CM}}{dt} = \frac{1}{R_{th,clf} + R_{th,sweq}} (T_{SWU} - T_{CM}) + \frac{1}{R_{th,clf} + R_{th,pweq}} (T_{PWU} - T_{CM}) + \frac{1}{R_{th,clf} + R_{th,sweq}} (T_{SWL} - T_{CM}) \\ + \frac{1}{R_{th,clf} + R_{th,pweq}} (T_{PWL} - T_{CM}) + \frac{2}{R_{th,crco}} (T_{CRL} - T_{CM}) + \frac{2}{R_{th,crco}} (T_{CRU} - T_{CM}) + P_{CM} \quad (140)$$

$$C_{COU} \frac{dT_{COU}}{dt} = \frac{2}{R_{th,crco}} (T_{CRU} - T_{COU}) + \frac{1}{R_{th,clf} + R_{th,sweq}} (T_{SWU} - T_{COU}) + \frac{1}{R_{th,clf} + R_{th,pweq}} (T_{PWU} - T_{COU}) \\ + \frac{1}{R_{th,hs}} (T_{am} - T_{COU}) + P_{COU} \quad (141)$$

$$C_{COL} \frac{dT_{COL}}{dt} = \frac{2}{R_{th,crco}} (T_{CRL} - T_{COL}) + \frac{1}{R_{th,clf} + R_{th,sweq}} (T_{SWL} - T_{COL}) + \frac{1}{R_{th,clf} + R_{th,pweq}} (T_{PWL} - T_{COL}) \\ + \frac{1}{R_{th,hs}} (T_{am} - T_{COL}) + P_{COL} \quad (142)$$

$$C_{CRU} \frac{dT_{CRU}}{dt} = \frac{1}{R_{th,crco}} (T_{COU} - T_{CRU}) + \frac{1}{R_{th,crswu}} (T_{SWU} - T_{CRU}) + \frac{1}{R_{th,crco}} (T_{CM} - T_{SWU}) + \frac{1}{R_{th,crco}} (T_{am} - T_{CRU}) + P_{CRU} \quad (143)$$

$$C_{CRL} \frac{dT_{CRL}}{dt} = \frac{1}{R_{th,crco}} (T_{COL} - T_{CRL}) + \frac{1}{R_{th,crswu}} (T_{SWL} - T_{CRL}) + \frac{1}{R_{th,crco}} (T_{CM} - T_{CRL}) + \frac{1}{R_{th,crco}} (T_{am} - T_{CRL}) + P_{CRL} \quad (144)$$

To represent the Eq. (127) – Eq (144) in a matrix format, the temperature matrix can be defined in the form represented in Eq. (145) and the differential equations can be represented using Eq. (146)

$$T = (T_{SWU} \quad T_{PWU} \quad T_{SWL} \quad T_{PWL} \quad T_{CM} \quad T_{COU} \quad T_{COL} \quad T_{CRU} \quad T_{CRL})^T \quad (145)$$

$$AT + BU = 0 \quad (146)$$

where the T is the temperature matrix defined in Eq. (145), U is the loss matrix or the input matrix defined in Eq. (149), the A is the thermal resistance matrix defined in Eq. (148), and B is defined in Eq (150):

$$T = -A^{-1}BU \quad (147)$$

$$A = \begin{pmatrix} R_{SWU} & 0 & 0 & 0 & \frac{1}{R_{th,pweq} + R_{th,clf}} & \frac{1}{R_{th,sweq} + R_{th,clf}} & 0 & \frac{1}{R_{th,crswu}} & 0 \\ 0 & R_{PWU} & 0 & 0 & \frac{1}{R_{th,pweq} + R_{th,clf}} & \frac{1}{R_{th,pweq} + R_{th,clf}} & 0 & \frac{1}{R_{th,crpwu}} & 0 \\ 0 & 0 & R_{SWL} & 0 & \frac{1}{R_{th,sweq} + R_{th,clf}} & 0 & \frac{1}{R_{th,sweq} + R_{th,clf}} & 0 & 0 \\ 0 & 0 & 0 & R_{PWL} & \frac{1}{R_{th,pweq} + R_{th,clf}} & 0 & \frac{1}{R_{th,pweq} + R_{th,clf}} & 0 & \frac{1}{R_{th,crpwl}} \\ \frac{1}{R_{th,clf} + R_{th,sweq}} & \frac{1}{R_{th,clf} + R_{th,pweq}} & \frac{1}{R_{th,clf} + R_{th,sweq}} & \frac{1}{R_{th,clf} + R_{th,pweq}} & R_{CM} & 0 & 0 & \frac{2}{R_{th,crclm}} & \frac{2}{R_{th,crclm}} \\ \frac{1}{R_{th,clf} + R_{th,sweq}} & \frac{1}{R_{th,clf} + R_{th,pweq}} & 0 & 0 & 0 & R_{COU} & 0 & \frac{2}{R_{th,crco}} & 0 \\ 0 & 0 & \frac{1}{R_{th,clf} + R_{th,sweq}} & \frac{1}{R_{th,clf} + R_{th,pweq}} & 0 & 0 & R_{COL} & 0 & \frac{2}{R_{th,crco}} \\ \frac{1}{R_{th,crswu}} & 0 & 0 & 0 & \frac{1}{R_{th,crclm}} & \frac{1}{R_{th,crco}} & 0 & R_{CRU} & 0 \\ 0 & 0 & \frac{1}{R_{th,crco}} & 0 & \frac{1}{R_{th,crclm}} & 0 & \frac{1}{R_{th,crswu}} & 0 & R_{CRL} \end{pmatrix} \quad (148)$$

$$U = (P_{SWU} \quad P_{SWL} \quad P_{PWU} \quad P_{PWL} \quad P_{COU} \quad P_{COL} \quad P_{CM} \quad P_{CRU} \quad P_{CRL} \quad T_{am})^T \quad (149)$$

$$B = \begin{pmatrix} 1 & 0 & 0 & 0 & 0 & 0 & 0 & 0 & 0 & 0 \\ 0 & 1 & 0 & 0 & 0 & 0 & 0 & 0 & 0 & 0 \\ 0 & 0 & 1 & 0 & 0 & 0 & 0 & 0 & 0 & 0 \\ 0 & 0 & 0 & 1 & 0 & 0 & 0 & 0 & 0 & 0 \\ 0 & 0 & 0 & 0 & 1 & 0 & 0 & 0 & 0 & 0 \\ 0 & 0 & 0 & 0 & 0 & 1 & 0 & 0 & 0 & \frac{1}{R_{th,hs}} \\ 0 & 0 & 0 & 0 & 0 & 0 & 1 & 0 & 0 & \frac{1}{R_{th,hs}} \\ 0 & 0 & 0 & 0 & 0 & 0 & 0 & 1 & 0 & \frac{1}{R_{th,crclm}} \\ 0 & 0 & 0 & 0 & 0 & 0 & 0 & 0 & 1 & \frac{1}{R_{th,crclm}} \end{pmatrix} \quad (150)$$

The diagonal elements in A matrix are defined using Eq. (151) – Eq. (159)

$$R_{CRL} = - \left( \frac{1}{R_{th,crco}} + \frac{1}{R_{th,crswu}} + \frac{1}{R_{th,crclm}} + \frac{1}{R_{th,crclm}} \right) \quad (151)$$

$$R_{CRU} = - \left( \frac{1}{R_{th,crco}} + \frac{1}{R_{th,crswu}} + \frac{1}{R_{th,crclm}} \right) \quad (152)$$

$$R_{COL} = - \left( \frac{2}{R_{th,crco}} + \frac{1}{R_{th,clf} + R_{th,sweq}} + \frac{1}{R_{th,clf} + R_{th,pweq}} + \frac{1}{R_{th,hs}} \right) \quad (153)$$

$$R_{COU} = - \left( \frac{2}{R_{th,crco}} + \frac{1}{R_{th,clf} + R_{th,sweq}} + \frac{1}{R_{th,clf} + R_{th,pweq}} + \frac{1}{R_{th,hs}} \right) \quad (154)$$

$$R_{CM} = - \left( \frac{1}{R_{th,clf} + R_{th,sweq}} + \frac{1}{R_{th,clf} + R_{th,pweq}} + \frac{1}{R_{th,clf} + R_{th,sweq}} + \frac{1}{R_{th,clf} + R_{th,pweq}} + \frac{2}{R_{th,crclm}} + \frac{2}{R_{th,crclm}} \right) \quad (155)$$

$$R_{PWL} = - \left( \frac{1}{R_{th,pweq} + R_{th,clf}} + \frac{1}{R_{th,pweq} + R_{th,clf}} + \frac{1}{R_{th,crpwl}} \right) \quad (156)$$

$$R_{SWL} = - \left( \frac{1}{R_{th,sweq} + R_{th,clf}} + \frac{1}{R_{th,sweq} + R_{th,clf}} + \frac{1}{R_{th,crswl}} \right) \quad (157)$$

$$R_{PWU} = - \left( \frac{1}{R_{th,pweq} + R_{th,clf}} + \frac{1}{R_{th,pweq} + R_{th,clf}} + \frac{1}{R_{th,crpwu}} \right) \quad (158)$$

$$R_{SWU} = - \left( \frac{1}{R_{th,sweq} + R_{th,clf}} + \frac{1}{R_{th,pweq} + R_{th,clf}} + \frac{1}{R_{th,crswu}} \right) \quad (159)$$

Now, it is necessary to define the values of the thermal resistances based on the physical properties of the system, Eq. (160) – Eq. (169) show the formulas for the thermal resistances.

$$R_{th,pweq} = \frac{2w_{litzins}}{\sigma_{ins} w_{litz}} + \frac{n_{sth}}{n_{stv} \sigma_{cu}} \quad (160)$$

$$R_{th,clf} = \frac{d_{cwp}}{l_c w_p \sigma_{ins}} \quad (161)$$

$$R_{th,sweq} = \frac{2w_{litzins}}{\sigma_{ins} w_{litz}} + \frac{n_{sth}}{n_{stv} \sigma_{cu}} \quad (162)$$

$$R_{th,crswu} = \frac{1}{\pi r_{ci} l_c h_{conv}} \quad (163)$$

$$R_{th,crpwu} = \frac{1}{\pi r_{ci} l_c h_{conv}} \quad (164)$$

$$R_{th,crpwL} = \frac{1}{\pi r_{ci} l_c h_{conv}} \quad (165)$$

$$R_{th,crclm} = \frac{\pi(r_{ci} + d_c)}{4d_c l_c \sigma_c} \quad (166)$$

$$R_{th,crco} = \frac{\pi(r_{ci} + d_c)}{4d_c l_c \sigma_c} \quad (167)$$

$$R_{th,crswu} = \frac{1}{\pi r_{ci} l_c h_{conv}} \quad (168)$$

$$R_{th,cram} = \frac{1}{(h_{conv} + h_{rad})\pi(r_{ci} + d_c)l_c} \quad (169)$$

The values of the core loss and winding loss for different parts of the HFPT can be calculated using Eq. (170) to Eq. (176):

$$P_{CO} = w_{cf} l_c d_c k_c f^\alpha B_m^\beta \quad (170)$$

$$P_{CR} = \pi r_{ci} d_c l_c k_c f^\alpha B_m^\beta \quad (171)$$

$$P_{CM} = 2P_{CO} \quad (172)$$

$$P_{SWU} = \sum_{i=1}^{n_{litz}} (l_c + \pi(r_{wsi} + (i-1)h_{litz})) \quad (173)$$

$$P_{SWL} = P_{SWU} \quad (174)$$

$$P_{PWU} = \sum_{i=1}^{n_{litz}} (l_c + \pi(r_{wpi} + (i-1)h_{litz})) \quad (175)$$

$$P_{PWL} = P_{PWU} \quad (176)$$

### 3.8 A design case study

A design case study is performed suitable for shipboard application with the H-bridge DAB DC-DC converter topology using SiC power module CAS300M17BM2. The rated values of the converter are provided in Table 12. The results of applying the design algorithm shown in Fig. 3 is shown in Fig. 17. The value of isolation voltage is assumed to be 60kV because this value is the maximum value in MV voltage range. Nanocrystalline Vitroperm500F is considered for the core material because of the thermal behavior and the manufacturing process that enables production of cut core pieces that are oval shape and they are suitable for the geometry that is considered in this study. Epoxy resin for coil former, CoolPolyD5108 for isolation layer and textile yarn for the insulation layer of the Litz wire are considered for optimization routine as it is shown in Fig. 17.

Table 12 HFPT design requirements for a design case study

Parameter	Description	Value	Unit
$P_{out}$	Rated output power	250	kW
$V_1$	Primary Voltage	1000	V
$V_2$	Secondary Voltage	1000	V
L	Leakage Inductance	18.6	$\mu$ H
n	Turns ratio	1	-
$V_{iso}$	Isolation Voltage	60000	V
f	Switching Frequency	40000	Hz
$T_{max}$	Maximum Temperature	80	$^{\circ}$ C
$T_{am}$	Ambient Temperature	55	$^{\circ}$ C

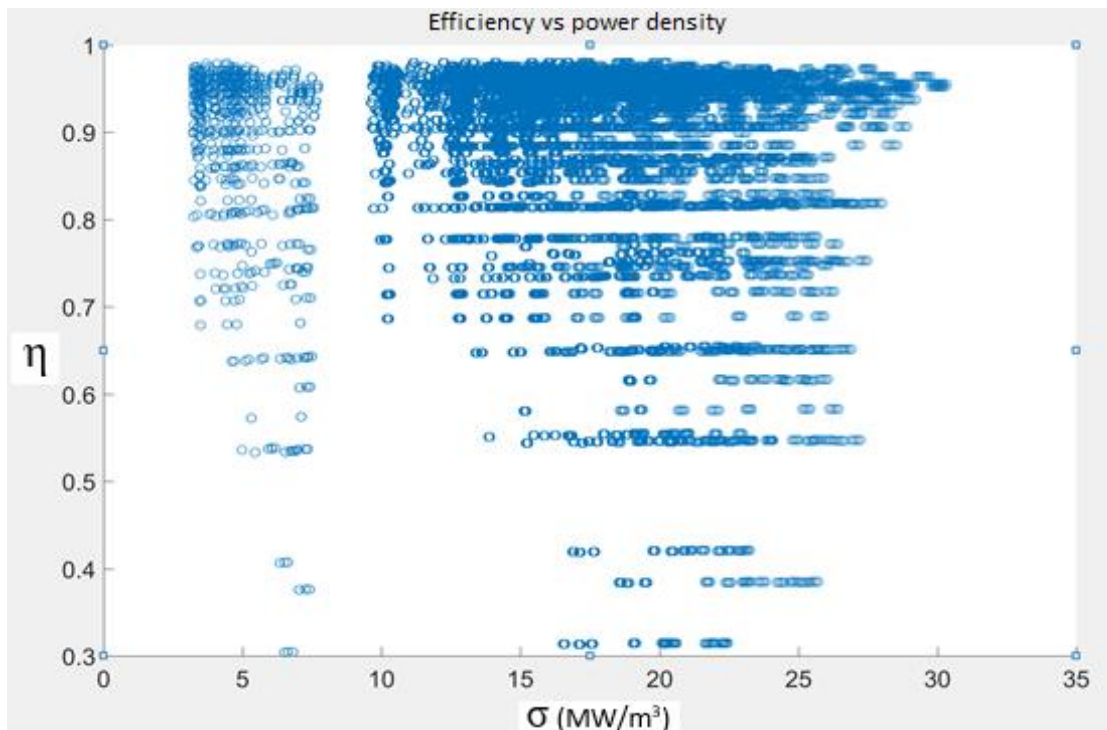


Fig. 17 Efficiency versus power density of transformer

Each circle in Fig. 17 corresponds to one design where the efficiency of the design and power density of the design ( $\text{MW}/\text{m}^3$ ) is plotted where the design parameters were swept through the design space and efficiency ( $\eta$ ) is defined as the ratio of output power to the input power ( $\eta = (P_{in} - P_{loss})/P_{in}$ ) and power density is the output power divided by the volume of the HFPT ( $\sigma = P_{out}/V_{HFPT}$ ) where  $V_{HFPT}$  is the volume of the transformer. This figure shows that with this topology and the limitations assumed for the analytical study, the power density as high as  $30 \text{ MW}/\text{m}^3$  ( $\text{kW}/\text{lit}$ ) and efficiency of about 98% can be achieved for the transformer. For example, the design with parameters that are shown in Table 13, the efficiency of 98% and the power density of  $20 \text{ MW}/\text{m}^3$  is calculated. The value of winding loss for this design is 3224 W and the value of core loss is 1820 W and the temperature matrix takes the values of  $T = [73 \ 73 \ 78 \ 78 \ 80 \ 75 \ 75 \ 76 \ 76]$ . The value of leakage inductance for this design is  $L=18.2 \ \mu\text{H}$ .

Table 13 Optimal values of the design variables for physics-based approach

Variable	Description	Optimal Value based on Fig 17	Unit
$x_1$	Diameter of the copper strand inside the Litz bundle	0.00060	m
$x_2$	Number of copper strands placed in a Litz bundle vertically	10.0000	-
$x_3$	Number of copper strands placed in a Litz bundle horizontally	21.0000	-



$x_4$	Width of the insulation layer of Litz wire	0.0020	m
$x_5$	Vertical distance between Litz bundles	0.00050	m
$x_6$	Horizontal distance between Litz bundles	0.00001	m
$x_7$	Number of Litz bundles placed horizontally in a core window	12.00000	-
$x_8$	Number of Litz bundles placed vertically in a core window	1.00000	-
$x_9$	Inner radius of the windings	0.01500	m
$x_{10}$	Thickness of the core	0.00130	m
$x_{11}$	Inner radius of the core	0.03750	m
$x_{12}$	Length of the magnetic core	0.12500	m
$x_{13}$	Width of the insulation layer	0.01000	m
$x_{14}$	Thickness of the insulation layer between the core and the winding	0.01000	m
$x_{15}$	Height of the heatsink	0.01500	m
$x_{16}$	Height of the base part of the heatsink	0.00200	m
$x_{17}$	Width of the fin	0.00300	m

If higher resolution of the temperature model along with larger design space is considered for the design problem, the computational power needed for the design will increase significantly. Therefore, more intelligent design method can be used. Optimization of the design is another aspect that is highly favorable. Multi-Objective Optimization (MO<sub>2</sub>) is needed for performing the optimization task. Optimization of HFPT using Genetic Algorithm (GA) will be discussed in chapter 4.

#### 4- OPTIMIZATION OF HFPT

Independent design parameters of the HFPT can be considered as a vector  $\vec{x}$  and the performance vector  $\vec{f}(\vec{x})$  is the criteria associated with the design vector and  $\vec{x} \in \Omega$  where  $\Omega$  is called the design space and  $\vec{f}(\vec{x}) \in Y$  where  $Y$  is the performance space. Eq. (177) and Eq. (178) show the design vector  $\vec{x}$  and the performance vector  $\vec{f}(\vec{x})$ . The components of design vector ( $\vec{x}$ ), are described in Table 4. First, we consider only the power density of the HFPT as a fitness function, therefore the optimization problem is a single objective optimization problem. Multi-objective optimization problem can be formulated when the fitness function takes a matrix format and for instance, cost, efficiency, reliability and manufacturability could be considered as a design criterion. However, this is considered as a future work and only single objective optimization is done in this study.

$$\vec{x} = (x_1, x_2, \dots, x_n) \quad (177)$$

$$\vec{f}(\vec{x}) = (f_1(\vec{x}), f_2(\vec{x}), \dots, f_m(\vec{x})) \quad (178)$$

$$x_i \in [x_{imin}, x_{imax}], i \in [1, n] \quad (179)$$

$$\Omega^* \equiv \arg \min f(x) = \{x^* \in \Omega : f(x^*) < f(x), \forall x \in \Omega\} \quad (180)$$

Objective function

Minimize

$$f(\vec{x}) = V_T(\vec{x}) \quad (181)$$

where:

$$\vec{x} = (x_1, x_2, \dots, x_{17})^T \quad (182)$$

$$f(\vec{x}) = \left(2x_7(x_1x_3 + 2x_4 + x_6 + x_{13} + 2(x_{11} + x_{10}))\right) \left((x_4x_2 + x_4 + x_5)(2x_8) + 4x_{14} + 4x_{10} + 2x_{16} + 2x_{15}\right) (x_{12} + 2x_{14} + (x_1x_2 + x_4 + x_5)(x_7) + x_9) \quad (183)$$

Such that:

$$g_1(\vec{x}) < L_{\max} \quad (184)$$

$$g_2(\vec{x}) < T_{\max} \quad (185)$$

where:

$$g_1(\vec{x}) = \mu_0(x_{12} + 2\pi x_8 x_9) \left(\frac{\delta}{x_2 x_3 \pi^2 x_1^2} e^{-\frac{2x_1}{\delta}} \left(e^{\frac{x_1}{\delta}} - 1\right) \left(\frac{1}{6}\right) x_5(x_5 + 1)(2x_5 + 1) + x_6 \frac{x_5(x_5+1)(x_2+1)}{4(x_2x_3)^2} x_3 \left(1 - \frac{\pi}{4}\right) + x_6 \frac{x_4(2x_4+x_7x_3)(1+x_2^2)}{(\pi x_1 x_2 x_3)^2} + x_4 \frac{x_5^2}{12} x_2 x_1 x_5(x_5 + 1)(2x_5 + 1) + (x_2 x_1 + 2x_4) \frac{x_{14}}{6} (x_7^3 + x_8^3) + \frac{2\mu_0\pi}{((x_1x_2+2x_4)x_5)^2} + 4 \frac{x_{13}\mu_0}{3((x_1x_2+2x_4)x_5)^2}\right) \quad (186)$$

$$g_2(\vec{x}) = (T_{SWU} \quad T_{PWU} \quad T_{SWL} \quad T_{PWL} \quad T_{CM} \quad T_{COU} \quad T_{COL} \quad T_{CRU} \quad T_{CRL})^T \quad (187)$$

where  $g_1(\vec{x})$  and  $g_2(\vec{x})$  refer to leakage inductance and temperature matrix respectively.

#### 4.1 Genetic algorithm

The genetic algorithm was developed first by John Holland [46] and then by David Goldberg [47]. Fig. 18 shows the diagram of the genetic algorithm to solve the optimization problem. A tensor representation,  $PT_{\xi\lambda}^{ij}$  is used to represent a design or a chromosome, where PT stands for Power

Transformer,  $i$  represents the  $i^{\text{th}}$  generation,  $j$  represents the  $j^{\text{th}}$  chromosome based on elitism sorting algorithm,  $\xi$  represents the gene number and  $\lambda$  is bit numbering variable where  $\lambda \in [0, n_{gb} - 1]$  and  $\lambda_{MSB} = 0$  and  $\lambda_{LSB} = n_{gb} - 1$  in  $n_b$  bit representation system. Eq. (188) and Eq. (189) show the Mutation operator and cross-over operator respectively:

$$\widehat{M}(PT_{\xi\lambda}^{ij}) = p_{mu}^{ij\xi\lambda} PT_{\xi\lambda}^{ij} \quad (188)$$

$$\widehat{C}(PT_{\xi_s\lambda}, PT_{\xi_t\lambda}^{ij} | n_{cro}) = p_{co}^{ij\xi\lambda} (PT_{\xi_t\lambda}^{ij}, PT_{\xi_s\lambda}^{ij}) \quad (189)$$

where  $p_{mu}^{ij\xi\lambda}$  and  $p_{co}^{ij\xi\lambda}$  are the probabilities of the mutation and cross-over processes for  $PT_{\xi\lambda}^{ij}$ .  $n_{cro}$  for cross-over process determines the number of bits considered for cross-over process. Various cross-over processes could be defined [48]. A computer program is developed to do the genetic algorithm optimization which is included in the appendix III.

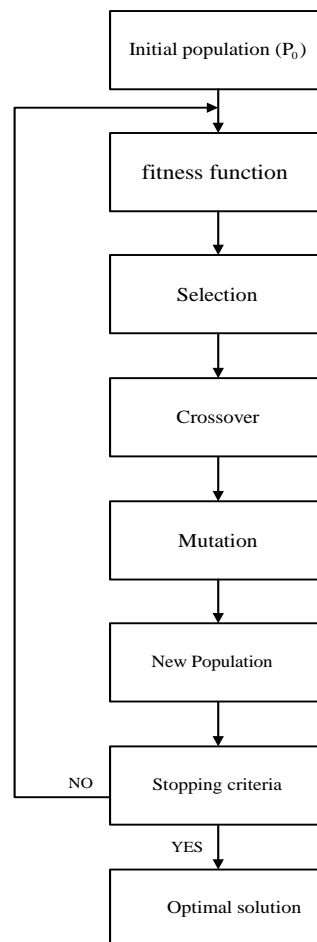


Fig. 18 Genetic algorithm for optimization

## 4.2 A design case study

A design space for an HFPT design case study problem is shown in Table 14. It should be noted that determination of the minimum value and maximum value associated with each gene is based on the information and insight about the HFPT that was obtained as a result of physics-based design that was performed in chapter 3. Some of the genes that directly impact the voltage isolation between the windings and the core and between winding to winding should take values that are above a minimum value that meets the required isolated voltage considering the application. For instance, the thickness of the insulating material used between the core and the windings should be high enough to provide this isolation voltage requirement. This is the reason that physics-based design needs to be performed before optimization using evolutionary algorithms. The number of values that each gene can take is  $n_x$  where in this case  $n_x = 11$ .  $T_{am} = 55^\circ\text{C}$ .

Table 14 Design space for an HFPT case study design

	<i>min</i>					<i>Mid</i>					<i>max</i>
$x_1$	0.00010	0.00020	0.00030	0.00040	0.00050	0.00060	0.00070	0.00080	0.00090	0.00100	0.00110
$x_2$	1.00000	2.00000	3.00000	4.00000	5.00000	6.00000	6.00000	8.00000	9.00000	10.0000	11.0000
$x_3$	1.00000	4.00000	7.00000	10.0000	13.0000	16.0000	19.0000	22.0000	25.0000	28.0000	32.0000
$x_4$	0.00010	0.00050	0.00100	0.00150	0.00200	0.00250	0.00300	0.00350	0.00400	0.00450	0.00500
$x_5$	0.00001	0.00002	0.00003	0.00004	0.00005	0.00006	0.00007	0.00008	0.00009	0.00010	0.00011
$x_6$	0.00001	0.00002	0.00003	0.00004	0.00005	0.00006	0.00007	0.00008	0.00009	0.00010	0.00011
$x_7$	1.00000	3.00000	5.00000	7.00000	9.00000	11.0000	13.0000	15.0000	17.0000	19.0000	21.0000
$x_8$	1.00000	2.00000	3.00000	4.00000	5.00000	6.00000	7.00000	8.00000	9.00000	10.0000	11.0000
$x_9$	0.01000	0.01400	0.01800	0.02200	0.02600	0.03000	0.03400	0.03800	0.04200	0.04600	0.05000
$x_{10}$	0.00500	0.00650	0.00800	0.00950	0.01100	0.01250	0.01400	0.01550	0.01700	0.01800	0.02000
$x_{11}$	0.01000	0.01400	0.01800	0.02200	0.02600	0.03000	0.03400	0.03800	0.04200	0.04600	0.05000
$x_{12}$	0.05000	0.09500	0.14000	0.18500	0.23000	0.27500	0.32000	0.36500	0.41000	0.45500	0.5000
$x_{13}$	0.0050	0.00650	0.00800	0.00950	0.01100	0.01250	0.01400	0.01550	0.01700	0.01850	0.02000
$x_{14}$	0.0001	0.00060	0.00110	0.00160	0.00210	0.00250	0.00300	0.00350	0.00400	0.00450	0.00500
$x_{15}$	0.0100	0.01400	0.01800	0.02200	0.02600	0.03000	0.03400	0.03800	0.04200	0.04600	0.05000
$x_{16}$	0.0010	0.00190	0.00280	0.00370	0.00460	0.00550	0.00640	0.00730	0.00820	0.00910	0.01000
$x_{17}$	0.0010	0.00190	0.00280	0.00370	0.00460	0.00550	0.00640	0.00730	0.00820	0.00910	0.01000

### 4.2.1 Binary encoding

The next step in the design using GA is creating an initial population of chromosomes. The number of initial chromosomes  $P_{init} = 3000$  is considered for the design case study. The initial population is formed randomly using a design space. A binary representation of one chromosome is tabulated in Appendix III. This is a chromosome where every gene takes the middle value in the assigned

range. In this example  $n_{gb} = 32$ . All the values that a gene can take are positive in the HFPT design problem, therefore it is not necessary to dedicate a bit to the sign of the gene. As a result,  $n_{chb}$  which is the number of bytes of memory that is needed to store the value of a chromosome is 68 bytes in this case. Consequently, the number of bytes needed to store a value of population is  $n_{pb} = n_p n_{chb}$ . For example, for the case of  $n_p = 3000$ ,  $n_{pb} = 204$  kB of memory is needed to store the information of the population.

The next step is calculating  $f(PT_{\xi\lambda}^{ij})$ ,  $g_1(PT_{\xi\lambda}^{ij})$  and  $g_2(PT_{\xi\lambda}^{ij})$  for this chromosome. The Table 15 shows the calculated values for these criteria for this chromosome.

Table 15 Calculated values for the considered  $PT_{\xi\lambda}^{ij}$

Chromosome	Value	Unit
$f(PT_{\xi\lambda}^{ij})$	0.0065	$m^3$
$g_1(PT_{\xi\lambda}^{ij})$	[74 74 78 78 80 75 75 76 76]	$C^\circ$
$g_2(PT_{\xi\lambda}^{ij})$	28	$\mu H$

#### 4.2.2 population formation and selection

This process is repeated for all the chromosomes in the initial population ( $n_{p0}$ ) and the results for those chromosomes that are in the feasible range are stored in memory. The next step is to apply elitism algorithm to sort the chromosomes and select pairs to generate the next generation. A parameter  $n_{elit}$  is defined to determine the number of chromosomes that are selected for reproduction compared to the total number of chromosomes that are in the feasible range. In a mathematical format  $n_{elit} = n_{pf} / \beta_p$  where  $n_{pf}$  is the total number of chromosomes that met the reproduction criteria and  $\beta_p$  is a production coefficient factor. In this example  $\beta_p = 5$  is considered. The next step is to convert the chromosome values to binary and then apply mutation and cross-over operations to generate the next generation. Next,  $f(PT_{\xi\lambda}^{ij})$ ,  $g_1(PT_{\xi\lambda}^{ij})$  and  $g_2(PT_{\xi\lambda}^{ij})$  should be calculated for the generated population and elitism algorithm should be applied. This process will continue to the point where either the population number is very small or if there is

not much improvement in the value of fitness function. Table 12 shows a calculated design based on this method for a random selection of initial generation. In this example for simplicity, a uniform probability distribution is considered for mutation and cross over with the values of 0.85 and 0.75 respectively.

#### 4.2.3 A design case study

A case study is done for the system values that are shown in Table 12. The code that was used to generate the results that are shown in Table 16 is provided in Appendix IV.

Table 16 Optimal values of the design variables based on the genetic algorithm optimization approach

Variable	Description	Optimal Value based on GA	Unit
$x_1$	Diameter of the copper strand inside the Litz bundle	0.00040	m
$x_2$	Number of copper strands placed in a Litz bundle vertically	11.0000	-
$x_3$	Number of copper strands placed in a Litz bundle horizontally	27.0000	-
$x_4$	Width of the insulation layer of Litz wire	0.00050	m
$x_5$	Vertical distance between Litz bundles	0.00050	m
$x_6$	Horizontal distance between Litz bundles	0.00001	m
$x_7$	Number of Litz bundles placed horizontally in a core window	11.00000	-
$x_8$	Number of Litz bundles placed vertically in a core window	1.00000	-
$x_9$	Inner radius of the windings	0.01500	m
$x_{10}$	Thickness of the core	0.00130	m
$x_{11}$	Inner radius of the core	0.03750	m
$x_{12}$	Length of the magnetic core	0.12500	m
$x_{13}$	Width of the insulation layer	0.02500	m
$x_{14}$	Thickness of the insulation layer between the core and the winding	0.00100	m
$x_{15}$	Height of the heatsink	0.01500	m
$x_{16}$	Height of the base part of the heatsink	0.00200	m
$x_{17}$	Width of the fin	0.00300	m

For this design,  $L = 18.12 \mu H$ ,  $\eta = 98.6\%$ ,  $\sigma = 22 \frac{kW}{lit}$ ,  $P_w = 954 (W)$ ,  $P_c = 1826 (W)$  was obtained where  $L$  is the leakage inductance and  $P_w$  and  $P_c$  show the winding loss and core loss respectively. The temperature vector was  $T = [73 \ 73 \ 78 \ 78 \ 80 \ 75 \ 75 \ 76 \ 76]$  was obtained for this design.

#### 4.2.4 Active cooling of the high frequency transformer

If a central cooling system is considered in the ship environment that provides a non-conductive coolant with temperature  $T_{ci}$  and speed of  $v_{ci}$  to the power electronic converter cabinet, The speed of the coolant is considered constant during the flow process. First, we start by creating a coordinate system for the problem.

The coordinate system that was used in Fig. 15 is considered for this chapter, therefore:  $x \in [-\frac{L_T}{2}, \frac{L_T}{2}]$ ,  $y \in [-\frac{W_T}{2}, \frac{W_T}{2}]$  and  $z \in [-\frac{H_T}{2}, \frac{H_T}{2}]$ . Eq. (190) shows the length of the transformer with active cooling:

$$L_T = n_c l_c + 2r_{wop} + 2(l_f + l_d) \quad (190)$$

where  $l_f$  is the length of fan and  $l_d$  is the distance between the fan and the outer point of the windings. The dimensions of the fan are  $w_f$ ,  $l_f$  and  $h_f$ . It should be noted that the converter drawers are electrically isolated and the number of converter drawers in one standing power electronic cabinet is  $n_{cd}$ . Considering the ship environment, using liquid cooling is assumed to be mandatory. Therefore, on the drawer level, there will also be coolant input and output for the power electronic modules and the flow of air in the cabinet is assumed in a way that one side of the converter cabinet is cooler than the other side.  $T_D^i(x,y,z)$  shows the value of temperature for converter drawer  $i$  at locations of  $(x,y,z)$  where  $i \in [1, n_{cd}]$ ,  $x \in [-\frac{L_D}{2}, \frac{L_D}{2}]$ ,  $y \in [-\frac{W_D}{2}, \frac{W_D}{2}]$  and  $z \in [-\frac{H_D}{2}, \frac{H_D}{2}]$  where  $L_D$  is the length of the converter drawer,  $W_D$  is the width of the converter drawer and  $H_D$  is the height of the drawer. The relation between these variables and the transformer design variables are:

$$L_D = L_T + L_{Dax} \quad (191)$$

$$W_D = W_T + W_{Dax} \quad (192)$$

$$H_D = H_T + H_{Dax} \quad (193)$$

Optimal determination of  $L_{Dax}$ ,  $W_{Dax}$  and  $H_{Dax}$  could be subject of research. It relates to system integration limitations, EMC compliance, converter safety, mechanical requirements of the converter, thermal management, etc. If converter optimization problem considered, these values should be considered in the design optimization problem [49].

Considering the arrangement of the drawers in the standing cabinet the following relations can be extracted for the temperature tensor.

$$T_D^i(x - \frac{L_D}{2}, y, z) = T_{ci} \quad (194)$$

$$T_D^i(x + \frac{L_D}{2}, y, z) = T_{co} \quad (195)$$

$$T_D^i(x, -\frac{W_D}{2}, z) = (T_x, T_{heo} + \frac{\Delta T_{he}}{W_D} (y + \frac{W_D}{2}), T_z) \quad (196)$$

$$T_D^i(x, \frac{W_D}{2}, z) = (T_x, T_{heo} + \frac{\Delta T_{he}}{W_D} (y - \frac{W_D}{2}), T_z) \quad (197)$$

$$T_D^i(x, y, z + \frac{H_D}{2}) = T_D^{i+1}(x, y, z - \frac{H_D}{2}) \quad (198)$$

where  $T_{heo}$  is the temperature of the output cold air flowing from the heat exchanger in the cabinet and  $T_{hei}$  is the input temperature of the heat exchanger or the temperature of the hot air in the cabinet and  $T_{hei} = T_{heo} + \Delta T_{he}$  where the  $\Delta T_{he}$  is the temperature difference between the air that goes into the heat exchanger and the air that flows out of the heat exchanger. The heat exchanger transfers the total thermal energy that is produced by the operation of the converter. In a mathematical format we can write:

$$Q_{ex} = n_{cd}(E_D) \quad (199)$$

where  $Q_{ex}$  is the total heat generated by the power electronic converter cabinet and  $E_D$  is the amount of energy that is turned into heat by the DAB converter is one drawer which consists of power electronic and high frequency transformer.

Approximation approach is used for the design. The first approximation method is to consider the medium temperature inside the power electronic converter equal to the ambient temperature during and use the thermal model developed in chapter 3. The same case study that was done in section 4.2.3 is solved with considering  $T_{am} = T_{heo} + \frac{\Delta T_{he}}{2}$ . The result of the optimization is shown in Table 16 for the case of  $T_{heo} = 60$  °C and  $\Delta T_{he} = 20$  °C. Detailed dynamic analysis such as using finite element method and Multi-physics simulation is considered as a future work.



Table 17 Optimal values of the HFPT design variables with active cooling

Variable	Description	Optimal Value	Unit
$x_1$	Diameter of the copper strand inside the Litz bundle	0.000375	m
$x_2$	Number of copper strands placed in a Litz bundle vertically	15.0000	-
$x_3$	Number of copper strands placed in a Litz bundle horizontally	25.0000	-
$x_4$	Width of the insulation layer of Litz wire	0.00021	m
$x_5$	Vertical distance between Litz bundles	0.00100	m
$x_6$	Horizontal distance between Litz bundles	0.00010	m
$x_7$	Number of Litz bundles placed horizontally in a core window	10.0000	-
$x_8$	Number of Litz bundles placed vertically in a core window	1.00000	-
$x_9$	Inner radius of the windings	0.01500	m
$x_{10}$	Thickness of the core	0.00150	m
$x_{11}$	Inner radius of the core	0.03750	m
$x_{12}$	Length of the magnetic core	0.14500	m
$x_{13}$	Width of the insulation layer	0.02500	m
$x_{14}$	Thickness of the insulation layer between the core and the winding	0.00200	m
$x_{15}$	Height of the heatsink	0.01500	m
$x_{16}$	Height of the base part of the heatsink	0.00200	m
$x_{17}$	Width of the fin	0.00300	m

For this design,  $L = 17.93 \mu H$ ,  $\eta = 98.9\%$ ,  $\sigma = 23 \frac{kW}{lit}$ ,  $P_w = 785 (W)$ ,  $P_c = 1726 (W)$  was obtained where  $L$  is the leakage inductance and  $P_w$  and  $P_c$  show the winding loss and core loss respectively. The temperature vector was  $T = [77 \ 77 \ 78 \ 78 \ 80 \ 74 \ 74 \ 78 \ 78]$  was obtained for this design.

## 5. CONCLUSION AND FUTURE WORK

A design and optimization methodology for a modular, high power and isolated DC-DC converter suitable for MVDC ship electrification is provided in this study. The input series output parallel configuration of dual active bridge DC-DC converter is considered for the MVDC DC-DC converter. The modular nature of the DAB is suitable for shipboard electrification and the need for high power density is addressed in the design process. Utilizing wide band gap (WBG) semiconductor switches is considered in this study and therefore high switching frequency is considered for the design of the high frequency power transformer.

The analytical loss formula is derived for the Silicon Carbide Power MOSFET considering liquid cooling and the mechanism for choosing the optimal switching frequency is explained. A novel design is proposed for the high frequency power transformer which is suitable for high power DC-DC converter with tunable leakage inductance, low profile structure, integrated heat sink and core topology.

Nanocrystalline based core material is considered for the magnetic core a rectangular Litz wire is considered for the winding. The thermal model and analysis for the high frequency power transformer is developed and the optimization process is carried out for reaching the highest power density with high efficiency for the transformer.

Several lessons learned from this study, for example, the systematic approach to design and optimization of power electronic converter and high frequency magnetic elements used in these converters. This process involves the recognition of design parameters and definition of design objective function and implication of limitations for the design process. The methodology for converting a hardware design problem to a mathematical optimization problem is an important lesson that was learned in this study. Utilizing evolutionary optimization algorithm like the genetic algorithm to extract the optimal design points is another lesson that was learned in this study.

With the methodology developed for design of high frequency power transformer a power density of up to 20 kW/lit is calculated while the efficiency of about 98% is calculated. The magnetic energy stored in all sections of the window is calculated and quantified. The results of this study show that it is possible to obtain the required power density for the shipboard electrification with this methodology.

The future work consists of improving the leakage inductance formula and the thermal model for the transformer to enable computation of the temperature of the core and winding with higher resolution. To improve the accuracy of the leakage inductance formula the superposition principle can be used in calculating the magnetic flux density in different components of the core window. For thermal model, the higher resolution can particularly be helpful for capturing the eddy current losses in the core causing hot spots. In the current model, the average temperature of different parts of the magnetic core is used. Extension of the optimization routine was done only for the high frequency power transformer to the converter level is the work that should be done in the future. To reach that goal, the junction temperature of the power module and the configuration of the drawers in power electronic cabinet and the size of the heat exchanger that was considered should be incorporated to the optimization problem. Once the optimization problem is solved for the converter, it can be extended further to the ship level where all the power electronic converters are interacting with each other and the dynamic of the system will depend on the design parameters inside the converters.

## References

- [1] W. McBride, "Technological change and the United States navy", JHU Press, vol.27., pp. 1865-1945, 2000.
- [2] R. Becker, "An overview in international environmental enforcement", *Geo. Int'l Env'tl. L. Rev.*, pp.10-625, 1997.
- [3] M. Julian, "The international convention for the prevention of pollution from ships", *Maritime Studies*, Vol. 113, pp. 16 - 23, 2000.
- [4] Third IMO Greenhouse Gas Study, International Maritime Organization, 2014
- [5] M. Cames, J. Graichen, A. Siemons, and V. Cook, "Emission reduction targets for international aviation and shipping", Directorate General for Internal Policies; European Parliamentary Policy Department, Economic and Scientific Policy: Bruxelles, Belgium, 2015.
- [6] N. Doerry, J. Amy, and C. Krolick, "History and the status of electricship propulsion, integrated power systems, and future trends in the us navy", *Proceedings of the IEEE*, Vol. 103, pp. 2243–2251, 2015.
- [7] L. Petersen, M. Ziv, D. Burns, T. Dinh, and P. Malek, "US navy efforts towards development of future naval weapons and in-tegration into an all-electric warship", *InIMarEST Engine as a Weapon (EAAW) Int. Symp. UK*, 2011.
- [8] Revision of "IEEE Recommended Practice for 1 kV to 35 kV Medium-Voltage DC Power Systems on Ships " *IEEE Std 1709-2010*, pp.1-54, 2 Nov. 2010, 2018.
- [9] IEEE Guide for Control Architecture for High Power Electronics (1 MW and Greater) Used in Electric Power Transmission and Distribution Systems," in *IEEE Std 1676-2010*, pp.1-47, 11 Feb. 2011.
- [10] R. Cuzner and V. Singh, "Future Shipboard MVdc System Protection Requirements and Solid-State Protective Device Topological Tradeoffs," in *IEEE Journal of Emerging and Selected Topics in Power Electronics*, vol. 5, no. 1, pp. 244-259, March 2017.
- [12] M. H. Kheraluwala, D. W. Novotny and D. M. Divan, "Design considerations for high power high frequency transformers," *21st Annual IEEE Conference on Power Electronics Specialists*, San Antonio, TX, USA, 1990, pp. 734-742.
- [13] M. H. Kheraluwala, "High-power high-frequency DC- to -DC converters", PhD Dissertation, The University of Wisconsin-Madison, 1991.

- [14] Irma Villar, "Multiphysical characterization of medium-frequency power electronic transformer" PhD dissertation, EPFL, 2010.
- [15] Amin Bahmani, "Design and Optimization Considerations of Medium-Frequency Power Transformers in High-Power DC-DC Applications" PhD dissertation, Chalmers university of technology, 2016.
- [16] Amin Bahmani, "Design and optimization of hf transformers for high power dc-dc applications", Master thesis, Chalmers university of technology, 2014.
- [17] J. Zheming, G. Sulligoi, R. Cuzner, L. Meng, J. Vasquez, and J. Guerrero. "Next-generation shipboard dc power system: Introduction smart grid and dc microgrid technologies into maritime electrical networks." IEEE Electrification Magazine 4, no. 2 (2016): 45-57.
- [18] R. M. Cuzner, R. Soman, M. M. Steurer, T. A. Toshon and M. O. Faruque, "Approach to Scalable Model Development for Navy Shipboard Compatible Modular Multilevel Converters," in IEEE Journal of Emerging and Selected Topics in Power Electronics, vol. 5, no. 1, pp. 28-39, March 2017
- [19] R. Soman, M. M. Steurer, T. A. Toshon, M. O. Faruque and R. M. Cuzner, "Size and Weight Computation of MVDC Power Equipment in Architectures Developed Using the Smart Ship Systems Design Environment," in IEEE Journal of Emerging and Selected Topics in Power Electronics, vol. 5, no. 1, pp. 40-50, March 2017
- [20] Ginn, H.; Cuzner, R. M., "The Shipboard Integrated Power System," in IEEE Electrification Magazine, vol. 3, no. 2, pp. 2-3, June 2015
- [21] Cuzner, R; Esmaili, A., "Fault tolerant shipboard MVDC architectures", International Conference on Electrical Systems for Aircraft, Railway, Ship Propulsion and Road Vehicles, 2015 IEEE (ESARS), March 3-5, 2015
- [22] Cuzner, R. M., "Power electronics packaging challenges for future warship applications," Integrated Power Packaging (IWIPP), 2015 IEEE International Workshop on, Chicago, IL, 2015, pp. 5-8.
- [23] R.W.A.A. De Doncker, D.M. Divan, M.H. Kheraluwala, "A Three-phase Soft-Switched High-Power-Density DC-DC Converter for High-Power Applications," IEEE Tran. on Industry Applications, Jan/Feb 1991, Vol. 27, No. 1, pp. 63-73.

- [24] G. Ortiz, "High-Power DC-DC Converter Technologies for Smart Grid and Traction Applications", PhD dissertation, ETH Zurich, 2014.
- [25] A. Rodríguez Alonso, J. Sebastian, D. G. Lamar, M. M. Hernando and A. Vazquez, "An overall study of a Dual Active Bridge for bidirectional DC/DC conversion," 2010 IEEE Energy Conversion Congress and Exposition, Atlanta, GA, 2010, pp. 1129-1135
- [26] R. T. Naayagi, A. J. Forsyth and R. Shuttleworth, "High-Power Bidirectional DC-DC Converter for Aerospace Applications," in IEEE Transactions on Power Electronics, vol. 27, no. 11, pp. 4366-4379, Nov. 2012.
- [27] E. De Din, H. A. B. Siddique, M. Cupelli, A. Monti and R. W. De Doncker, "Voltage Control of Parallel-Connected Dual-Active Bridge Converters for Shipboard Applications," in IEEE Journal of Emerging and Selected Topics in Power Electronics, vol. 6, no. 2, pp. 664-673, June 2018.
- [28] M. A. Bahmani and T. Thiringer, "Accurate Evaluation of Leakage Inductance in High-Frequency Transformers Using an Improved Frequency-Dependent Expression," in IEEE Transactions on Power Electronics, vol. 30, no. 10, pp. 5738-5745, Oct. 2015.
- [29] I. Villar, U. Viscarret, I. Etxeberria-Otadui and A. Rufer, "Global Loss Evaluation Methods for Nonsinusoidally Fed Medium-Frequency Power Transformers," in IEEE Transactions on Industrial Electronics, vol. 56, no. 10, pp. 4132-4140, Oct. 2009.
- [30] M. A. Bahmani, T. Thiringer and M. Kharezy, "Design Methodology and Optimization of a Medium-Frequency Transformer for High-Power DC-DC Applications," in IEEE Transactions on Industry Applications, vol. 52, no. 5, pp. 4225-4233, Sept.-Oct. 2016.
- [31] J. Biela and J. W. Kolar, "Cooling Concepts for High Power Density Magnetic Devices," 2007 Power Conversion Conference, Nagoya, 2007, pp. 1-8.
- [32] G. Ortiz, J. Biela and J. W. Kolar, "Optimized design of medium frequency transformers with high isolation requirements," IECON 2010 - 36th Annual Conference on IEEE Industrial Electronics Society, Glendale, AZ, 2010, pp. 631-638.
- [33] G. Ortiz, L. Fässler, J. W. Kolar and O. Apeldoorn, "Application of the magnetic ear for flux balancing of a 160kW/20kHz DC-DC converter transformer," 2013 Twenty-Eighth Annual IEEE

Applied Power Electronics Conference and Exposition (APEC), Long Beach, CA, 2013, pp. 2118-2124.

[34] P. Shuai and J. Biela, "Design and optimization of medium frequency, medium voltage transformers," 2013 15th European Conference on Power Electronics and Applications (EPE), Lille, 2013, pp. 1-10

[35] I. Villar, U. Viscarret, I. Etxeberria-Otadui and A. Rufer, "Global Loss Evaluation Methods for Nonsinusoidally Fed Medium-Frequency Power Transformers," in IEEE Transactions on Industrial Electronics, vol. 56, no. 10, pp. 4132-4140, Oct. 2009.

[36] M. Rashidi, "Design and implementation of a multi-port solid state transformer for flexible DER integration", PhD dissertation, University of Wisconsin-Milwaukee, 2017.

[37] R. Petkov, "Optimum design of a high-power, high-frequency transformer," in IEEE Transactions on Power Electronics, vol. 11, no. 1, pp. 33-42, Jan. 1996.

[38] L. Heinemann, "An actively cooled high power, high frequency transformer with high insulation capability," APEC. Seventeenth Annual IEEE Applied Power Electronics Conference and Exposition (Cat. No.02CH37335), Dallas, TX, USA, 2002, pp. 352-357 vol.1.

[39] L. Heinemann, R. Ullrich and H. Grotstollen, "Transfer function and calculation of parameters for high frequency multiwinding transformers," PESC '91 Record 22nd Annual IEEE Power Electronics Specialists Conference, Cambridge, MA, USA, 1991, pp. 659-666.

[40] W. Shen, F. Wang, D. Boroyevich and C. W. Tipton, "Loss Characterization and Calculation of Nanocrystalline Cores for High-frequency Magnetics Applications," APEC 07 - Twenty-Second Annual IEEE Applied Power Electronics Conference and Exposition, Anaheim, CA, USA, 2007, pp. 90-96.

[41] S. D. Sudhoff, "Power magnetic devices, a multi-objective design approach", Wiley, 2014.

[42] W.G. Hurley, W. H. Wolfle, "Transformers and inductors for power electronics", John Wiley, 2013.

[43] P. L. Dowell, "Effects of eddy currents in transformer windings," in Proceedings of the Institution of Electrical Engineers, vol. 113, no. 8, pp. 1387-1394, August 1966.

- [44] David Jiles, "introduction to magnetism and magnetic materials", CRC Press, Jun 16, 1998 - Technology & Engineering.
- [45] Randy L. Haupt, Sue Ellen Haupt "Practical Genetic Algorithms", John Wiley & Sons , Inc, 1998.
- [46] John Holland, "Adaptation in Natural and Artificial Systems", University of Michigan Press. 1975.
- [47] David Goldberg, "Genetic algorithm in Search, Optimization and Machine Learning", New York, 1989.
- [48] P. Larranaga, C. M. H. Kuijpers, R. H. Murga and Y. Yurramendi, "Learning Bayesian network structures by searching for the best ordering with genetic algorithms," in IEEE Transactions on Systems, Man, and Cybernetics - Part A: Systems and Humans, vol. 26, no. 4, pp. 487-493, July 1996.
- [49] R. Cuzner, S. Cruz, Frank Ferrese, R. Hosseini," Power converter metamodeling approach for the smart ship design environment", IEEE Electric Ship Technologies Symposium (ESTS), Arlington, VA, USA, 2017.



## Appendix I

The code for Semiconductor module thermal calculation

```

vi=950;
vo=1050;
d=vo/vi;
L = 1.5e-5;

f=40000;
w=2*pi*f;
Phi = pi*[0.1 0.2 0.3 0.4 0.45 0.5];
rq=0.01;

% L1 = 1e-5*[1 1.5 2 2.5 3 3.5 4];
% Phi = pi*[1/12 1/6 1/4 1/3 1/2]; % phase shift
% for j=1:5
% %   L=L1(j)
%   phi=Phi(j);
%   phi = pi/3;

theta = 0:0.001:2*pi;
t = theta/w;
N = length(theta);

I = zeros(1,N);
PDMV = zeros(1,N);
PDLV = zeros(1,N);
PQMV = zeros(1,N);
PQLV = zeros(1,N);
PSWMV = zeros(1,N);
PSWLV = zeros(1,N);

```

```

%% % instantaneous power loss % % %
% for j=1:length(PHI)
% phi = PHI(j);
for j=1:length(Phi)
    phi = Phi(j)
    I0 = -vi/w/L*((1-d)*pi/2+d*phi)
    I_phi = -vi/w/L*((1-d)*pi/2-phi)
    n1 = ceil(N*abs(phi)/2/2/pi);
    n2 = ceil(abs(phi)/2/pi*N)
    n3 = ceil(pi/2/pi*N);
    n4 = ceil((pi+abs(phi))/2/2/pi*N);
    n5 = ceil((pi+abs(phi))/2/pi*N);
    PSWMV (n3)=Poff;
    PSWMV(1) = Poff;
    % PSWMV (1) = Poff;
    PSWLV (n2) = Poff;
    PSWLV (n5)=Poff;
    for i = 1:n1

        I(i)=(vi+vo)/w/L*theta(i) + I0;
        PDMV (i) = (Vfd1 + abs(Rfd1*I(i)))*abs(I(i));
        PQMV (i) = 0;
        PDLV (i) = (Vfd1 + abs(Rfd1*I(i)))*abs(I(i));
        PQLV (i) = 0;

    end
    for i=n1+1:n2

        I(i)=(vi+vo)/w/L*theta(i) + I0;
        PDMV (i) = 0;

```

$$\text{PQMV}(i) = (r_q * I(i)) * I(i);$$

$$\text{PDLV}(i) = 0;$$

$$\text{PQLV}(i) = (r_q * I(i)) * I(i);$$

end

for i=n2+1:n3

$$I(i) = (v_i - v_o) / w / L * (\theta(i) - \phi) + I_{\phi};$$

$$\text{PDMV}(i) = 0;$$

$$\text{PQMV}(i) = (r_q * I(i)) * I(i);$$

$$\text{PDLV}(i) = (V_{fd1} + \text{abs}(R_{fd1} * I(i))) * \text{abs}(I(i));$$

$$\text{PQLV}(i) = 0;$$

end

for i = n3+1:n4

$$I(i) = -((v_i + v_o) / w / L * (\theta(i) - \pi) + I_0);$$

$$\text{PDMV}(i) = (V_{fd1} + \text{abs}(R_{fd1} * I(i))) * \text{abs}(I(i));$$

$$\text{PQMV}(i) = 0;$$

$$\text{PDLV}(i) = (V_{fd1} + \text{abs}(R_{fd1} * I(i))) * \text{abs}(I(i));$$

$$\text{PQLV}(i) = 0;$$

end

for i=n4+1:n5

$$I(i) = -((v_i + v_o) / w / L * (\theta(i) - \pi) + I_0);$$

$$\text{PDMV}(i) = 0;$$

$$\text{PQMV}(i) = (r_q * I(i)) * I(i);$$

$$\text{PDLV}(i) = 0;$$

$$\text{PQLV}(i) = (r_q * I(i)) * I(i);$$

```

end
for i=n5+1:N

    I(i) = -((vi-vo)/w/L*(theta(i)-pi-phi)+I_phi);
    PDMV (i) = 0;
    PQMV (i) = (rq*I(i))*I(i);
    PDLV (i) = (Vfd1 + abs(Rfd1*I(i)))*abs(I(i));
    PQLV (i) = 0;

end

%%% power loss %%%
PDMVave = sum(PDMV)/2/N
PQMVave = sum(PQMV)/2/N
PDLVave = sum(PDLV)/2/N
PQLVave = sum(PQLV)/2/N
PMMV = (PDMV + PQMV +PSWMV);
PMMVave = sum(PMMV)/N
PMLV = (PDLV + PQLV + PSWLV);
PMLVave = sum(PMLV)/N
PMV= 2*PMMV;
PMVave=sum(PMV)/N
PLV=2*PMLV;
PLVave=sum(PLV)/N
PDAB = 2*(PMMV + PMLV);
PDABave = sum(PDAB)/N

%%% Thermal Calculation %%%
T_max = zeros(1,4);
T_min = zeros(1,4);
TA = 5:5:35;
lq=0.062;
wq=0.106;

```

```

RSA = 1/(lq*wq*1550*2); % ?
RCS = 0.03; %?
RJCQ = 0.071;
RJCD = 0.065;
TSMV = TA + RSA*2*(PMMVave);
TCMV = TSMV + RCS * PMMVave;
TJQMV = TCMV + RJCQ*PQMVAve;
T_max(1) = max (TJQMV);
T_min(1)=min (TJQMV);
TJDMV = TCMV + RJCD * PDMVAve;
T_max(2) = max (TJDMV);
T_min(2)=min (TJDMV);
TSLV = TA + RSA*2*(PMLVAve);
TCLV = TSLV + RCS * PMLVAve;
TJQLV = TCLV + RJCQ*PQLVAve;
T_max(3) = max (TJQLV);
T_min(3)=min (TJQLV);
TJDLV = TCLV + RJCD * PDLVAve;
T_max(4) = max (TJDLV);
T_min(4)=min (TJDLV);
p(j)=vi*vo*sin(phi)/w/L;
p2(j)=vi^2/w/L*d*phi*(1-abs(phi)/pi);
TJ_max (j) = max(T_max)
TJ_min (j) = min(T_min)
end

```

## APPENDIX II

## Computer code for leakage inductance calculation

```
%% converter parameters
```

```
fsw =40000; %switching frequency
```

```
I = 200; %winding current
```

```
%% Independent parameters
```

```
dst = 0.5e-3; % diameter of Copper strand
```

```
nstv = 10; %number of strands placed in the Litz bundle vertically
```

```
nsth = 30; % number of strands placed in the Litz bundle horizontally
```

```
wLitzins = 0.001; % width of the insulation layer of Litz bundle
```

```
dLitzv = 0.001; % vertical distance between the Litz bundles
```

```
dLitzh = 0.001; % horizontal distance between the Litz bundles
```

```
nLitzh = 10; % number Litz bundles placed in the core horizontally
```

```
nLitzv = 1; % numer of Litz bundles placed in the core vertically
```

```
rwi = 0.015; %inner radius of the winding
```

```
lc = 0.03; % length of the magnetic core
```

```
wiso = 0.01; %width of the insulation layer
```

```
dcwv = 0.01; % thickness of the isolation layer between the winding and core
```

```
nc = 10; % number of core stacks
```

```
%% Dependent Parameters
```

```
hLitz = nstv*dst + 2*wLitzins; %height of Litz bundle
```

```
wLitz = nsth*dst + 2*wLitzins; %width of Litz bundle
```

```
lcore = nc*lc; %total length of magnetic core
```

$lw = 2*(l_{core} + \pi*r_{wi});$  % length of winding

$nst = n_{stv} * n_{sth};$  % total number of strands in Litz bundle

$I_{st} = I/nst;$  % current in one strand

$\mu_0 = 1.25663753e-6;$  % permeability of air (H/m)

$\sigma = 5.87e7;$  % conductivity of copper (S/m)

$skin = \sqrt{2/(\pi/fsw/\mu_0/\sigma)};$  % skin depth

%% Leakage Inductance

$E_{cu} = n_{Litzh} * n_{stv} * n_{sth} * lw * \mu_0 * I_{st}^2 * skin / 4 * \pi / \pi / dst / dst * \exp(-2 * dst / skin) * (\exp(dst / skin)) * (\exp(dst / skin - 1)) * (1/6) * n_{Litzv} * (n_{Litzv} + 1) * (2 * n_{Litzv} + 1)$

$E_{bair} = lw * n_{Litzh} * n_{Litzv} * (n_{Litzv} + 1) / 2 * n_{stv} * (n_{stv} + 1) / 2 * n_{sth} * dst^2 * (1 - \pi/4) * \mu_0 * I_{st}^2 / \pi / \pi / dst / dst$

$E_{ins} =$

$n_{Litzh} * lw * \mu_0 * I_{st}^2 / \pi / \pi / dst / dst * (w_{Litzins} * w_{Litz} * (1 + n_{stv}^2) + 2 * w_{Litzins} * n_{Litzv}^2 / 4 * (h_{Litz} - 2 * w_{Litzins})) * (1/6) * n_{Litzv} * (n_{Litzv} + 1) * (2 * n_{Litzv} + 1)$

$E_{intwh} =$

$lw * n_{Litzh} * \mu_0 * I^2 * d_{Litzh} / 3 * h_{Litz} / h_{Litz} / n_{sth} / n_{sth} * (1/6) * (n_{Litzv}) * (n_{Litzv} + 1) * (2 * n_{Litzv} + 1)$

$E_{intwv} =$

$lw * n_{Litzv} * \mu_0 * I^2 * d_{Litzv} / 3 * n_{stv} / n_{stv} * w_{Litz} / w_{Litz} * (1/6) * n_{Litzh} * (n_{Litzh} + 1) * (2 * n_{Litzh} + 1)$

$E_{isowcl} = lw * w_{Litz} * n_{Litzh}^3 * \mu_0 * I^2 * dcwv / 6$

$E_{isowcu} = lw * w_{Litz} * n_{Litzh}^3 * n_{Litzv}^2 * \mu_0 * I^2 * dcwv / 6$

$E_{iso} = lw * 2 * \mu_0^2 * I^2 * w_{iso} / 3 * h_{Litz} / h_{Litz}$

$E_{airch} = lw * 2 * \mu_0^2 * I^2 * \pi / h_{Litz} / h_{Litz} / n_{Litzv} / n_{Litzv}$

$E_{cw} = 2 * (E_{cu} + E_{bair} + E_{ins} + E_{intwh} + E_{intwv} + E_{isowcl} + E_{isowcu} + E_{airch}) + E_{iso}$

$L = 2 * E_{cw} / I^2$

## APPENDIX III

Computer code for design of HFPT

tic

loop=0;

%% 1- System requirements

vdc1 = 1e3;

vdc2 = 1e3;

n = vdc2/vdc1; % definition

Pout =250e3;

Viso =60e3;

Tmax = 80;

Tc=[5 15 25 35];

% required leakage calculation

% voltage tolerance

vdc1max = vdc1\*1.05;

vdc2max = vdc2\*1.05;

vdc1min=vdc1\*0.95;

vdc2min=vdc2\*0.95;

% d calculation

dmax=vdc2max/vdc1min/n;

dmin=vdc2min/vdc1max/n;

% soft switching requirement

phimin1= pi\*(dmax-1)/2/dmax; % if d&gt;1



```

phimin2=pi*(1-dmin)/2; % if d<1
phimin =min(phimin1,phimin2);

%% frequency calculation

VFD1 = 1.5; % forward bias of diode

RFD1 = 0.05; % diode forward resistance

Vfd1 = 1.5; % MV side module's diode thershold voltage

Rfd1 = 0.005; % MV side module's diode on resistance

RQ1 = 0.01; % MV side modules MOSFET ON resistance

I_max=300;

fsw=4000;

Eoff = 0.033*I_max*0.001; % data sheet

Poff = Eoff*fsw; % data sheet

f=fsw;

Lmax = vdc1*vdc2*phimin*n*(pi-phimin)/2/Pout/pi/pi/fsw;

%----- DAB -----

phi=pi/12; % ?

d = vdc2/vdc1;

phi1 = (pi+2*phi*d-pi*d)/(2*(1+d));

t1 = (pi+2*phi*d-pi*d)/(4*pi*f*(1+d));

tphi = phi/(2*pi*f);

```

$$Z1 = (n*vdc1 + vdc2)/(n*Lmax);$$

$$Z2 = (n*vdc1 - vdc2)/(n*Lmax);$$

$$Ts = 1/f;$$

$$IT1 = Z1*(sqrt((4*t1^2*tphi + Ts*t1^2 - 4*tphi^2*t1 - Ts*t1*tphi + Ts*tphi^2)/(3*Ts)));$$

$$ID1avg = -Z1*phi^2/4/pi/2/pi/f;$$

$$IS1avg = Z1/4/pi/2/pi/f*(phi1^2-2*phi1*phi+pi*phi1);$$

$$ID1rms = Z1*phi1/2/pi/f*sqrt(phi1/6/pi);$$

$$IS1rms = Z1/2/pi/f*sqrt(phi*(pi-2*phi1)*(phi-phi1)+phi1^2*(pi-phi1)/6/pi);$$

$$ID5avg = Z1/4/pi/n/2/pi/f*(phi1^2+pi*phi-phi^2);$$

$$IS5avg = -Z1/4/pi/n/2/pi/f*(phi-phi1)^2;$$

$$ID5rms = Z1/n/2/pi/f*sqrt(((phi^2+phi1^2)*(pi+phi1-phi)-pi*phi*phi1)/6/pi);$$

$$IS5rms = Z1/4/n/pi/2/pi/f*(phi-phi1)*sqrt((phi-phi1)/6/pi);$$

%-----

%% 2- Fixed Parameters

%% 2-1 Magnetic Core

%nanocrystalline vitroperm500F

$$Bmax = 0.8* 1.2;$$

$$K = 0.48; \% \text{ what is this?}$$

$$\text{alphacore}=1.8;$$

$$\text{betacore} =2.3;$$

$$\text{rocore}=7300; \% \text{kg/m}^3$$

kc= 0.75; %filling factor of the core (M. A. Bahmani, etal"Core loss behavior in high frequency high power transformers effect of core topoloty"

%% 2-2 Litz wire

% rectangular Litz wire with Nst round strands

wLitzins=5e-4; %thickness of the insulation layer of the Litz bundle

dst = 2e-4; %diameter of the copper strand

nstv = 10; % number of strands vertical

nsth=30; % number of strands horizontal

nst = nsth\*nstv; % total number of strands in the Litz bundle

wLitz = nsth\*dst+2\*wLitzins; %width of the Litz wire

hLitz = nstv\*dst+2\*wLitzins; %height of the Litz wire

dLitzbh= 2e-4; %horizontal distance between Litz bundles

dLitzbv= 2e-4; %vertical distance between Litz bundles

% cost\_Litz = 1; % \$ cost of Litz bundle per meter

% lifetime\_Litz = 2; % life time of Litz wire / years

%% 2-3 Isolation layer

% CoolPoly-D5108 - Thermally conductive, electrically insulative

Eins= 29; %kV/mm

tansigma = 0.022; % @100kHz

epsilon\_r = 4.8; %(kV/mm)

ksaf= 0.3; % safty factor for the dielectric strength

%% 3- Isolation & Clearance calculation

```

dcwv = ceil(vdc2/1000/(ksaf*Eins))/1000; % thickness of the resine materials for coil
former (m)

diso = 1e-3; %thickness of the isolation layer material

wisomin = ceil(Viso /1000/ (ksaf*Eins))/1000; % width of the isolaiton layer (m)

%% 4- Free parameters

%   ncc = linspace(1,6,6);    %number of core stacks

%   AA = 1e-3* linspace(10,90,5);    %frontal side of the core cross section

%   nLitzv1 = linspace(5,14,10);

%   AR1 = linspace(1,10,10); % aspect ratio of the primary Litz bundle- ratio between the
respective total height and width

%   Jmax = 1e9*linspace(1,10,10) ;    % maximum allowed RMS value of the current
density through a conductor ?? (A/m^2)

%

Ntot=length(ncc)*length(AA)*length(nLitzv1)*length(nLitzv1)*length(dst1)*length(dst1)*lengt
h(AR1)*length(AR21)*length(Jmax);

%   Vtotal=zeros(1,Ntot);

%   etatotal=zeros(1,Ntot);

%   sigmatotal=zeros(1,Ntot);%power density

%% 5- Dimension

%% 5-1 Litz Dimensions

%   nst = 4*IT1/(pi*dst^2*Jmax); % number of strands in primary Litz bundle

```

```

%      k = wLitzins * (1-AR);

%      nsth = floor ((k + sqrt(k^2 + nst*dst^2*AR)/(dst*AR)));      % number of strands in
each internal row of Litz bundle for primary

%      nstv = ceil (nst/nsth);      % nuber of strands in each internal column within a Litz
bundle of primary windings

%% 5-2 core window

%----- take core information -----

rci = 0.02; % inner radius of the core

wc = .15; %total width of the core (m)

dc=0.005; %thickness of the core (m)

hc = rci+dc; % height of the core

lcc = 0.01; %depth of one core (m)

% ---- calculate the nc -----

nc = 20; % number of core stacks

lc = nc*lcc; % total depth of the core

% ----- calculate the number of winding -----

wiso = wisomin; % width of the isolation layer

wcf = wc-2*(dc+rci); % width of the flat part of the core (m)

nLitzv = ceil((2*hc - 2*dc-2*dcwv)/hLitz); % number of Litz wires placed vertically

```

```

nLitzh = ceil((wcf-wisomin)/2/wLitz); % number of Litz wire placed horizontally

wp = (wcf-wisomin)/2; % width of the primary windings

%% length of winding and isolation layer

rwi = rci; % radius of the winding

lw = 2*nLitzv*nLitzh*(lc+pi*rwi+(nLitzv-1)*(dLitzbv+hLitz)); % Mean length turn of the
primary winding

riso = 0; %radius of the isolation

niso = ceil((2*hc - 2*dc-2*dcwv)/diso); % number of layers of the isolation material

liso = 2*niso*lc+pi*(2*niso*riso+diso*niso*(niso-1)); % length of the isolation material (m)

%----- skin depth ----

mu0 = 4*pi*1e-7; %H/m

ro_cu = 2e-8; %ohm.m for copper at 60-C (what about at operating temperature?)

sigma = sqrt(ro_cu/pi/f/mu0); %skin depth at any particular frequency

alpha = (1+1i)/sigma;

%-----

delta = nstv*dst/sigma; %delta is defined for foil as dcu/sigma, for Litz wire the dcu is
replaced by nstv*dst

Leakage=mu0*Iw/nLitzh/wLitz*( nstv*dst/3/delta^2 *( (4*nLitzv^2-1)*(sinh(2*delta)-
sin(2*delta))/(cosh(2*delta)-cos(2*delta)) - 2*(nLitzv^2-1)*(sinh(delta)-sin(delta))/(cosh(delta)-
cos(delta)) )+wiso+wLitzins*(nLitzv-1)/nLitzv ); % leakage inductance

%% 6- Power Loss Calculations

%% 6-1 Core Losses

% Vc = 4*nc*A*B*(H+2*A) + 4*nc*A*B*G;

%Psc =

```

```

%k,ki

k=1;

ki=1;

FWC=pi/4; % for square wave (DAB)

Vc = dc*lc*(2*wcf+pi*(2*rci*dc+dc^2));% volume of the coree

mcore=Vc*rocore;

Pcore = FWC*(f/1000)^alphacore*Bmax^betacore*mcore;% core loss (W)

%% 6-2 Winding Losses

nh =10; %number of harmonics considered

RFh = zeros (nh,2); % column 1: primary, column 2: secondary

Ih = zeros (nh,2); % column 1: primary, column 2: secondary

VT=zeros(nh,2);

deltavlp = zeros (nh,1);

Pw11=zeros(1,nh);

Pw22=zeros(1,nh);

for i=1:nh

%D

%   D1=0.5;

%   D2=0.5;

%   deltaphi(i) = atan(cot(pi*i*D1)) - atan(cot(pi*i*D2))+i*phi; %

%   deltavlp(i)=4*vdc l/pi/i*sqrt((sin(pi*i*D1)^2)+(d*sin(pi*i*D2))^2-

(2*d*abs(sin(pi*i*D1)*sin(pi*i*D2))*cos(deltaphi(i)))); %

```

```

%      %phd

%      Ih(i,1) = deltavlp(i)/2/pi/f/i/Lmax; %RMS of ith harmoinc of the current at the primary

%      Ih(i,2) = Ih(i,1)/n; % n-> turns ratio

%master

Ih(i,1) = 4*vdc1 * sqrt(1+d^2-2*d*cos(i*phi))/2/sqrt(2)/pi/pi/f/i^2/Lmax; %resistance
factor for windings - From Bahmani phd eq. (5.42) - From

%Dowell originally

sigma_i = sqrt(ro_cu/pi/f/i/mu0);

delta_i = nstv*dst/sigma_i;

delta_i = dst/2*sqrt(2)/2/sigma_i*sqrt(nLitzh*nsth*dst*sqrt(pi)/2/(2*hc-2*dc));

RFh(i,1) = delta_i*((sinh(2*delta_i))+sin(2*delta_i))/((cosh(2*delta_i))-cos(2*delta_i))
+ (nLitzv^2-1)/3*2*delta_i*(((sinh(delta_i))-sin(delta_i))/(cosh(delta_i)+cos(delta_i)));
%Litz wire resistance variation with frequency for primary

% RFh(i,2) = delta2*((sinh(2*delta2))+sin(2*delta2))/((cosh(2*delta2))-cos(2*delta2)) +
(nLitzv^2-1)/3*2*delta2*(((sinh(delta2))-sin(delta2))/(cosh(delta2)+cos(delta2)));      %Litz
wire resistance variation with frequency for secondary

RFh(i,2)=RFh(i,1);

con_cu = 5.96*1e7; %copper conductivity at 20C

Rdc1 = ro_cu*4*lw/pi/dst^2/nst;

Rdc2 = ro_cu*4*lw/pi/dst^2/nst;

Pw11(i) = Rdc1*RFh(i,1)*Ih(i,1)^2; %primary winding loss

Pw22(i) = Rdc2*RFh(i,2)*Ih(i,2)^2; %secondary winding loss

end

Pw1 = sum(Pw11);

```



$$Pw2 = \text{sum}(Pw22);$$

$$Pw2=Pw1;$$

%% 6-3 Dielectric Losses

% Uniform distribution of magnetic field is considered within

% the isolation distance, coil former distance and clearing

% distance

$$\text{deltaVins}=\text{Viso}; \text{ \% ??}$$

$$\text{Cins} =1; \text{ \% ??}$$

$Pins = \text{deltaVins}^2 * 2 * \pi * f * \text{Cins} * \text{tansigma} * 1e-12$  ; %Cins capacitance of the dielectric medium , deltaVins the voltage over the dielectric medium

$$\text{\% } C(\text{LV-HV})=$$

$$\text{\% } C(\text{LV-C})=$$

$$\text{\% } C(\text{HV-C})=$$

$$\text{\% } P_{die}=$$

$$PT = P_{core}+Pw1+Pw2+Pins;$$

%% 7- Thermal Calculations and Constraints

$$\text{\% } AT+BU=0 \rightarrow T=-(A^{-1})BU$$

$k_{pol}=10$ ;%(W/mK) Thermal conductivity of the thermally conductive polymeric material

$k_{cc}=1$ ;% Thermal conductivity of the core material

$k_{iso}=1$ ;% Thermal conductivity of the isolation materials

$\text{sigma}_{ins} = 10$ ; %(W/mK) Thermal conductivity of the thermally conductive polymeric material

sigma\_cu=1;%CHANGE

sigma\_ins=1;%CHANGE

sigma\_c=1;%change

rthpweq = 2\*wLitzins/sigma\_ins/wLitz+nsth/nstv/sigma\_cu;

rthclf = dcwv/lc/wp/sigma\_ins;

rthsweq = 2\*wLitzins/sigma\_ins/wLitz + nsth/nstv/sigma\_cu;

g=9.8;

Ts=120;

Ta=40;

cp = 0.9; % for aluminum (J/gmK)

k = 0.027; %w/mk

pr=cp\*mu0/k;

pr=0.715;

v=1e-5; %kinematic viscosity m^2/s

hconv = (0.68+0.67\*(g\*2/(Ts+Ta))\*(Ts-Ta)\*Vc\*pr/v^2)^0.25/(1+(0.492/pr)^9/16)^4/9)\*k/Vc;

sigma\_sb=5.67e-8; % stefan-boltzmann constant

epsilon=8.85e-12; % permittivity of free space

hrad=epsilon\*sigma\_sb\*(Ts^4-Ta^4)/(Ts-Ta);

rthcrpwu = 1/pi/rci/lc/hconv;

rthcrpwl = 1/pi/rci/lc/hconv;

$$rthcrcm = \pi * (rci + dc) / 4 / dc / lc / \sigma_c;$$

$$rthcrswu = 1 / \pi / rci / lc / hconv;$$

$$rthcram = 1 / (hconv + hrad) / \pi / (rci + dc) / lc;$$

$$rthcrco = rthcrcm; \% \text{ change}$$

$$rthhs = rthcrcm; \% \text{ change}$$

$$rthcrswl = rthcrpwl;$$

$$rcrl = -(1 / rthcrco + 1 / rthcrswu + 1 / rthcrcm + 1 / rthcram);$$

$$rcru = -(1 / rthcrco + 1 / rthcrswu + 1 / rthcrcm);$$

$$rcol = -(2 / rthcrco + 1 / (rthclf + rthsweq) + 1 / (rthclf + rthpweq) + 1 / rthhs);$$

$$rcou = -(2 / rthcrco + 1 / (rthclf + rthsweq) + 1 / (rthclf + rthpweq) + 1 / rthhs);$$

$$rcm = -$$

$$(1 / (rthclf + rthsweq) + 1 / (rthclf + rthpweq) + 1 / (rthclf + rthsweq) + 1 / (rthclf + rthpweq) + 2 / rthcrcm + 2 / rthcrswl);$$

$$rpwl = -(1 / (rthpweq + rthclf) + 1 / (rthpweq + rthclf) + 1 / rthcrpwl);$$

$$rswl = -(1 / (rthsweq + rthclf) + 1 / (rthsweq + rthclf) + 1 / rthcrswl);$$

$$rpwu = -(1 / (rthpweq + rthclf) + 1 / (rthpweq + rthclf) + 1 / rthcrpwu);$$

$$rswu = -(1 / (rthsweq + rthclf) + 1 / (rthpweq + rthclf) + 1 / rthcrswu);$$

$$pco = wcf * lc * dc * kc * f^{\alpha_{core}} * B_{max}^{\beta_{core}};$$

$$pcr = \pi * rci * dc * lc * kc * f^{\alpha_{core}} * B_{max}^{\beta_{core}};$$

$$pcm = 2 * pco;$$

$$pwsu = nLitzh * lc + hLitz * 0.5 * nLitzh * (nLitzh - 1);$$

$$pswl = pwsu;$$

```

ppwu = nLitzh*lc + pi*nLitzh*rwi+0.5*nLitzh*(nLitzh-1);

ppwl=pswl;

pcou=pco;

pcol=pco;

pcru=pcr;

pcrl=pcr;

Tam=40;

% T=[tswu tpwu tswl tpwl tcm tcou tcol tcru tcrl];

U = [pwsu; pswl; ppwu; ppwl; pcou; pcol; pcm; pcru; pcrl; Tam];

B = zeros(9,10);

for i=1:9

    B(i,i)=1;

end

B(6,10)=rthhs^-1;

B(7,10)=rthhs^-1;

B(8,10)=rthcram^-1;

B(9,10)=rthcram^-1;

A=zeros(9,9);

A(1,1) = rswu;

A(1,5)=(rthpweq+rthclf)^-1 ;

A(1,6)=(rthsweq+rthclf)^-1 ;

A(1,8)= (rthcrswu)^-1 ;

A(2,2) = rpwu;

```

$$A(2,5)=(rthpweq+rthclf)^{-1} ;$$

$$A(2,6)=(rthpweq+rthclf)^{-1} ;$$

$$A(2,8)= (rthcrpwu)^{-1} ;$$

$$A(3,3)=rswl ;$$

$$A(3,5) = (rthsweq+rthclf)^{-1} ;$$

$$A(3,7)= (rthpweq+rthclf)^{-1};$$

$$A(4,4)=rpwl;$$

$$A(4,5)=(rthsweq+rthclf)^{-1} ;$$

$$A(4,7)=(rthpweq+rthclf)^{-1} ;$$

$$A(4,9)=(rthcrpwl)^{-1};$$

$$A(5,1)=(rthsweq+rthclf)^{-1} ;$$

$$A(5,2)=(rthpweq+rthclf)^{-1} ;$$

$$A(5,3) = (rthsweq+rthclf)^{-1};$$

$$A(5,4) = (rthpweq+rthclf)^{-1} ;$$

$$A(5,5)= rcm ;$$

$$A(5,8)= 2/rthcrqm ;$$

$$A(5,9)=2/rthcrqm;$$

$$A(6,3)= (rthsweq+rthclf)^{-1} ;$$

$$A(6,4)=(rthpweq+rthclf)^{-1} ;$$

$$A(6,7)= rcol ;$$

$$A(6,8)=2/rthcrco ;$$

$$A(7,3)=(rthsweq+rthclf)^{-1} ;$$

$$A(7,4)=(rthpweq+rthclf)^{-1} ;$$

$$A(7,7) = rcol;$$

$$A(7,9) = 2/rthcrco;$$

$$A(8,1) = rthcrswu^{-1};$$

$$A(8,5) = rthcrcm^{-1} ;$$

$$A(8,6) = rthcrco^{-1} ;$$

$$A(8,8) = rcru ;$$

$$A(9,3) = rthcrco ;$$

$$A(9,5) = rthcrcm ;$$

$$A(9,7) = rthcrswu^{-1} ;$$

$$A(9,9) = rcrl;$$

$$\% \quad A = [rswu \quad 0 \quad 0 \quad 0 \quad (rthpweq+rthclf)^{-1} \quad (rthsweq+rthclf)^{-1} \quad 0 \\ (rthcrswu)^{-1} \quad 0 \quad ;$$

$$\% \quad 0 \quad rpwu \quad 0 \quad 0 \quad (rthpweq+rthclf)^{-1} \quad (rthpweq+rthclf)^{-1} \quad 0 \quad (rthcrpwu)^{-1} \\ 1 \quad 0 \quad ;$$

$$\% \quad 0 \quad 0 \quad rswl \quad 0 \quad (rthsweq+rthclf)^{-1} \quad 0 \quad (rthpweq+rthclf)^{-1} \quad 0 \\ 0 \quad ;$$

$$\% \quad 0 \quad 0 \quad 0 \quad rpwl \quad (rthsweq+rthclf)^{-1} \quad 0 \quad (rthpweq+rthclf)^{-1} \quad 0 \\ (rthcrpwl)^{-1};$$

$$\% \quad (rthsweq+rthclf)^{-1} \quad (rthpweq+rthclf)^{-1} \quad (rthsweq+rthclf)^{-1} \quad (rthpweq+rthclf)^{-1} \quad rcm \quad 0 \\ 0 \quad 2/rthcrcm \quad 2/rthcrcm;$$

$$\% \quad (rthsweq+rthclf)^{-1} \quad (rthpweq+rthclf)^{-1} \quad 0 \quad 0 \quad 0 \quad rcou \quad 2/rthcrco \quad 0 \\ ;$$

$$\% \quad 0 \quad 0 \quad (rthsweq+rthclf)^{-1} \quad (rthpweq+rthclf)^{-1} \quad 0 \quad 0 \quad rcol \quad 0 \\ 2/rthcrco;$$

$$\% \quad rthcrswu^{-1} \quad 0 \quad 0 \quad 0 \quad rthcrcm^{-1} \quad rthcrco^{-1} \quad 0 \quad rcru \quad 0 \quad ;$$

```
%      0      0      rthcrco      0      rthrcrm      0      rthcrswu^-1      0      rcr1]
```

```
T = -1*inv(A)*B*U;
```

```
% if (L <= Lmax && T(2) <= Tmax)
```

```
% %Saving The Results
```

```
% % i-> nc, j-> A, t-> nLitzv, s-> nLitzv, k -> ds1, bb -> ds2, dd -> AR, ff -> AR2
```

```
% % Lbox(ii,j,t,s,kk,bb,dd,ff,jj) =Ltot ;
```

```
% % Wbox(ii,j,t,s,kk,bb,dd,ff,jj)=Wtot;
```

```
% % Hbox(ii,j,t,s,kk,bb,dd,ff,jj)=Htot;
```

```
% % Vbox(ii,j,t,s,kk,bb,dd,ff,jj)=Vtot;
```

```
% % Ps(ii,j,t,s,kk,bb,dd,ff,jj)=Pout+PT;
```

```
% % eta(ii,j,t,s,kk,bb,dd,ff,jj)=Pout/Ps;
```

```
% % else
```

```
%
```

```
% loop=loop+1;
```

```
% Vtotal(loop)=Vtot;
```

```
% etatotal(loop)=Pout/Ps;
```

```
% sigmatotal(loop)=Pout/Vtot;
```

```
% end
```

```
%Go To 4 (Choose a new set of parameters and continue)
```

```
toc
```

### Appendix IV

Binary equivalent of one chromosome where each gene takes the mid-point of the design space.

0	0	0	0	0	0	0	0	0	0	0	0	0	0	0	0	0	0	0	0	0	0	1	0	1	0	0	0	1	1		
0	0	0	0	0	0	0	0	0	0	1	1	0	0	1	0	0	0	0	0	0	0	0	0	0	0	0	0	0	0	0	
0	0	0	0	0	0	0	0	1	0	0	1	0	1	1	0	0	0	0	0	0	0	0	0	0	0	0	0	0	0	0	
0	0	0	0	0	0	0	0	0	0	0	0	0	0	0	0	0	0	0	0	0	0	0	0	1	0	1	0	0	0	1	1
0	0	0	0	0	0	0	0	0	0	0	0	0	0	0	0	0	0	0	0	0	0	0	1	0	1	0	0	0	1	1	
0	0	0	0	0	0	0	0	0	0	0	0	0	0	0	0	0	0	0	0	0	0	0	1	0	1	0	0	0	1	1	
0	0	0	0	0	0	0	0	0	0	0	0	0	1	1	1	1	0	0	0	0	0	0	0	0	0	0	0	0	0	0	
0	0	0	0	0	0	0	0	0	0	0	0	0	1	1	1	1	0	0	0	0	0	0	0	0	0	0	0	0	0	0	
0	0	0	0	0	0	0	0	0	0	0	0	0	0	0	0	0	0	0	0	0	0	1	1	0	0	1	1	0	0	1	0
0	0	0	0	0	0	0	0	0	0	0	0	0	0	0	0	0	0	0	0	0	0	1	1	1	1	1	0	1	0	1	1
0	0	0	0	0	0	0	0	0	0	0	0	0	0	0	0	0	0	0	0	0	0	1	1	1	1	1	0	1	0	1	1
0	0	0	0	0	0	0	0	0	0	0	0	0	0	0	0	0	0	0	0	0	0	0	0	0	0	0	0	0	0	0	
0	0	0	0	0	0	0	0	0	0	0	0	0	0	0	0	0	0	0	0	0	0	1	1	1	1	1	0	1	0	1	1
0	0	0	0	0	0	0	0	0	0	0	0	0	0	0	0	0	0	0	0	0	0	0	1	0	1	0	0	0	1	1	
0	0	0	0	0	0	0	0	0	0	0	0	0	0	0	0	0	0	0	0	0	0	1	1	0	0	1	1	0	0	1	0
0	0	0	0	0	0	0	0	0	0	0	0	0	0	0	0	0	0	0	0	0	0	1	1	0	0	1	1	0	0	1	1
0	0	0	0	0	0	0	0	0	0	0	0	0	0	0	0	0	0	0	0	0	0	1	1	1	1	0	1	0	1	1	



## Appendix V

The code for genetic algorithm optimization

```
clear all
```

```
clc
```

```
pco = 0.75; % probability of cross over
```

```
pmu = 0.85; % probability of mutation process
```

```
% ----- creating the design space
```

```
nx=11; % number of values each gene can take in a range
```

```
ng=7; % number of genes in the problem
```

```
rcimin = 0.01;
```

```
rcimax = 0.1;
```

```
ncmin = 1;
```

```
ncmax = 50;
```

```
dcmin = 0.005;
```

```
dcmax= 0.05;
```

```
dstmin = 0.00001;
```

```
dstmax = 0.005;
```

```
wcmin = 0.05;
```

```
wcmax = 0.3;
```

```
rwimin = 0.01;
```

```
rwimax = 0.1;
```

```
hsmin = 0.01;
```

```
hsmax = 0.05;
```

```

rci1 = linspace(rcimin,rcimax,nx);

nc1 = round(linspace(ncmin,ncmax,nx));

dc1 = linspace(dcmin,dcmax,nx);

dst1 = linspace(dstmin,dstmax,nx);

wc1 = linspace(wcmin,wcmax,nx);

rwi1 = linspace(rwimin,rwimax,nx);

hs1 = linspace(hsmin,hsmax,nx);

% -----binary encoding

n = 16;    % number bits for integer part of your number

m = 16;    % number bits for fraction part of your number

% g1 = zeros(nx,m+n);

for i = 1:nx

    d2b = [ fix(rem(fix(rci1(i))*pow2(-(n-1):0),2)), fix(rem( rem(rci1(i),1)*pow2(1:m),2))];

    g1(i,:)=d2b;%

end

for i = 1:nx

    d2b = [ fix(rem(fix(nc1(i))*pow2(-(n-1):0),2)), fix(rem( rem(nc1(i),1)*pow2(1:m),2))];

    g2(i,:)=d2b;%

end

for i = 1:nx

    d2b = [ fix(rem(fix(dc1(i))*pow2(-(n-1):0),2)), fix(rem( rem(dc1(i),1)*pow2(1:m),2))];

    g3(i,:)=d2b;%

```

```
end
```

```
for i = 1:nx
```

```
    d2b = [ fix(rem(fix(dst1(i))*pow2(-(n-1):0),2)), fix(rem( rem(dst1(i),1)*pow2(1:m),2))];
```

```
    g4(i,:)=d2b;%
```

```
end
```

```
for i = 1:nx
```

```
    d2b = [ fix(rem(fix(wc1(i))*pow2(-(n-1):0),2)), fix(rem( rem(wc1(i),1)*pow2(1:m),2))];
```

```
    g5(i,:)=d2b;%
```

```
end
```

```
for i = 1:nx
```

```
    d2b = [ fix(rem(fix(rw1(i))*pow2(-(n-1):0),2)), fix(rem( rem(rw1(i),1)*pow2(1:m),2))];
```

```
    g6(i,:)=d2b;%
```

```
end
```

```
for i = 1:nx
```

```
    d2b = [ fix(rem(fix(hs1(i))*pow2(-(n-1):0),2)), fix(rem( rem(hs1(i),1)*pow2(1:m),2))];
```

```
    g7(i,:)=d2b;%
```

```
end
```

```
a1=ceil(rand*nx);
```

```
a2=ceil(rand*nx);
```

```
a3=ceil(rand*nx);
```

```
a4=ceil(rand*nx);
```

```
a5=ceil(rand*nx);
```

```

a6=ceil(rand*nx);
a7=ceil(rand*nx);
chb1 = [g1(a1,:); g2(a2,:);g3(a3,:);g4(a4,:);g5(a5,:);g6(a6,:);g7(a7,:)];
b1=ceil(rand*nx);
b2=ceil(rand*nx);
b3=ceil(rand*nx);
b4=ceil(rand*nx);
b5=ceil(rand*nx);
b6=ceil(rand*nx);
b7=ceil(rand*nx);
chb2 = [g1(b1,:); g2(b2,:);g3(b3,:);g4(b4,:);g5(b5,:);g6(b6,:);g7(b7,:)];
chb = [chb1,chb2]; % a random binary pair of chromosomes (parents)
for i=1:ng
chdp1(i,:) = chb(i,1:32)*pow2([n-1:-1:0 -(1:m)].');
chdp2(i,:) = chb(i,33:64)*pow2([n-1:-1:0 -(1:m)].');
end
chdp=[chdp1,chdp2] % a random decimal pair of chromosomes (parents)
% cross over
if rand>(1-pco)
chb11=chb1;
index = ceil(rand*ng);
chb11(index,n+1:n+4)=chb2(index,n+1:n+4); % cross over
chbn1= chb11;

```

```

chb22=chb2;

chb22(index,n+1:n+4)=chb1(index,n+1:n+4); %cross over

chbn2 = chb22;

chbn = [chbn1,chbn2]; % cross overed pair of new chromosomes

% mutation process

if rand>(1-pmu)

[a,b] = size (chbn);

if chbn(ceil(rand(1)*a),ceil(rand(1)*b))==0

    chbn(ceil(rand(1)*a),ceil(rand(1)*b))=1;

else chbn(ceil(rand(1)*a),ceil(rand(1)*b))=0

end

end

end

% mutation

if rand>(1-pmu)

[a,b] = size (chbn);

if chbn(ceil(rand(1)*a),ceil(rand(1)*b))==0

    chbn(ceil(rand(1)*a),ceil(rand(1)*b))=1;

else chbn(ceil(rand(1)*a),ceil(rand(1)*b))=0

end

end

chbn;

for i=1:ng

```

```
chdn1(i,:) = chbn(i,1:n+m)*pow2([n-1:-1:0 -(1:m)].');  
chdn2(i,:) = chbn(i,n+m+1:2*(n+m))*pow2([n-1:-1:0 -(1:m)].');  
  
end  
  
chdn=[chdn1,chdn2]
```

# CURRICULUM VITAE

SEYED RASOUL HOSSEINI

## ACADEMIC BACKGROUND

PhD, Electrical Engineering, University of Wisconsin-Milwaukee, Milwaukee, WI, USA (2015, 2020)

MS, Electrical Engineering, University of Wisconsin-Milwaukee, Milwaukee, WI, USA (2012, 2014)

MS, Solid State Physics, University of Kurdistan, Sanandaj, Iran (2007,2010)

BS, Electrical Engineering, KNTU University of Technology, Tehran, Iran (2003, 2007)

## EMPLOYEMENT

- Research Assistant, Power electronic/Power System Laboratory, University of Wisconsin-Milwaukee, Milwaukee, WI [Jan. 2015, May. 2018] (3.5 years)
  - o Funded by office of Naval research (ONR)
  - o Research project:
    - o Design and optimization of high frequency transformer for DC-DC power converter utilizing Dual Active Bridge topology
    - o Computer simulation of dual active bridge DC-DC converter for medium voltage direct current (MVDC) power system
    - o Methodology for characterization of common mode conducted electromagnetic emission in high frequency power converters
    - o Development of three phase solar inverter with SiC power MOSFET modules
    - o Studied the electromagnetic compatibility problem of three phase inverter with switching frequency of 100 kHz and power rating of 100 kW
    - o Computer simulation of multiple power electronic converter systems
    - o Proposal writing, poster preparation, technical publication and presenting the overall flow of the project for technical and non-technical audience
  
- Intern, electrical engineering, research and development, Rockwell Automation, Mequon campus, WI [Sept. 2017, Sept. 2018] (1 year)
  - o Research project: (High power Laboratory)
  - o Laboratory Investigation of utilizing wide band gap semiconductor materials for active front end (AFE) converter used for power factor correction (PFC) in regenerative motor drive
  - o Dynamic measurement of gate source voltage for high frequency gate driver board for SiC module control
  - o Double pulse test of SiC power module for extracting the switching loss of the high current SiC module
  - o Comparison of short circuit protection methodology for SiC MOSFET power module
  
- Teaching Assistant, Electromechanical Energy Conversion Lab, University of Wisconsin-Milwaukee, Milwaukee, WI [Spring 2019, Fall 2019 and Spring 2020] (1.5 years)
  - o Single phase measurement

- Three phase measurement
- Single phase Transformer
- Three phase Transformer
- DC machine
- AC Induction machine
- Synchronous generator
- 
- Research Assistant, Photonic Laboratory, University of Wisconsin-Milwaukee, Milwaukee, WI, USA [Sept. 2012, Dec. 2014] (2.5 years)
- Funded by National Science Foundation (NSF)  
Research project: (Laser Laboratory)
  - Anderson localized modes in a disordered glass optical fiber
  - Computer simulation of the optical wave propagation in optical fiber
  - Modal analysis of the impact of the boundaries on transverse Anderson localization in a one-dimensional disordered optical lattice
  - Laser coupling optimization to Anderson optical fiber
  - Development of Anderson disordered glass optical fiber
- Teaching Assistant, Digital logic discussion, University of Wisconsin-Milwaukee, Milwaukee, WI [Fall 2013] (0.5 year)
  - Digital logic gate circuits
  - Flip flops
  - Timing analysis
  - Introduction to FPGA
  - Logical programming
- Teaching Assistant, Electronics Lab, University of Wisconsin-Milwaukee, Milwaukee, WI [Spring 2014] (0.5 year)
  - Differential amplifiers
  - Op-amp
  - Feedback temperature control circuit
  - Oscillators
  - Diode bridge rectifier
- Teaching Assistant, electric circuit Lab, University of Wisconsin-Milwaukee, Milwaukee, WI [Spring 2014] (0.5 year)
  - Voltage division
  - Current division
  - Series and parallel circuits
  - Thevenin and Norton equivalent circuits
  - Circuit networks



- Technical Project Expert, National Cartographic Center, Tehran [Sept. 2010 – Sept. 2012] (2 years)
  - o Responsible for development of a national data streaming network with 120 outdoor stations equipped with high accuracy GPS and GLONASS receivers – worth of the project: \$ 50M
  - o Responsible for planning, negotiation, purchase, testing, configuration, installation and maintenance of 120 outdoor stations equipped with outdoor rack, electric power, uninterruptable power supply, battery, solar cell, temperature control, security camera, multiple communication link, GPS receiver and antenna
  - o Responsible for preparing multiple contracts with third party companies
  - o Responsible for presenting the development of the project to the minister
  
- Utility power system supervisor, National Engineering Association, Tehran [Sept. 2010 – Sept. 2012] (2 years)
  - o Designed the layout of the power system for the residential facilities
  - o Supervised the implementation of the residential power system according to the design
  - o Mentored the technicians to choose the right equipment and follow the guidelines provided in the design
  
- Research Assistant, Optoelectronics Laboratory, University of Kurdistan, Sanandaj, Iran [Sept. 2009 – Sept. 2010] (1 year)
  - o Modeling and simulation of ultra-short pulse propagation in semiconductor optical amplifier (SOA)
  - o Solving nonlinear Schrodinger equation for Semiconductor optical amplifier (SOA)
  - o Modelling the impact of Kerr effect in nonlinear medium
  - o Investigation of pulse width, medium loss and gain effect during the pulse propagation in semiconductor medium
  
- Research Assistant, Complex system simulation laboratory, University of Kurdistan, Sanandaj, Iran [Sept. 2008 – Sept. 2009] (1 year)
  - o Modeling and simulation of dynamics of nonlinear and chaotic granular material
  - o Prediction of motion of multi-particle system in lossy medium
  
- Intern, electrical engineering, Asia Wire, Malayer [Summer 2005] (0.5 years)
  - o Speed control of the induction motors rated for Medium Voltage
  - o Factory electrical system supervisory and maintenance
  - o Machinery maintenance in the facility

#### PUBLICATIONS

1. A. Lemmon, R. Cuzner, J. Gafford, S. R. Hosseini, A. Brovont, M. Mazzola, “Methodology for Characterization of Common-Mode Conducted Electromagnetic Emissions in Wide-Bandgap Converters for Ungrounded Shipboard Applications”, IEEE Journal of Emerging and Selected Topics in Power Electronics, vol. 6, No. 1, page 300-314, 2018.

2. B. Abaei, S. R. Hosseini, S. Karbasi, A. Mafi, "Modal analysis of the impact of the boundaries on transverse Anderson localization in a one-dimensional disordered optical lattice", *Optics communication Journal*, Vol 365, P.g. 208-2014, 2016.
3. S. R. Hosseini, M. Razaghi, N. Das, "Investigation of input pulsewidth, medium loss and gain effect on the output pulse characteristics of semiconductor optical amplifiers" *Optical engineering journal*, Vol. 51, No.7, 2012.
4. S. R. Hosseini, M. Razaghi, N. Das, "Analysis of non-linear refractive index influences on four-wave mixing conversion efficiency in semiconductor optical amplifiers" *Journal of optics and laser technology*, Vol. 44, No. 3 2012.
5. S. R. Hosseini, M. Razaghi, N. Das, "Analysis of ultrafast nonlinear phenomena's influences on output optical pulses and four-wave mixing characteristics in semiconductor optical amplifiers" *Journal of optical and quantum electronics*, Vol. 42, No. 11, 2011.
6. S. R. Hosseini, R. Cuzner, "Design and optimization of a High Frequency Power Transformer for solid state transformer", Submitted to the IEEE Energy Conversion Congress and Exposition (ECCE), Detroit, Michigan, 2020.
7. S. R. Hosseini, R. Cuzner, "A High Frequency Power Transformer for isolated and bidirectional DC-DC Converter used for MVDC Collection System in Wind Farms", presented at the IEEE International conference on renewable energy and applications (ICRERA), Slovenia, November 2019.
8. Robert Cuzner, S. Cruz, F. Rerrese, S. R. Hosseini "Power Converter metamodeling approach for the smart ship design environment", IEEE Electric Ship Technologies Symposium (ESTS), page 118-125, 2017.
9. Q. Jiao, S. R. Hosseini, R. Cuzner, "A comparison between silicon carbide based current source rectifier and voltage source rectifier for applications in community DC microgrid", IEEE International conference on Renewable Energy and Applications (ICRERA), page 544-549, 2016.
10. R. Cuzner, S. R. Hosseini, A. Lemmon, J. Gafford, M. Mazzola, "Methodology for the volume minimization in non-isolated SiC based PV inverters", IEEE Applied Power Electronic Conference and Exposition (APEC), page 1577-1584, 2016.
11. W. Fu, Q. Jiao, S. R. Hosseini, R. Cuzner, A. Lemmon "Methodology for the volume minimization in non-isolated SiC based PV inverters" IEEE International conference on renewable energy and applications (ICRERA), page 1236-1242, 2015.
12. S. Karbasi, S. R. Hosseini, K. w. Koch, T. Hawkins, J. Ballato, A. Mafi," Anderson localized modes in a disordered glass optical fiber", *Photonic and phononic properties of engineerd nanostructures IV*, Vol 8994, 2014.
13. S. R. Hosseini, M. Razaghi, N. Das, "Four-wave mixing in semiconductor optical amplifiers for high-speed communications" 5<sup>th</sup> international conference on Computers and Devices for communication (CODEC), Vol. 42, No. 11, 2012

14. S. R. Hosseini, M. Razaghi, N. Das, "Input pump pulse energy optimization to maximise four-wave mixing conversion efficiency in semiconductor optical amplifier" IEEE 10<sup>th</sup> international conference on Numerical Simulation of Optoelectronic Devices (NUSOD), page 43-44, 2010.